

NONUNIFORMLY SPACED ARRAY ELEMENTS

THESIS

Daniel Robert Richards Jr., Captain, USAF

AFIT/GE/ENG/00M-14

**DEPARTMENT OF THE AIR FORCE
AIR UNIVERSITY**

AIR FORCE INSTITUTE OF TECHNOLOGY

Wright-Patterson Air Force Base, Ohio

APPROVED FOR PUBLIC RELEASE, DISTRIBUTION UNLIMITED.

20000815 173

The views expressed in this thesis are those of the author and do not reflect the official policy or position of the Department of Defense or the U. S. Government.

NONUNIFORMLY SPACED ARRAY ELEMENTS

THESIS

Presented to the Faculty

Graduate School of Engineering and Management

Air Force Institute of Technology

Air University

Air Education and Training Command

In Partial Fulfillment of the Requirements for the
Degree of Master of Science in Electrical Engineering

Daniel Robert Richards Jr., B.S.E.E.

Captain, USAF

March 2000

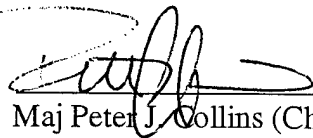
APPROVED FOR PUBLIC RELEASE, DISTRIBUTION UNLIMITED.

NONUNIFORMLY SPACED ARRAY ELEMENTS

Daniel Robert Richards Jr.

Captain, USAF

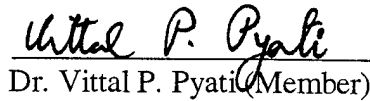
Approved:


Maj Peter J. Collins (Chairman)

15 MAR 00
date


Dr. Michael A. Temple (Member)

15 March 00
date


Dr. Vittal P. Pyati (Member)

15 Mar 00
date

ACKNOWLEDGMENTS

First, I would like to thank my Lord and Savior, Jesus Christ, for the opportunity and ability to not only endure AFIT, but also graduate. I also thank my wife, Mary Helen, and my son, Daniel, for what patience and understanding they have had while their loved one is at his second home.

I would also like to thank, my advisor, Major Peter Collins, for his insight, direction, and patience with this endeavor. I would also like to thank my sponsor and future supervisor, Dr Stephen Schneider, for giving me such an impossible endeavor, and then somehow convincing me that it was all my idea. I want to also thank the honorable “Doc” John Mehr formerly of Mission Research Center, for his superb engineering knowledge and experience. Without him as a sounding board, this thesis would not have been possible. I would also like to thank Sir, Dr., Maj. (Retired), Professor Mike Temple, for his insight and advice on the focus of the AFIT experience.

Lastly, I want to thank the other AFIT RASCALS, Lt Mike “Snitch” Saville, and Lt Geoff “Mr. Bean” Akers, for their late night discussions and support with this thesis.

Daniel Robert Richards Jr.

TABLE OF CONTENTS

1 Introduction	1
1.1 Problem Statement	4
1.2 Assumptions	5
1.3 Scope	6
1.4 Resources	6
1.5 Overview	7
2 Background	8
2.1 Periodic Arrays	8
2.1.1. Pattern Factor	8
2.1.2. Sidelobes	10
2.1.3. Grating Lobes	11
2.1.4. Scanning	13
2.1.5. Mutual Coupling	13
2.2 Aperiodic Arrays	14
2.2.1. Pattern Factor	14
2.2.2. Deterministic Array Thinning	15
2.2.3. Random and Statistical Array Thinning	20
2.3 Aperiodic vs. Periodic	23
2.3.1. Similarities	23
2.3.2. Advantages	23
2.3.3. Disadvantages	24
3 Theory	25
3.1 Periodic Arrays	25
3.1.1. Spacing	25
3.1.2. Current	26
3.2 Deterministic Approach	27
3.3 Statistical Theory for Random Arrays	29
3.3.1. Average Array Factor	31
3.4 Statistical Approaches	32
3.4.1. Statistical Density Taper	33
3.4.2. Random Array	37
3.4.3. Peak Sidelobe Indicator Statistics	42
4 Application	45
4.1 Planar Array Pattern Factor	45
4.2 Parameter Values	49
4.2.1. Uniform and Baseline Arrays	49
4.2.2. Deterministic Array	50
4.2.3. Statistical Array	51
4.2.4. Random Array	52
4.3 Comparison Analysis Methodology	54
4.3.1. Requirements	54
4.3.2. Metric	55
5 Results and Analysis	57
5.1 Process	57
5.2 Results	59
5.2.1. Array Performance	61
5.2.2. Element Counts	78
5.3 Analysis	79

5.3.1. Statistical Array.....	79
5.3.2. Random Array.....	79
5.3.3. Deterministic Array.....	80
6 Conclusions and Recommendations	81
6.1 Conclusions	81
6.2 Recommendations.....	81
6.3 Future Topics.....	82
Appendix A: C++ Flowcharts	83
Appendix B: Boresight Pattern Factors	90
Appendix C: Boresight Plots of Larger Arrays with Higher β Values.....	114
Appendix D: Nonprintable Materials List	121
Bibliography	123
Vita	125

TABLE OF FIGURES

Figure 1.1 Low and Medium Earth Orbit Altitudes.....	2
Figure 1.2 Networked Cluster of Space Based Radars	3
Figure 1.3 Large Effective Aperture	4
Figure 2.1 Spherical coordinate system	9
Figure 2.2 Normalized Radiation Pattern For A Uniform Aperture Distribution	11
Figure 2.3 Example Of A Linear Deterministic Array Element Distribution	16
Figure 3.1 Tapered Current Distribution On A 4 M2 Array With Maximum Value Of 1 And Axes Normalized To L , The Length Of The Array.	27
Figure 3.2 Sample random array.....	30
Figure 3.3 The PDF For Both The Random And Statistical Array Approaches.	33
Figure 3.4 Peak Sidelobe Estimator.....	41
Figure 4.1 Example Symmetric 4 Element Array.....	47
Figure 4.2 Peak Sidelobe Level Vs Confidence Level For Various Array Sizes.....	53
Figure 5.1 Process Of Data Generation And Analysis.....	58
Figure 5.2 HPBW Comparison on 4m ² Arrays.....	61
Figure 5.3 PSL Comparison on 4m ² Arrays.....	62
Figure 5.4 Uniform 4m ² Array Metric Breakdown.....	62
Figure 5.5 Deterministic 4m ² Array Metric Breakdown.....	63
Figure 5.6 Statistic 4m ² Array Metric Breakdown	63
Figure 5.7 Random 4m ² Array Metric Breakdown.....	64
Figure 5.8 Random2 4m ² Array Metric Breakdown.....	64
Figure 5.9 HPBW Comparison on 8m ² Arrays.....	65
Figure 5.10 PSL Comparison on 8m ² Arrays.....	65
Figure 5.11 Uniform 8m ² Array Metric Breakdown.....	66
Figure 5.12 Deterministic 8m ² Array Metric Breakdown.....	66
Figure 5.13 Statistic 8m ² Array Metric Breakdown.....	67
Figure 5.14 Random 8m ² Array Metric Breakdown.....	67
Figure 5.15 Random2 8m ² Array Metric Breakdown.....	68
Figure 5.16 HPBW Comparison on 12m ² Arrays.....	68
Figure 5.17 PSL Comparison on 12m ² Arrays.....	69
Figure 5.18 Uniform 12m ² Array Metric Breakdown.....	69
Figure 5.19 Deterministic 12m ² Array Metric Breakdown.....	70
Figure 5.20 Statistic 12m ² Array Metric Breakdown.....	70
Figure 5.21 Random 12m ² Array Metric Breakdown.....	71
Figure 5.22 Random2 12m ² Array Metric Breakdown.....	71
Figure 5.23 HPBW Comparison on 16m ² Arrays.....	72
Figure 5.24 PSL Comparison on 16m ² Arrays.....	72
Figure 5.25 Uniform 16m ² Array Metric Breakdown.....	73
Figure 5.26 Deterministic 16m ² Array Metric Breakdown.....	73
Figure 5.27 Statistic 16m ² Array Metric Breakdown.....	74
Figure 5.28 Random 16m ² Array Metric Breakdown.....	74
Figure 5.29 Random2 16m ² Array Metric Breakdown.....	75
Figure 5.30 Random2 16m ² Array ($\beta=.999$) Metric Breakdown	75

Figure 5.31 Element Count Trend For Each Array vs. Array Size.....	76
Figure 5.32 Boresight Trend For Each Array vs. Array Size.....	76
Figure 5.33 HPBW Trend For Each Array vs. Array Size.....	77
Figure 5.34 PSL Trend For Each Array vs. Array Size	77

Abstract

This thesis provides a method to reduce physical resource requirements along with cost reduction in Space Based Radar (SBR) platforms, and provides a rule of thumb for randomization effects on arrays. A trend analysis is performed on 4, 8, 12, and 16 square meter arrays. Three aperiodic thinning approaches are examined. They are an equal current density element distribution, a random periodic grid of elements, and random element distribution based a peak sidelobe indicator. According to the metrics used, the statistical and deterministic array thinning approaches performed best for these small arrays. However, the statistical arrays have a scan angle limitation of $\theta_0=30^\circ$ due to the interelement spacing of two wavelengths. The deterministic does poorly with peak sidelobes. The random array performance was limited due to the relatively small array sizes for the random approach used. The small size limits the array's capability to meet the peak sidelobe threshold requirement, due to a reduced confidence level, along with limiting the effective area to be randomized. However, as the array size increased, the thinning levels and performance increased to become competitive with the other array approaches. If trends continue as array size increases, the random array is the ideal solution.

NONUNIFORMLY SPACED ARRAY ELEMENTS

1 Introduction

The United States Air Force has a vital interest in providing continual, all-weather surveillance of large geographical areas. The breakup of major world powers coupled with the ease of access, purchase, and use of lethal weapons, has reduced regional stability overseas. Ironically, the dispersion of lethal threats takes place concurrent with a decrease in US foreign presence and an increase in restrictions on US military use of foreign airspace. This results in a need for a worldwide surveillance capability to protect national security, assets, and interests abroad. This capability requires wide angle scanning over large coverage areas and precision target tracking in high-density electromagnetic environments.

One emerging solution to address this need is space-based radar. With its ability to cover large geographical areas continuously under all weather conditions without regard to airspace restrictions or forward presence, it has become a primary candidate for meeting this critical need. However, using radar platforms in a space environment introduces problems of platform weight, limited power, flexibility, and cost. It also requires overcoming major technological challenges of wide-angle precision tracking and multiple target discrimination from low earth orbit (LEO) and medium earth orbit (MEO) trajectories (see Figure 1).

The following example provides insight into the problem by comparing the capabilities and requirements for air breathing radar platforms with those of space based platforms, operating at 12 GHz. In particular, the example compares the array sizes and element counts for an unmanned aerial vehicle (UAV), a fighter and an SBR. A UAV with a 1.1 by 1.1-meter array will have approximately 2,000 elements if populated at half a wavelength interelement spacing. Similarly, a fighter with a 1 by 1-m array has over 1,600 elements. Finally, a SBR of 10 by 10-meters would require over 640,000 elements to populate the array at half a wavelength interelement spacing.

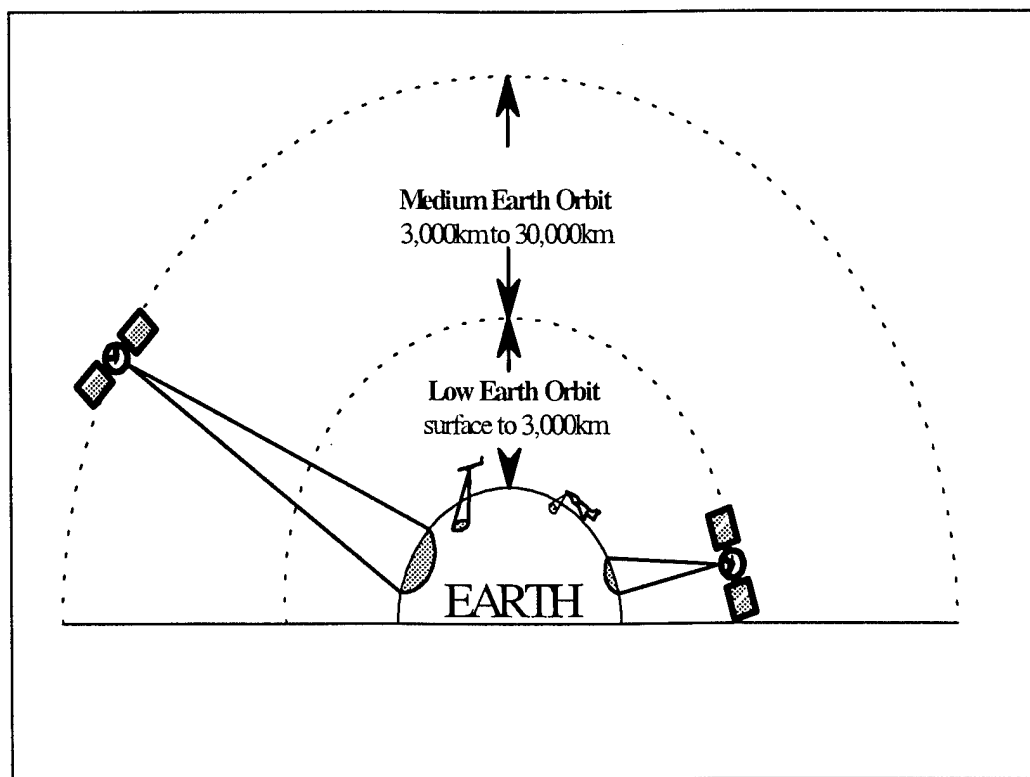


Figure 1.1 Low and Medium Earth Orbit Altitudes

Taking the element counts above and looking at the power, size, weight and cost limitations, it is evident that the implementation of a SBR is not a simple problem. The demands of space-based platforms require an unconventional look at how to achieve the same performance with less power, smaller size and lighter weight.

Some approaches involve using constellations or clusters of multiple smaller platforms networked together (Figure 1.2), collapsible parabolic apertures, and splitting large apertures into smaller pieces to create a larger effective aperture (Figure 1.3). This research focuses on yet another approach by reducing the number of array elements with non-uniform interelement spacing. Concepts from this approach could prove useful for the above approaches and other large array applications.

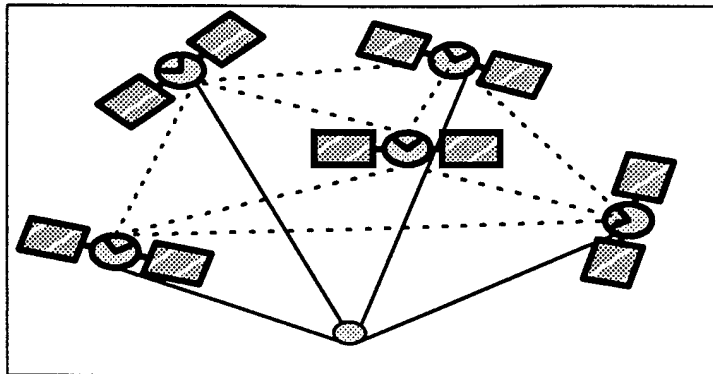


Figure 1.2 Networked Cluster of Space Based Radars

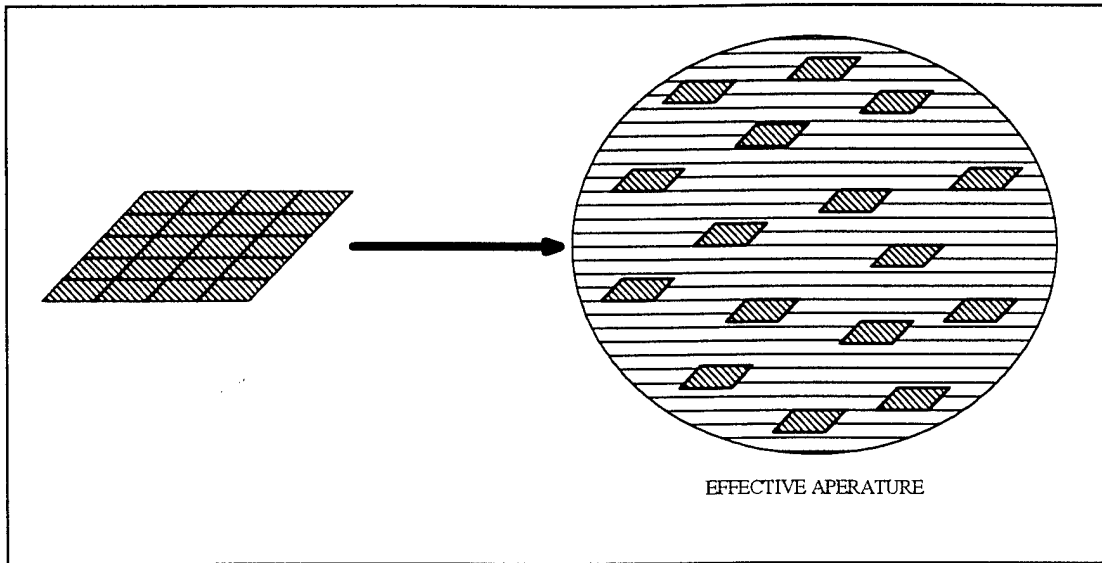


Figure 1.3 Large Effective Aperture

1.1 Problem Statement

This research focuses on determining an optimal array design to minimize the number of radiating elements by utilization of non-periodic array structures. There are many methods of creating a non-periodic array structure. The specific methods of interest in this thesis are:

- Deterministic: element locations based on an algorithmic approach, in particular a variant of the equal current area or volume approach.
- Random: element locations randomly selected from a probability distribution function (pdf). The pdf used is the tapered current distribution on the baseline uniform array.
- Statistical: periodic grid with interelement spacing of two wavelengths. Randomly selected element locations are “turned off” or not used based upon

a pdf. The pdf used is the tapered current distribution on the baseline uniform array.

1.2 Assumptions

The assumptions used in this research and modeling process are:

- The mutual coupling between the array elements is negligible.
- The elements are isotropic radiators.
- The array structure is assumed symmetric in each quadrant. This results in a reduction in complexity and cost in the manufacturing process, eases transport and construction requirements in space, and most importantly, decreases computational and implementation complexity.
- The pattern factor is symmetric about the scan angle of θ_0 for all ϕ and the scan angle ϕ_0 since the array structure is symmetric.
- The computations for scan angles are only requested in the two principle planes defined by $\phi_0=0^\circ$ and $\phi_0=90^\circ$.
- Due to symmetry about the mainbeam, θ is sampled from 0° to 90° and ϕ is sampled from ϕ_0 to ϕ_0 plus 180° .

1.3 Scope

The approaches covered in this thesis are applicable to any size array. For trend analysis purposes and in interest of time, the focus is on arrays of 4, 8, 12, and 16 square meters. This thesis has the following tasks:

- Find an optimal element reduction approach out of the three approaches mentioned previously.
- Determine the optimal approach for the 4, 8, 12, and 16 square meter arrays that best meets the following operating requirements.
 - $\pm 50^\circ$ scan capability
 - Peak sidelobe level (PSL) threshold of -13.5 dB or less for aperiodic arrays.
 - 2 GHz to 12 GHz frequency range
- Provide a metric for determining the effects of randomization on an array.
- Provide a trend analysis for aperiodic arrays as the array size gets larger.

1.4 Resources

The computational program was developed using Microsoft Visual C++[®] V6. The graphical user interface and representation of results are in MATLAB[®]. Various PC platforms were used to execute the program. They ranged from a Pentium 133 to a Pentium III 550, running either Windows 98 or NT.

1.5 Overview

This document contains a review of significant works in non-uniform arrays, the theory behind the deterministic, statistical, and random approaches, the selection of the optimal non-uniform approach, and the optimal approach applied to four different sized arrays. Chapter 2 contains a review of periodic arrays and literature review of significant writings on non-uniform, random, and non-periodic array theory and synthesis. The third chapter is devoted to the theory behind the approaches used in this effort. Chapter 4 contains the application of the non-uniform element reduction approaches to the arrays and the methodology used to determine the optimal array approach. The fifth chapter provides the results and analysis from the application in Chapter 4. Chapter 6 contains conclusions and recommendations based on the results presented in Chapter 5.

2 Background

This chapter lays a foundation for both periodic and aperiodic linear arrays. It concludes with a summary of the advantages and disadvantages that are inherent to each array type.

2.1 Periodic Arrays

An array can be broken down into its individual radiating elements. The array's pattern factor is just the summation of the radiation pattern from each element in the array.

2.1.1. Pattern Factor

The pattern factor for a single element is

$$f(\Psi) = I \exp(j\Psi) \quad (2.1)$$

where

$$\Psi = \beta \sin(\theta)$$

$$\beta = \frac{2\pi}{\lambda} .$$

The far field pattern is the summation of each individual radiating element's contributions in a given direction. For N isotropic, in-phase elements spaced along the x -axis, the pattern factor is equivalent to

$$f(\theta) = \sum_{n=1}^N i_n \exp(j\beta d_n \sin(\theta)) \quad (2.2)$$

where

i_n = the current on the n th element

d_n = the distance of the n th element from the point of origin in meters

θ is referenced off of the z -axis (see Figure 2.1)

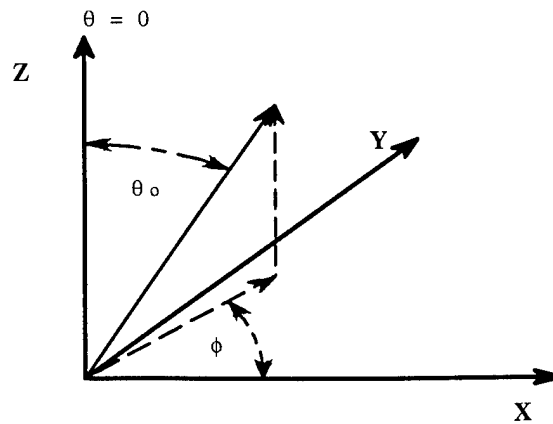


Figure 2.1 Spherical coordinate system

The two independent design variables are the element locations d_n and the element weighting or currents i_n . However, for equally spaced arrays, the element locations are normally fixed to half a wavelength, leaving the elements' weighting as the only design parameter (Steinberg, 1974:124).

Since the current magnitude of the antenna is equal to the sum of the individual element currents, the equally spaced array with a uniform current distribution has a normalized current magnitude, I , of one. Therefore, the excitation coefficients or weightings become

$$I = N \cdot i_n \quad n = 1, 2, 3, \dots, N \quad (2.3)$$

and

$$i_n = I / N \quad (2.4)$$

Now for $I=1$, i_n becomes

$$i_n = 1 / N \quad n = 1, 2, 3, \dots, N \quad (2.5)$$

Reducing the array factor by substituting Equation (2.5) into Equation (2.2) gives

$$f(\theta) = \frac{1}{N} \sum_{n=1}^N \exp \left[\frac{j2\pi d(n-1) \sin \theta}{\lambda} \right] \quad (2.6)$$

where d is the interelement spacing. With the excitation being uniform, the last design freedom is no longer available.

2.1.2. Sidelobes

Sidelobes are minor lobes in the array pattern (see Figure 2.2). Reductions in sidelobe levels are desirable since they are a large source of power loss. The number of sidelobes in one period of the pattern factor relates directly to the number of elements in the array. For N elements, there is one mainlobe and $N-2$ sidelobes in each period. The sidelobe widths are $2\pi/N$ while the main and grating lobes are twice this width. As N

increases, the number of sidelobes increases while their width and peak values decrease. As N approaches infinity, the sidelobe levels approach that of a uniform line source (Stutzman, 1998:100).

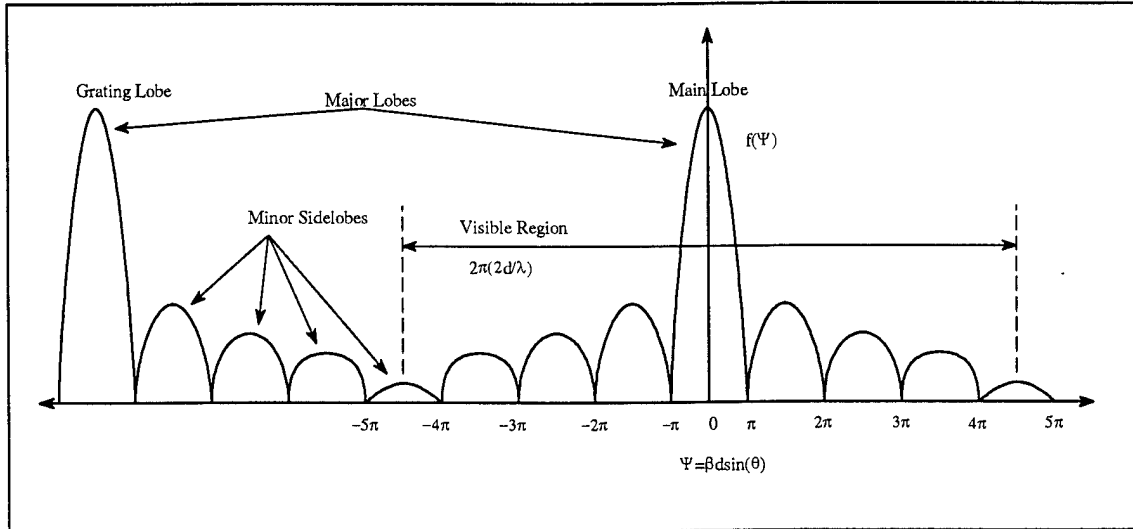


Figure 2.2 Normalized Radiation Pattern For A Uniform Aperture Distribution

2.1.3. Grating Lobes

The largest source of periodic array limitations and power loss is the grating lobe. Grating lobes are additional major lobes (see Figure 2.2) whose power intensity is equal to that of the mainlobe (Stutzman, 1998:99). These lobes are a result from the coherent sum of all the elements' radiation at angles other than the steering angle (Steinberg, 1976:125). In a periodic array, to avoid grating lobes from appearing in the visible region, the interelement spacing needs to be less than half a wavelength. This stems from the fact that for $d = \lambda/2$ only one period of the array factor appears in the visible region ($-\pi/2 < \theta < \pi/2$) (Stutzman, 1998:98). The portion of the array factor that appears in the

visible region is determined by setting the period of the pattern factor to the phase progression over the visible region,

$$\Psi(\theta) = \alpha + \frac{2\pi \sin(\theta)}{\lambda} \quad (2.7)$$

Substituting the limits on θ into Equation (2.7) gives

$$\alpha - \frac{2d\pi}{\lambda} < \Psi(\theta) < \alpha + \frac{2d\pi}{\lambda} \quad (2.8)$$

or

$$\Psi(\theta) < \frac{4d\pi}{\lambda} \quad (2.9)$$

For one period (2π) to be in the visible region, Ψ must equal 2π . Then Equation (2.9) becomes

$$2\pi < \frac{4d\pi}{\lambda} \quad (2.10)$$

Finally, solving for d

$$d = \frac{\lambda}{2} \quad (2.11)$$

which is the half wavelength interelement spacing.

Grating lobes further affect array capabilities by limiting the scan angle of the array. The maximum scan angle of an array is the maximum steering angle prior to the introduction of grating lobes in the visible region.

2.1.4. *Scanning*

Electronic beam scanning occurs through cumulative changes in phase. By progressively shifting the phase (α) on each element, the summation of the phases results in the mainbeam being directed off boresight. This electronic form of beam steering allows scanning without physically moving the aperture. The new direction of the main beam is found by solving Equation (2.12) for θ_0 , and then finding the angle where the array factor is a maximum. This maximum occurs where $\Psi=0$. So setting

$$\Psi(\theta) = \alpha + \frac{2\pi \sin(\theta)}{\lambda} \quad (2.12)$$

to 0, and solving for α results in

$$\alpha = -\frac{2\pi \sin(\theta_0)}{\lambda} \quad (2.13)$$

Then solving for θ_0

$$\theta_0 = \pi - \text{asin}\left(\frac{\alpha\lambda}{2d\pi}\right) \quad (2.14)$$

Equation (2.14) determines the maximum scanning angle for the array.

2.1.5. *Mutual Coupling*

Mutual coupling is another design consideration with arrays. Coupling can occur from the feed structure and surface paths, along with reflections at the antenna terminals, and element radiation (Steinberg, 1976:124). Each element's radiation induces currents

upon all the other elements in the array. The radiation-coupling coefficient, c_{mn} , between elements m and n is

$$c_{mn} = \frac{\sin(d_{mn}\beta)}{d_{mn}\beta} . \quad (2.15)$$

Coupling affects gain, effective element pattern, and transmitter load (Steinberg, 1976:125). Theoretically, coupling effects are calculable; however, in practice they are not. The best approach to dealing with mutual coupling is to make it negligible. One way this can be accomplished is by thinning or over spacing the array elements. The drawback of thinning is that it reintroduces the problem of grating lobes, unless the array is aperiodic (Steinberg, 1976:125).

2.2 Aperiodic Arrays

As stated in the introduction, very large arrays with equal spacing require a large number of elements. With aperiodic structures using fewer elements, it is possible to gain a higher direction finding resolution than with periodic arrays (Andreasen, 1962:138). Furthermore, aperiodic arrays have wider scan capability over a larger frequency band (Andreasen, 1962:137).

2.2.1. Pattern Factor

The previous section stated that an array's pattern can be broken down to its individual elements' radiation pattern. This is still applicable to aperiodic arrays.

The only change occurs in the parameter d_n in order to account for phase progression along the array. The pattern factor is still

$$f(\theta) = \sum_{n=1}^N i_n \exp \left[\frac{j d_n 2\pi \sin(\theta)}{\lambda} \right] \quad (2.16)$$

where

i_n = the current on the n th element

d_n = distance from the center of the array to the n th element in meters

However, aperiodic arrays differ from the periodic in that their element positions d_n are not chosen to be equally spaced along the array. In the past, the selection of element locations for aperiodic arrays was a trial and error process due to the limited computational capability. Trial and error approaches are highly inefficient and require an abundance of time. A more efficient method for the selection of element positions is the use of deterministic sampling algorithms.

2.2.2. Deterministic Array Thinning

The deterministic approach uses an algorithm to choose the element locations. A common deterministic approach is density tapering. Density or spatial tapering on an aperiodic array is directly equivalent to current or amplitude tapering of a periodic array (Sandler, 1960:496). This is where the selection of element locations are found by dividing the area under the current excitation function into equal subsections. Then the elements are placed in the middle of each equal area subsection (see Figure 2.3). This is the deterministic approach used in this research. Chapter 3 will discuss this method further.

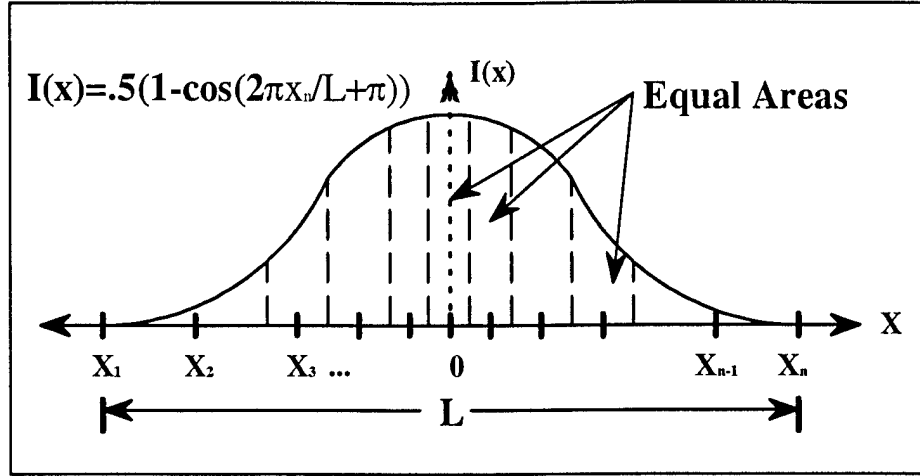


Figure 2.3 Example Of A Linear Deterministic Array Element Distribution

The reciprocal current density is another deterministic algorithm, similar to the equal area approach. Each successive element's location is relative to the previous element's position based on the reciprocal of the current excitation on that previous element. The first spacing is

$$d_{01} = \frac{D}{i(x_0)} \quad (2.17)$$

where D is the designer proportionality constant. With the first element located at $x_0=0$, the next element is located at

$$x_1 = x_0 + d_{01} = \frac{D}{i(x_0)} \quad (2.18)$$

For the second element, the distance from x_1 is

$$d_{12} = \frac{D}{i(x_1)} \quad (2.19)$$

placing x_2 at

$$x_2 = x_1 + d_{12} = D \left(\frac{1}{i(x_0)} + \frac{1}{i(x_1)} \right) . \quad (2.20)$$

Therefore, the n th element location is

$$x_n = D \sum_{j=0}^{n-1} \frac{1}{i(x_j)} . \quad (2.21)$$

A deterministic approach taken by Sheldon Sandler is based on spatial frequency.

“Spatial frequency is a measure of the variation of each element contribution with far field angle” (Sandler, 1960:496). In this approach, elements are spaced from each other based on harmonic frequencies of the uniformly spaced array.

$$f(\theta) = 1 + 2 \sum_{m=1}^{(N-1)/2} \cos(2dm\pi \cos(\theta)) \quad (2.22)$$

where

d = element spacing in fractions of a wavelength

N = total number of elements.

In Equation (2.22), the lowest array frequency is associated with the center element, with the fundamental frequency given by the $m=1$ term, the first harmonic given by the $m=2$, up to the $m=(N-1)/2$ term. For instance, take 3 elements in a line. Make one the center and place the other two a distance d , from the center. The distance d determines the fundamental frequency for the 3-element array. Now take two more elements and place them $2d$ from the center. These last two elements, due to the periodicity (integer multiples of length d) of their location, will determine the first harmonic frequency of the array. Add two more elements and place them $3d$ from the center and this generates the

3rd harmonic frequency. The harmonic frequencies are due to the periodicity of the element locations. Since the uniform array is composed of multiple pairs located by integer multiple of d away from the center, there are multiple harmonics. Applying this concept to a nonuniformly spaced array results in an unevenly distributed spatial frequency spectrum. This approach determines the element locations based on desired frequency capability of the desired array.

Some other deterministic approaches are log density taper, primes, arithmetic progression, controlled cosines, and elimination of multiples. (King and others, 1960) The log density taper places the k th element at a location $1-\log(10-k)$ from the center of the array. For prime numbers spacing, the element locations are generated by taking a set of successive prime numbers, doubling those numbers, and scaling them down by dividing by 100 (see Table 2.1).

The arithmetic progression is generated with an initial spacing of 1 and a common difference of $1/7$. In other words, each element location is given by d_n

$$d_n = 1 + \frac{n}{7} \quad (2.23)$$

where d_n is the distance between the element and array center.

Table 2.1 Prime Number Element Spacing

Element	Prime	Prime Doubled	Derived Spacing	Distance
1	53	106	1.06	1.06
2	59	118	1.18	2.24
3	61	122	1.22	3.46
4	67	134	1.34	4.80
5	71	142	1.42	6.22
6	73	146	1.46	7.68
7	79	158	1.58	9.26
8	83	166	1.66	10.92

The controlled cosines is generated by

$$A = 20 \log \left[\frac{c + 2 \sum_{k=1}^n \cos(2\pi Z \frac{d_k}{\lambda})}{2n + c} \right] \quad (2.24)$$

where

A = the magnitude of the pattern factor in dB,

$Z = S_{min}(\sin \theta - \sin \theta_0)$

S_{min} = the smallest of the set of unequal spacings in wavelengths,

θ = the angle to which the beam is steered,

θ_0 = the azimuth angle measured from broad side,

$2n+c$ = the number of elements in the array

$c=1$ for odd elements and $c=0$ for even elements

d_k/λ = the distance in wavelengths from the center of the array to the k th element.

The element locations, d_k , are a set of distances that evenly spread the product Zd_k/λ , from 0 to 1 for all Z from .05 to 2. This will minimize the sidelobes in the range of Z from .05 to 2.

The elimination of multiples is just the placement of the elements such that no spacing between two elements is a multiple of one-half. Table 2.2 gives sample location for the first 7 elements of each of the linear array types.

Table 2.2 Other Deterministic Array Element Locations (In Wavelengths)

Array Type	X₀	X₁	X₂	X₃	X₄	X₅	X₆
Uniform	0	0.5	1.0	1.5	2.0	2.5	3.0
Logarithmic	0	1.0	2.1	3.4	4.9	6.6	8.7
Prime Numbers	0	1.06	2.24	3.46	4.8	6.22	7.68
Arithmetic Progression	0	1.0	2 1/7	3 3/7	4 6/7	6 4/7	8 3/7
Elimination of Multiples	0	1.0	2.05	3.15	4.3	5.6	6.95
Controlled Cosines	0	1.0	2.1	3.4	4.9	6.6	8.5

There are many deterministic approaches to choose from, determining which approach is best is not an easy task. One has to look at how each affects desired pattern parameters and select one that best meets performance requirements. One way to skirt that selection process is to use a statistically controlled aperiodic thinning technique.

2.2.3. Random and Statistical Array Thinning

These two are grouped together since they are both handled via application of statistical theory. An array constructed with element locations chosen by some random process is a random array. In the statistical approach, the element spacing is initially

uniform. A fraction of the elements are randomly removed. Both array-thinning methods share the same statistical properties even though they involve different design approaches (Steinberg, 1976:140).

The statistical density taper approach evolved from the study of random amplitude and phase errors in an array. The same mathematics is applicable to random errors in element location. This evolved into an approach of taking a filled array and removing elements according to some random or statistically process.

Another approach is to let a random process supply the element locations. For instance, take the current distribution on a uniformly spaced array and make it the probability density function for the random process that selects the element's location. Now randomly select a probability density function (pdf) level and find random location values that produce a pdf value less than the random pdf value selected (see Figure 3.3). This process is repeated until the desired number of elements is reached.

Selecting the number of elements can be based on desired thinning levels, average sidelobe levels (ASL), or peak sidelobe detection (PSD). Thinning level is just a percentage reduction in the number of elements from a fully populated array. The ASL is based on selecting an average sidelobe level and using the normalized theoretical average sidelobe level of

$$ASL = \frac{1}{N} \quad (2.25)$$

to determine the number of elements, N , for the array (Steinberg, 1972). These are non-complex approaches to deriving the number of elements. However, they do not provide

decent sidelobe control. A random method that provides more control is by a random process described by a tapered probability distribution. This would result in fewer elements at the outskirts of the array, resulting in lower sidelobe levels.

In an approach presented by Maffett, a method is given to design an aperiodic linear array. This array is composed of one-fourth the number of elements needed by a uniformly spaced array, with no mainlobe beamwidth sacrifice, and only a 5-dB sidelobe sacrifice (Maffett, 1962:131). The number of elements is found by first taking the sampled version of the desired pattern factor G

$$G(u) = \sum_{n=0}^N \varepsilon_n b_n \cos(kx_n u), \quad \varepsilon_n = \begin{cases} 1, & n = 0 \\ 2, & n \neq 0 \end{cases} \quad (2.26)$$

where

$$u = \cos\theta - \cos\theta_0$$

θ = observation angle

θ_0 = beam steer angle

b_n = the amplitude factor

n_n = element location

and dividing it by the total source current A . Taking the moments of G/A , for suitable values for the length L of the array and the number of elements N , the expression for G/A can be approximated by the normal distribution (Maffett, 1962:133). The advantage of the normal distribution is that it provides a very useful statistical description for the random array.

Steinberg also presents another technique that combines sidelobe levels and the required number of elements for statistical arrays in his articles discussing the theory of

peak sidelobe indicators. Y. T. Lo also presents a variant of this method (Lo, 1967:231). The maximum peak sidelobe is predicted given a desired confidence level that sidelobes will not exceed the predicted level. Chapter 3 covers this technique in more detail.

2.3 Aperiodic vs. Periodic

This section gives a brief summary of the similarities, advantages, and disadvantages of the aperiodic and periodic arrays.

2.3.1. Similarities

Some things are relatively unchanged between periodic and aperiodic arrays. As mentioned earlier, the fundamentals of the array factor do not change. Since beamwidth is primarily dependent on array size, it remains unaffected by using variable interelement spacing in an array, assuming the thinning is not excessive.

2.3.2. Advantages

The primary advantage of aperiodic arrays is the reduction in the number of elements required to populate the array. Depending on the extent of thinning, the reduction can provide significant cost and weight savings.

Another major advantage of aperiodic arrays is that the average spacing can be designed to be over several wavelengths, without running into grating lobes (Lo, 1968:425). This allows for greater beam steering range. Increased spacing also reduces the effects of radiation coupling. From Equation (2.15), it is apparent that the effects of radiation coupling are dependent on the spacing of the two elements in consideration. As d_{mn} increases, the coupling decreases. The reason for not allowing d_{mn}

to be larger than half a wavelength in a periodic array is due to the introduction of grating lobes into the visible region. With aperiodic arrays, the periodicity of the structure is not there to allow the development of grating lobes (Steinberg, 1976:125).

Finally, the variation in the elements' location allow for better array performance over a larger band of frequencies. Since the distance from the origin of each element varies, the frequencies with wavelengths equal to or multiples of those distances, will radiate more efficiently with an aperiodic array.

2.3.3. Disadvantages

The improvements in scan angle, bandwidth, and fewer elements, comes at a cost. The major expense is in design control of the radiation pattern in the sidelobe region. With a reduction in the number of elements, the sidelobe levels not only increase but also lose their predictability outside the neighborhood (past the third null) of the main beam. The other cost encountered is gain loss. With fewer radiating elements, the total array gain is going to be less than that of the periodic array of the same size with the same element types and feed structure.

With the foundation laid down in this chapter on periodic and aperiodic array structures, the next chapter will further develop the aperiodic array thinning techniques that are used in this thesis.

3 Theory

This chapter examines in depth, the three approaches chosen as possible optimal design methods. All three approaches are referenced to a baseline or control array of equally spaced, uniformly excited elements. Coverage of the baseline array is first along with an equally spaced array employing an amplitude taper. Then a discussion is provided on the deterministic approach, followed by a brief section on random array statistics. Finally, a detailed look at the last two approaches, statistic and random array thinning, is presented.

3.1 Periodic Arrays

3.1.1. Spacing

The baseline array is a fully populated array with elements separated by half a wavelength. The choice of wavelength is determined by the operating frequency. Since the array is to operate over a range of frequencies, one must decide which of those frequencies determines the spacing. For this thesis, the frequency selection is based on the idea that the element locations are sampling intervals for the current distribution producing the desired pattern factor. At the lower frequencies, the wavelengths are larger providing lower sampling resolution for the higher frequencies. However, using the high frequency for element locations, provides over sampling of the current distribution at lower frequencies. Since it is more advantageous to have over sampling than under sampling, the highest operating frequency will determine the design wavelength.

3.1.2. Current

The baseline array has a uniform current excitation. An equally spaced array with amplitude tapering is also used. This amplitude-tapered array provides an equally spaced array that is optimized for low sidelobe levels. This optimized equispaced array provides a low sidelobe array for approximation purposes by the aperiodic arrays. A commonly used tapered current excitation is the raised cosine, given by

$$i_T(x_n) = \frac{1}{2} \left(1 - \cos\left(\frac{2x_n\pi}{L} + \pi\right) \right) \quad (3.1)$$

where

$i_T(x_n)$ = the current on the n th element in the uniform array

L = the length of the array in meters

At the edges, $-L/2$ and $L/2$, the current drops down to zero, while reaching a max of one at the center of the array ($x_n=0$). The design array is a two dimensional, planar array, so i_T must also be planar to produce the same current excitation along the y -axis. The current excitation for the array is just a product of the x and y current functions. In this case, i_T becomes

$$i_T(x_n, y_n) = \frac{1}{2} \left(1 - \cos\left(\frac{2x_n\pi}{L} + \pi\right) \right) \left(1 - \cos\left(\frac{2y_n\pi}{W} + \pi\right) \right) \quad (3.2)$$

where

W = the width of the array

y_n = n th element location on the y -axis, ranging from $-W/2$ to $W/2$.

Figure 3.1 contains an example plot of the tapered current distribution for a 4-m2 array.

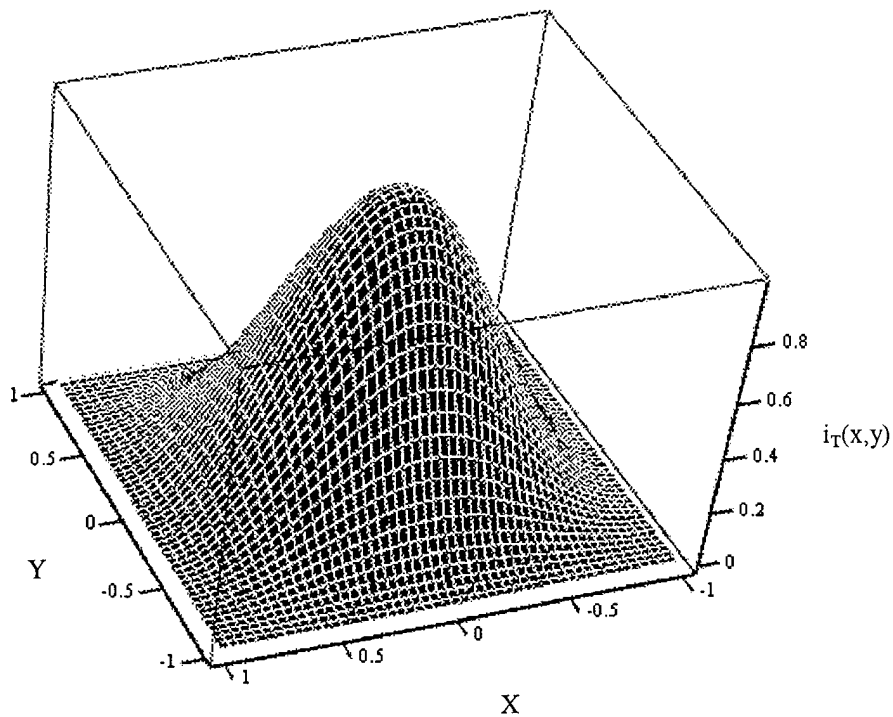


Figure 3.1 Tapered Current Distribution On A 4 M2 Array With Maximum Value Of 1 And Axes Normalized To L , The Length Of The Array.

3.2 Deterministic Approach

One of the easier array thinning approaches to implement is the deterministic approach. A modified equal area element distribution is chosen as the deterministic thinning approach. It is a spatial taper approach based on element location dispersion due to equal area regions under the current excitation function (see Figure 3.1). The modification comes from placing elements at the ends of the array in order to maintain

the beamwidth requirements. Otherwise, the rest of the process follows the spatial taper approach described in Chapter 2.

As previously stated, a periodic array can be viewed as a continuous current distribution sampled at equally spaced intervals. Each of these samples has a magnitude equal to the excitation current at each sample point. This gives a sampled approximation of the array's excitation current $i(x)$. For this deterministic approach, the first step is to divide the total area under the current distribution curve into equal area subsections. The cumulative current distribution as a function of x is

$$I(x) = \int_{-L/2}^x i(x') dx' . \quad (3.3)$$

Integrating over the length of the array gives the total area under $i(x)$. Labeling it I_T ,

$$I_T = \int_{-L/2}^{L/2} i(x) dx \quad (3.4)$$

and then dividing it into $N-2$ equal subsections of area, gives

$$I_{eq} = \frac{I_T}{N-2} \quad (3.5)$$

which is the equal area value that each interval or subsection of $i(x)$ must contain. Once the intervals are found, the element locations are placed at the midpoint of the interval. Therefore, each element location is determined by combining (3.4) and (3.5).

$$I_{eq} = \frac{I_T}{N-2} = \int_{a_{n-1}}^{a_n} i(x) dx . \quad (3.6)$$

The value for the first non edge element, x_1 , is

$$x_1 = \frac{a_1 - 0}{2} \quad (3.7)$$

In Equation (3.7), x_1 is located halfway between a_0 and a_1 . The value for a_1 is determined by solving Equation (3.6) for a_n . When $n=1$, Equation (3.6) becomes

$$I_{eq} = \frac{I_T}{N - 2} = \int_0^{a_1} i(x) dx \quad (3.8)$$

Using Equations (3.6) through (3.8), the location of the n th element is found to be

$$x_n = \frac{a_n - a_{n-1}}{2} \quad (3.9)$$

For example take a five element linear array. At a frequency of 3 GHz, the wavelength is 0.1 meters. Since the desired minimum interelement spacing is two wavelengths, the first pair of elements will be located at ± 0.2 meters about the center element of the array. Taking 0 and 0.2 as the limits of integration for Equation (3.6) the equal cumulative current density is found. The next pair of elements are located where a_n sets the integral in Equation (3.6) equal to the I_{eq} . Repeating this process determines the locations for the rest of the elements.

3.3 Statistical Theory for Random Arrays

The following development is based on Steinberg's "Theory of the Random Array" (Steinberg, 1976:139-188). It starts with a linear random array of N elements that have corresponding element locations of x_n on the x -axis. The location values of x_n are

from a set of independent random variables. These variables have some arbitrary probability density distribution $w_I(x)$.

In Figure 3.2, the length of the array is L and has a current density of $i(x)$, which is a sum of δ functions at each x_n on L .

$$i(x) = \sum_{n=1}^N \delta(x - x_n) \quad (3.10)$$

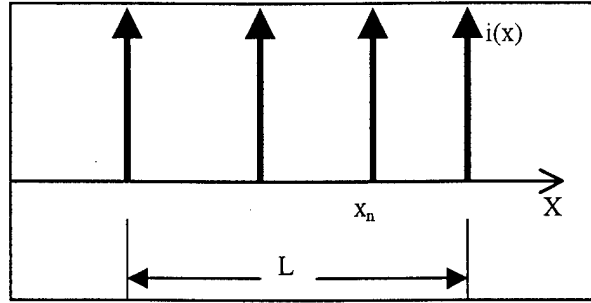


Figure 3.2 Sample random array

The Fourier transform of $i(x)$ is the complex far-field radiation pattern $f(u)$. The pattern is proportional to the sum of unit vectors, since $i(x)$ is a set of δ functions whose Fourier transform is one. i.e.,

$$f(u) = \sum_{n=1}^N \exp(jkx_n u) \quad (3.11)$$

where

x_n = distance of the n th element from the array center

$$u = \sin(\theta) - \sin(\theta_0) \quad (3.12)$$

$$k = \beta = \frac{2\pi}{\lambda} \quad (3.13)$$

The amplitude on the mainlobe is going to be equal to the number of elements, N . The RMS amplitude of the sidelobes is \sqrt{N} . The mean of the sidelobe power pattern is N , which is the square of the RMS amplitude. The power ratio of average sidelobe (N) to mainlobe (N^2) is N/N^2 , which simplifies to $1/N$. This is the theoretical average sidelobe level.

3.3.1. Average Array Factor

Since the random array's element locations differ from one run to the next, the pattern factor needs to be in terms of averages. Therefore, the next item of interest is the ensemble average of random arrays. The ensemble average of a pattern factor is

$$\overline{f(u)} = \frac{1}{N} \overline{\left(\sum_{n=1}^N \exp(jkx_n u) \right)} \quad (3.14)$$

where the over bar represents the average value.

Since all the random variables x_n are from the same population, each term has the same average value. In addition, the average value of the sum is equal to the sum of the average values. This reduces the pattern factor to

$$\overline{f(u)} = \overline{\exp(jkx_n u)} \frac{1}{N} \sum_{n=1}^N 1 = \overline{\exp(jkx_n u)} \quad (3.15)$$

An important statistical attribute to notice with Equation (3.15) is that it is the characteristic equation for the random value x , which in turn is the average value of $\exp(jkx_n u)$. The characteristic equation is also equal to

$$\overline{\exp(jkx_n u)} = \int w_1(x) \exp(jkx_n u) dx \quad (3.16)$$

This is similar to the desired array pattern factor of

$$f_d(u) = \int i_0(x) \exp(jkx_n u) dx \quad (3.17)$$

If $f_0(u)$ is the normalized pattern factor then $i_0(x)$ is normalized, and by setting the weighting function to the normalized current excitation

$$w_1(x) = i_0(x) \quad (3.18)$$

then the following equivalency can be made

$$\overline{f(u)} = f_0(u) \quad (3.19)$$

This is an important relationship since it states that the ensemble average of the complex random array can be matched to any radiation pattern with a real current density. This is accomplished by selecting the pdf of element locations according to Equation (3.18).

3.4 Statistical Approaches

The statistical approach is another type of random array thinning. It originated from analysis on periodic arrays with random element failure, and phase or amplitude errors. It essentially looks at the results of randomization on periodic structures.

3.4.1. Statistical Density Taper

The starting point is a periodic grid with an interelement spacing of two wavelengths. The randomization comes into play through a random process controlling each element's excitation. The normalized tapered current $i_N(x_n, y_n)$, that would excite the n th element, is compared to a randomly generated number from a uniform distribution. If the random number is less than I_N , the element is turned on with a current amplitude of one. If it is greater, than the element is off or not present in the array. Looking at Figure 3.3, if $p(n)=.25$ for the n th element, that means there is only a 25% chance that the element is "on". There are more numbers (between 0 and 1) greater than 0.25, than there are less than 0.25. Therefore, by setting the "on" state dependent upon the random number being less than $p(n)$, results in the appropriate probability that the element is "on".

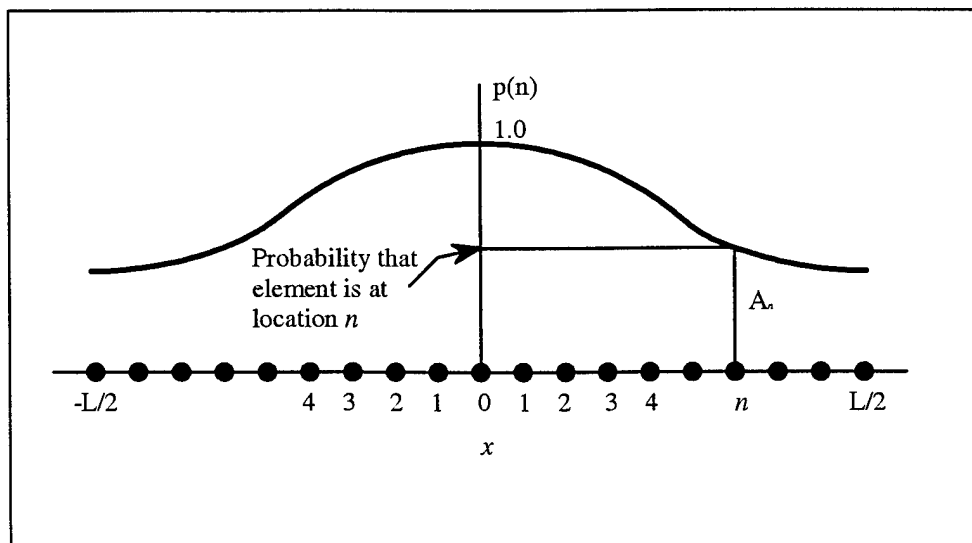


Figure 3.3 The PDF For Both The Random And Statistical Array Approaches.

If there is an N element filled array, the array factor is

$$f(\theta, \phi) = \sum_{n=1}^N F_n \exp(j\Psi_n) \quad (3.20)$$

where

F_n = element on/off factor, either 0 or 1

Ψ_n = phase on the n th element.

In this array, F_n is selected randomly to be either one or zero. It is chosen randomly from element to element so that its ensemble average is

$$\overline{F_n} = k \cdot A_n \quad (3.21)$$

where

k = the degree of thinning

A_n = the amplitude of the current excitation on a filled array whose pattern factor,

f_0 , is being modeled.

When $k=1$, an array is naturally thinned. Depending on array geometry, natural thinning reduces the number of elements to 40 to 60 percent of the element count of the original array.

The desired or modeled pattern factor is

$$f_0(\theta, \phi) = \sum_{n=1}^N A_n \exp(j\Psi_n) \quad (3.22)$$

Since F_n is random process, so is the pattern factor f . If the number of elements, N , is large, the central limit theorem states that the distribution for $f(\theta, \phi)$, for a given θ and ϕ , will be approximately Gaussian (Collin, 1969:221). Furthermore, due to independence of the random variable x , the mean value of the sum is the sum of the means. Just as in the previous section, the average pattern factor is identical to that of the amplitude tapered array. Therefore combining Equation (3.21) with Equation (3.23), for $k=1$, the ensemble average of the reduced element array is equivalent to the modeled array f_0 .

$$\begin{aligned} \overline{f(\theta, \phi)} &= \sum_{n=1}^N \overline{F_n} \cdot \exp(j \cdot \Psi_n) = \\ &= \sum_{n=1}^N A_n \cdot \exp(j \cdot \Psi_n) = f_0(\theta, \phi) \end{aligned} \quad (3.23)$$

Squaring the ensemble average in Equation (3.21), results in the power pattern

$$\begin{aligned} \overline{|f(\theta, \phi)|^2} &= \overline{f(\theta, \phi) \cdot f(\theta, \phi)^*} = \\ &= \sum_n \sum_m \overline{F_n F_m \exp(j(\Psi_n - \Psi_m))} \end{aligned} \quad (3.24)$$

The mean of a product of independent random variables is equal to the product of those means. Since F_n and F_m are independent, when $n \neq m$, the average becomes

$$\overline{|f(\theta, \phi)|^2}_{m \neq n} = \sum_n \sum_m \overline{F_n F_m \exp(j(\Psi_n - \Psi_m))} + \sum_n \overline{F_n^2} \quad (3.25)$$

The values for F_n and F_m are either zero or one, therefore the second summation in Equation (3.25) becomes

$$\overline{\sum_n F_n^2} = \sum_n \overline{F_n^2} = \sum_n A_n^2 \quad (3.26)$$

Applying the theorem for the sum of the averages to the first sum in Equation (3.25) results in

$$\sum_n \sum_{\substack{m \\ n \neq m}} A_n A_m \exp(\Psi_n - \Psi_m) \quad (3.27)$$

In order to make Equation (3.27) equivalent to the square of the modeled pattern factor in Equation (3.22), the $n=m$ components need to be added. Adding and subtracting the $n=m$ components gives

$$\overline{|f(\theta, \phi)|^2} = \left| f_0(\theta, \phi) \right|^2 + \sum_n A_n (1 - A_n) \quad (3.28)$$

Looking at the two terms above, we see that the first term is the power pattern for the amplitude-tapered array. The second term is only dependent on the number of elements and the amplitude tapered array's illumination current and not on θ and ϕ . This implies that the average radiation pattern is predictable based on the illumination currents of the tapered array. An important note about Equation (3.28) is that the second term dominates the pattern outside the neighborhood of the main beam and defines the average sidelobe level of the statistical sidelobes (Collin, 1969:223).

3.4.2. Random Array

The following development is from Steinberg's peak sidelobe theory for random arrays (Steinberg, 1976). Steinberg provides a method to control the statistical sidelobe levels. While theoretically complex, it is simple to implement mathematically. First, a revisit of the average power pattern, with a slightly different approach, is necessary.

The power pattern is the product of the pattern factor and its conjugate. The normalized ensemble average of the power pattern is

$$\overline{|f(u)|^2} = \overline{f \cdot f^*} = \frac{1}{N^2} \cdot \sum_{n=1}^N \sum_{m=1}^N \overline{\exp(jk(x_n - x_m)u)} \quad (3.29)$$

Through the following reduction

$$\overline{|f(u)|^2} = \frac{1}{N^2} \cdot \sum_n^N \sum_m^M \overline{\exp(jk(x_n - x_m)u)} \quad (3.30)$$

$$\overline{|f(u)|^2} = \frac{1}{N^2} (N + \overline{\exp(jkxu)\exp(-jkxu)}(N^2 - N)) \quad (3.31)$$

$$\overline{|f(u)|^2} = \frac{1}{N^2} (N + f_o(u)f_o^*(u)(N^2 - N)) \quad (3.32)$$

the average pattern becomes

$$\overline{|f(u)|^2} = |f_o(u)|^2 \cdot (1 - \frac{1}{N}) + \frac{1}{N} \quad (3.33)$$

In other words, Equation (3.33) states that near the mainlobe region of the design pattern (where $|f_o(u)|^2 \approx 1$), the amplitude of the mainlobe and nearby sidelobes are greater than $1/N$, so the patterns are relatively unchanged. In the statistical sidelobe region, the sidelobe values of the design pattern fall below the $1/N$ average sidelobe power of the random component and disappear leaving the region controlled by the random component (Steinberg, 1976:144).

The next step is to determine the peak statistical sidelobe levels using the peak sidelobe estimator B . The peak sidelobe indicator predicts, to a certain confidence level, β , that n number of samples of the pattern factor will not exceed some desired threshold level, A_0 . The probability that any sample out of the n samples of the sidelobe pattern, at some angle u , falls between A_0 and some δ above A_0 is

$$\Pr(A_0 \leq A \leq A_0 + \delta A) = \int_{A_0}^{A_0 + \delta A} w_1(A) dA . \quad (3.34)$$

Letting δ go to infinity gives the integral

$$\alpha = \int_{A_0}^{\infty} w_1(A) dA = \exp \left[\frac{-(A_0)^2}{N} \right] . \quad (3.35)$$

If n independent samples of the sidelobe pattern are taken, the probability that none of those samples exceeds the threshold level A_0 is

$$\beta = (1 - \alpha)^n = \left[1 - \exp \left[\frac{-(A_0)^2}{N} \right] \right]^n . \quad (3.36)$$

The quantity $(A_0)^2/N$ is the power ratio B . The parameter B , which is also the peak sidelobe estimator, is the ratio between the normalized threshold level and the theoretical average sidelobe level $(1/N)$. To normalize the threshold level, it is divided by the peak power of the mainlobe, which is N^2 . Substituting B into Equation (3.36) and solving for B gives

$$B = -\ln(1 - \beta^{1/n}) . \quad (3.37)$$

Finally, the number of samples that needs to be taken for a desired B , must be determined. The value of n brings in all the relevant array properties (length, frequency, and scan angle) with the exception of the number of elements, N . The number of samples to be taken is chosen by using the Nyquist sampling theorem. This theorem states that for a band limited wave, with a maximum bandwidth of W , can be determined uniquely by values sampled at uniform intervals of T_s seconds, where $T_s=2W$ (Sklar, 1988:58). The minimum sampling rate is two times the length of the array divided by the wavelength (Steinberg, 1976:154). This results in the number of samples being equal to the number of $2*L/\lambda$ intervals there are in the visible region. Since the visible region changes when scanning occurs, the number of intervals will change. At endfire, there are two lengths in the visible region, but at other angles, this is not the case and therefore fewer samples are required. This leads to

$$n = \frac{2L}{\lambda} (1 + |u_0|) = \frac{2L}{\lambda} (1 + |\sin(\theta_0)|) \quad (3.38)$$

samples to specify the complex radiation pattern. However, since the pattern is symmetrical, only half the number of samples is needed (Steinberg, 1976:154).

Therefore, n becomes

$$n = \frac{L}{\lambda} (1 + |\sin(\theta_0)|) . \quad (3.39)$$

Taking Equations (3.37) and (3.39), and solving for N , results in the number of elements required for a specified threshold, A_0 , for an L length array, with a maximum desired scan angle of θ_0 . i.e.,

$$N = \frac{A_0^2}{B} = \frac{A_0^2}{-\ln(1 - \beta \left[\frac{\lambda}{L(1 + |\sin(\theta_0)|)} \right])} . \quad (3.40)$$

However there is one problem with Equation (3.40). The estimator B is biased. Look at Figure 3.4, which is a sample of a section of sidelobes from a power pattern. The highest peak is B_p . The process up to this point gives a peak-sampled maximum of B . The location of B is a distance ΔU away from the true peak B_p . Since ΔU is always greater than zero, then B is always less than B_p making B a downward biased estimator.

To account for this, an average for ΔB is needed in order to add to B and remove the bias (Steinberg, 1976:161). This average is found by choosing a sample point close to the peak B_p and then approximating the power pattern around that point using Taylor's expansion. Through differentiation, averages, and further approximations (Steinberg 161-165), the average becomes

$$\Delta B = 1 + \frac{2}{B} . \quad (3.41)$$

Adding ΔB to B gives the new peak sidelobe estimator B_p

$$B_p = B + 1 + \frac{2}{B} . \quad (3.42)$$

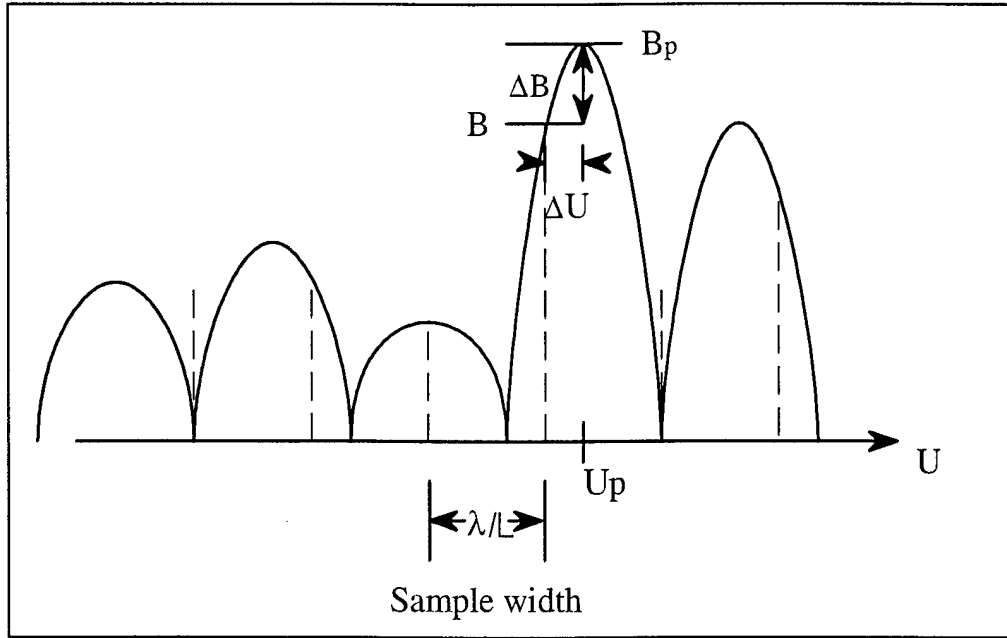


Figure 3.4 Peak Sidelobe Estimator

The estimator B_p is the ratio of the unnormalized peak sidelobe to the average sidelobe level N . The value of A_0^2 is the normalized peak sidelobe power, so multiplying it by the power of the mainlobe, N^2 , and substituting into B_p gives

$$B_p = NA_0^2 . \quad (3.43)$$

Finally, solving for N .

$$N = \frac{B_p}{A_0^2} . \quad (3.44)$$

In terms of B , N becomes

$$N = \frac{B + 1 + \frac{2}{B}}{A_0^2} \quad (3.45)$$

This expression is used to generate the number of elements required for the random approach.

3.4.3. Peak Sidelobe Indicator Statistics

Looking at the statistical behavior of B will give some insight on what to expect from B_p , along with expected results. The probability distribution function of B is simply β . The probability density function is simply the derivative of β taken with respect to B .

$$W(B) = \frac{d\beta}{dB} = n(1 - \exp(-B))^{n-1} \exp(-B) \quad (3.46)$$

The first moment is the average of B , and the second moment gives the variance about the average. The characteristic function of B is

$$\Phi_B(S) = -\int_0^{\infty} W(B) \exp(SB) dB = n \int_0^{\infty} (1 - \exp(-B))^{n-1} \exp((S-1)B) dB \quad (3.47)$$

Using the method of cumulants on the characteristic function gives the moments of B through the logarithm of the characteristic function

$$\ln(\Phi_B(S)) = -\sum_{k=1}^{\infty} \ln\left(1 - \frac{S}{k}\right) \quad (3.48)$$

Using the power series expansion of the logarithm and solving for semiinvariants yields

$$\lambda_r = (r-1)! \sum_{k=1}^n k^{-r} \quad (3.49)$$

Therefore, for $r=1$, the first moment of B , or its mean, is

$$\mu = \lambda_1 = \sum_{k=1}^n \frac{1}{k} \quad (3.50)$$

where n is still the array parameter.

The variance of B is

$$\sigma^2 = \lambda_2 = \sum_{k=1}^n \frac{1}{k^2} \quad (3.51)$$

An important fact about the variance is that as the array size gets larger the variance goes to

$$\sigma^2 = \lambda_2 = \sum_{k=1}^n \frac{1}{k^2} \Rightarrow \frac{\pi^2}{6} \text{ as } n \rightarrow \infty . \quad (3.52)$$

Which is independent of the array size.

Before going into the next chapter, let's review the important points developed thus far. For the average quantities of the random arrays:

1. The ensemble average array factor is equivalent to the desired array pattern factor.
2. Randomization does not significantly affect the mainlobe and nearby sidelobes.
3. Randomization does dominate the sidelobe structure outside the mainlobe region.

The peak sidelobe theory provides a method to estimate the probability β , that the statistical or random sidelobes do not exceed a sidelobe threshold level A_0 , for some maximum steering angle θ_0 . As the size of the array increases the variance of the peak sidelobe indicator B_p , remains constant

4 Application

This chapter goes into detail on the implementation of the concepts of each approach covered in Chapter 3. It starts with the pattern factor for a symmetric planar array, and then summarizes the mathematics for the array parameters of interest. The theory applicable to the linear array is also applicable to the planar array. The conversion of the pattern factor from a linear planar array is simple. The current excitation and phase progression simply contains a y component to account for the added array dimension.

4.1 Planar Array Pattern Factor

The pattern factor for a planar array is

$$f(\theta, \phi) = \sum_{n=1}^N \sum_{m=1}^M I_{mn} \exp(j\beta \Psi_{mn}(\theta, \phi)) \quad . \quad (4.1)$$

Except for the non-uniformly excited uniform array, the current amplitude, I_{mn} , is equal to one. The uniform array has a tapered current of

$$I_{mn} = \frac{1}{4} \left(1 - \cos\left(\pi + \frac{2x_m\pi}{W}\right) \right) \left(1 - \cos\left(\pi + \frac{2y_n\pi}{L}\right) \right) \quad . \quad (4.2)$$

The phase $\Psi_{mn}(\theta, \phi)$ is equal to

$$\Psi_{mn}(\theta, \phi) = x_m (\sin \theta \cos \phi - \sin \theta_0 \cos \phi_0) + y_n (\sin \theta \sin \phi - \sin \theta_0 \sin \phi_0) \quad (4.3)$$

where θ_0 and ϕ_0 are the beam steering angles.

Combining the three equations above, the pattern factor is dependent on θ , ϕ , θ_0 , ϕ_0 , x , and y . These variables have ranges of $0 \leq \theta \leq \pi/2$, $0 \leq \phi \leq \pi$, $-W/2 \leq x \leq W/2$ and $-L/2 \leq y \leq L/2$, respectively. Computing the pattern factor over these ranges takes up a lot of computation time. The total number of iterations or loops required is equal to the number of elements in the array times the number of sample points in ϕ times the number of sample points in θ . That gives the number of iterations for one run for one approach with no scan or frequency analysis performed. For the simulations in this thesis, there are three scan angle runs (one boresight and then $\theta_0=50^\circ$ in the xz and the yz principle planes), times the eleven frequency intervals. For a four square meter array with one degree angular sampling, the total number of iterations for the uniform array at 12 GHz would be

$$(180 \text{ deg of } \phi)(90 \text{ deg of } \theta)(11 \text{ frequencies})(3 \text{ scan angles}) * \\ (160 * 160 \text{ elements}) = 1.3685760e+10 \text{ iterations.}$$

For sixteen square meter array, the number of elements is 4 times that of the four square meter array. For proper sampling of a pattern, there needs to be $16*\pi$ times the area of the array in wavelengths. That is $16\pi A/\lambda^2$ samples of the full pattern. Due to angular symmetry, only a fourth of the sampling needs to be done. Recalculating the above four square meter array example results in

$$(16*\pi*4/\lambda^2)(11)(3)(160*160)/4 = 6.794284e+10 \text{ iterations.}$$

As can be seen, the computational time required becomes enormous as the array sizes increase. In order to reduce this time, the array is assumed to be symmetric. Each quadrant is a mirror image of the two quadrants it borders. With symmetry, the pattern

factor can be reduced to computations in only one quadrant. Take a simple example of four elements symmetrically located in each quadrant of the x-y plane as seen in Figure 4.1.

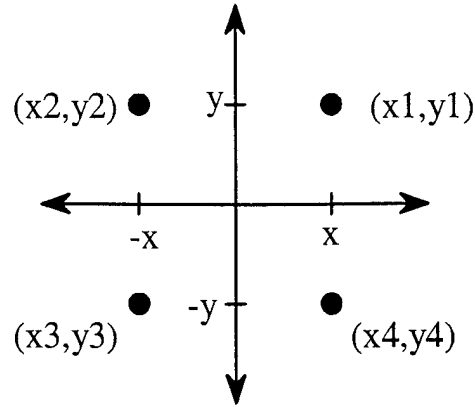


Figure 4.1 Example Symmetric 4 Element Array

For the array above, the pattern factor is

$$f(\theta, \phi) = \sum_{m=1}^M \sum_{n=1}^N I_{mn} \exp \left[j\beta(x_m(\sin \theta \cos \phi - \sin \theta_0 \cos \phi_0) + y_n(\sin \theta \sin \phi - \sin \theta_0 \sin \phi_0)) \right] \quad (4.4)$$

For notation simplicity, let the steering angles be zero, then the pattern factor for the above array would be

$$\begin{aligned} f(\theta, \phi) = & i_1 \exp[j\beta(x_1 \sin \theta \cos \phi + y_1 \sin \theta \sin \phi)] \\ & + i_2 \exp[j\beta(x_2 \sin \theta \cos \phi + y_2 \sin \theta \sin \phi)] \\ & + i_3 \exp[j\beta(x_3 \sin \theta \cos \phi + y_3 \sin \theta \sin \phi)] \\ & + i_4 \exp[j\beta(x_4 \sin \theta \cos \phi + y_4 \sin \theta \sin \phi)] \end{aligned} \quad (4.5)$$

Since the current is symmetric also, then the current on each is also equal.

Furthermore, the physical locations are related by $x_1 = x_4 = -x_3 = -x_2$ and $y_1 = y_2 = -y_3 = -y_4$.

Substituting a corresponding value of $x=x_1$ and $y=y_1$ into Equation (4.5) results in

$$\begin{aligned} f(\theta, \phi) = & i \exp[j\beta(x \sin \theta \cos \phi + y \sin \theta \sin \phi)] \\ & + i \exp[j\beta(-x \sin \theta \cos \phi + y \sin \theta \sin \phi)] \\ & + i \exp[j\beta(-x \sin \theta \cos \phi - y \sin \theta \sin \phi)] \\ & + i \exp[j\beta(x \sin \theta \cos \phi - y \sin \theta \sin \phi)] \end{aligned} \quad (4.6)$$

Using the trigonometric substitution of

$$\exp(\pm j\beta) = \cos(\beta) \pm j \sin(\beta) \quad (4.7)$$

in Equation (4.6) and applying further trigonometric substitutions, the final pattern factor is

$$f(\theta, \phi) = 4 \cos(x\beta \sin \theta \cos \phi) \cos(y\beta \sin \theta \sin \phi) \quad (4.8)$$

This means that each set of four symmetric elements can be reduced to Equation (4.8). Those elements lying on the axis are in pairs so their combined pattern factor is half of that found in Equation (4.8). Therefore, the total pattern factor for a symmetric planar array is

$$\begin{aligned} f(\theta, \phi) = & 1 + 2 \sum_{n=1, x \neq 0}^{N_x} \cos(x\beta(\sin \theta \cos \phi - \alpha_x)) \\ & + 2 \sum_{n=1, y \neq 0}^{N_y} \cos(y\beta(\sin \theta \sin \phi - \alpha_y)) \\ & + 4 \sum_{n=1, x \neq 0, y \neq 0} (\cos(x\beta(\sin \theta \cos \phi - \alpha_x)) * \cos(y\beta(\sin \theta \sin \phi - \alpha_y))) \end{aligned} \quad (4.9)$$

where

N_q = the number of elements in the first quadrant

α = the beam steering phase progression for the corresponding x or y.

This reduced form of the pattern factor only requires the first quadrant to be processed, reducing the computational time by approximately seventy-five percent.

4.2 Parameter Values

The values used for each approach are shown next. A summary of the parameters for each approach is given at the end of this section.

4.2.1. *Uniform and Baseline Arrays*

For the uniform equispaced array, the parameters for the array are constant. The interelement spacing is .0125 meters for a max operating frequency at 12 GHz. The maximum operating frequency is used to determine interelement spacing since at that spacing the lower frequencies will have more sampling elements. The maximum number of elements is equal to each dimension of the array divided by the wavelength. The product of these two becomes the total number of elements needed to fill the array.

The current distribution on uniform array is tapered. It is a raised cosine function. As previously mentioned, the tapering reduces sidelobe levels. The current $I(x,y)$ was given earlier in Equation (4.2) for the equispaced array. The aperiodic arrays will have a uniform current distribution.

The baseline array is used for comparison purposes and has the same structure as the uniform array above but has a uniform current excitation. Element and beamwidth are given in Table 4.1.

Table 4.1 Uniform And Baseline Element Counts And First Null Beamwidth (FNBW)

Array Area (m ²)	Number of Elements	FNBW (rad)	FNBW (deg)
4	25600	0.01250	0.71656
8	51200	0.00884	0.50668
12	76800	0.00722	0.41371
16	102400	0.00625	0.35828
32	204800	0.00442	0.25334
100	640000	0.00250	0.14331

4.2.2. *Deterministic Array*

Element positions are determined by equal area integrals of the tapered current density distribution applied to the uniform array. It is also desirable to have a minimum interelement spacing of two wavelengths to avoid mutual coupling. For the deterministic approach, elements will be closest in the center of the array due to the larger percentage of the volume under the current curve there. Therefore, taking in consideration the two wavelength lower limit, the current is integrated from zero to two wavelengths to get the equal area value for determining the remaining element locations.

Table 4.2 Deterministic Array Element Counts

Array Area (m ²)	Number of Elements
4	441
8	961
12	1369
16	1681

4.2.3. Statistical Array

The statistical approach implementation is rather straightforward. A periodic grid is created with an interelement separation of two wavelengths. Then the value of the current at that x-y location in Equation (4.2) is calculated. A random number from zero to one is compared to the current value. If the random number is less than the current value, then the element is on by giving it a current value of one. This results in the element probability distribution being the same equation as the current function of the uniform array. Table 4.3 provides the maximum expected element counts for the statistical array if all elements are in the “on” status.

Table 4.3 Maximum Element Count For Statistical Array

Array Area (m ²)	Max Number of Elements
4	1600
8	3200
12	4800
16	6400

4.2.4. Random Array

For the random approach, there are several items of interest. First, a desired peak sidelobe level A_0 , is selected, followed by the confidence level β , that the sidelobes will not exceed that level. Then the number of elements N , is determined.

First, an upper limit has to be determined for the number of elements. This sets the minimum attainable confidence level and peak sidelobe levels. In order to be feasible, the number of elements in the random array needs to be less than the number in the filled array. By setting N to the number of elements in the equispaced array

$$N = \frac{LW}{\lambda^2} \quad (4.10)$$

and placing Equation (4.10) into Equation (3.40), the lower limit of A_0^2 is

$$A_0^2 = \frac{LW}{\lambda^2} \left(-\ln(1 - \beta^{\frac{\lambda}{L(1 + |\sin(\theta_0)|)}) \right) \quad (4.11)$$

Figure 4.2 contains plots of Equation (4.11) for array sizes of 4, 8, 12, 16, and 100 square meters versus the confidence levels. The peak sidelobe level threshold is -13.5 dB. This threshold value was chosen since it is the minimum peak sidelobe value for a uniform line source. Table 4.4 contains is a break down of the calculated values for N , n , B , β , B_p , and A_0^2 for the array sizes of interest and larger sized arrays. The larger arrays are included to demonstrate that the behavior of the element counts with respect to array size for random arrays.

Table 4.4 Random Array Parameters

Array Area (m ²)	Confidence Level β	PSL (dB) A_0^2	B	Bp	PSL Samples n	Linear Array N	Planar Array N
4	0.65	-13.5	4.92	6.33	59.01	141	20080
8	0.65	-13.5	5.27	6.65	83.45	148	22154
12	0.65	-13.5	5.47	6.84	102.20	153	23426
16	0.65	-13.5	5.61	6.97	118.02	156	24355
32	0.65	-13.5	5.96	7.30	166.90	163	26681
100	0.65	-13.5	6.53	7.84	295.05	175	30776

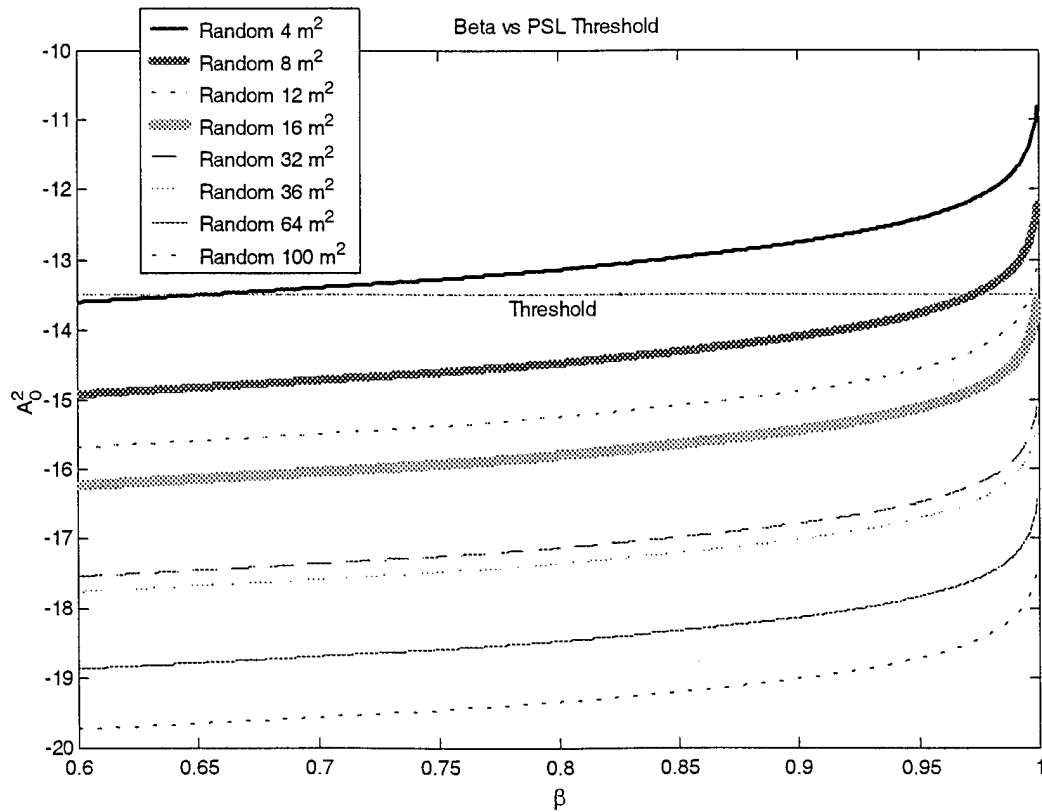


Figure 4.2 Peak Sidelobe Level Vs Confidence Level For Various Array Sizes

The value for β is set at 65% since it is the maximum confidence level possible for 4-m² array (see Figure 4.2). This is because for the given frequency, the element count for a higher confidence level would exceed the number of elements required for the half wavelength equal spaced array. To keep all arrays on a level field, the confidence level remained at 65% for the larger arrays as well. Table 4.5 shows some of the expected parameters for higher β values for various array sizes.

Table 4.5 Random Array Parameters For Higher β

Array Area (m ²)	Confidence Level β	PSL (dB) A_0^2	B	Bp	PSL Sample $s n$	Planar Array N	Elements in Uniform Array
8	0.95	-13.5	7.39	8.67	83.453	37632	51200
12	0.998	-13.5	10.84	12.03	102.21	72473	76800
16	0.999	-13.5	11.68	12.85	118.02	82749	102400
32	0.999	-13.5	12.02	13.19	166.91	87207	204800
100	0.999	-13.5	12.59	13.75	295.05	94799	640000

4.3 Comparison Analysis Methodology

4.3.1. Requirements

The performance requirements for the arrays are in the areas of beamwidth, beam scanning, frequency range, and element reduction. For comparison and analysis, all thinning approaches referenced the performance of a baseline (uniform amplitude, equally spaced) array of equal size. Metrics are used to compare the different thinning

approaches and determine the overall optimal array performance. The next section discusses these metrics.

4.3.2. *Metric*

The metric is broken down into four areas. These areas are boresight, xz plane, yz plane, and element count. The first three areas are the three different mainbeam directions. The directions include each array's performance over the frequency band (2-12 GHz). Under each of these position categories, are subcategories for half power beamwidth (HPBW) and peak sidelobe level (PSL). Table 4.6 provides a breakdown of the metric along with the weightings that are used in the analysis in Chapter 5. The HPBW is found by simply finding the half power point for each array for both the xz and yz planes. Linear interpolation is applied if the half power point lies between two sample points. The HPBW is then determined by taking the square root of the product of the beamwidth in each plane giving the beamwidth, bw_A , for that approach. The same method determines the beamwidth, bw_B , for the baseline array.

The final value used in the metric is

$$HPBW = 1 - \left(\frac{bw_B - bw_A}{bw_B + bw_A} \right) . \quad (4.12)$$

The PSL value is calculated by determining the number of angular samples greater than the threshold level of -13.5 dB and comparing that to the number of samples in the baseline array that exceeds the same threshold. The metric value is determined by the following

$$PSL = 1 - \left(\frac{psl_B - psl_A}{psl_B + psl_A} \right) \quad (4.13)$$

where

psl_B = baseline PSL value

psl_A = thinning approach PSL value.

Table 4.6 Breakdown Of Array Performance Metric

Boresight (20%)	Half Power Beamwidth (50%)
	Peak Sidelobe Levels (50%)
XZ Plane (20%)	Half Power Beamwidth (50%)
	Peak Sidelobe Levels (50%)
YZ Plane (20%)	Half Power Beamwidth (50%)
	Peak Sidelobe Levels (50%)
Number of Elements (40%)	

The metric for the element count is found by subtracting from one, the ratio of the number of elements in the aperiodic array to that in the baseline array.

Now that a metric (one of many possible metrics) has been defined, the next step is to apply that metric to each array to determine the optimal thinning approach.

5 Results and Analysis

This chapter discusses the outcome of applying the covered theories, thinning approaches, and metrics. A brief process description is given, followed by the results of applying the metric formed in Chapter 4. Then the metric values are changed to emphasize HPBW, PSL, and boresight performance rather than element count. Next trend analysis plots for all the arrays are shown. Finally, the chapter concludes with an overall analysis section.

5.1 Process

The overall process from pattern factor generation to data analysis and results is shown in Figure 5.1. Appendix A contains flowcharts for the first two sections of the computational process. These two sections are C++ programs. The first program generated all the pattern factor data for the given parameters of length, width, frequency range, number of sampling points for θ and ϕ , start and stop values for θ , desired confidence level, and PSL threshold. The second program was a data compilation program that sorted and compiled the data from multiple runs for analysis in MATLAB[®].

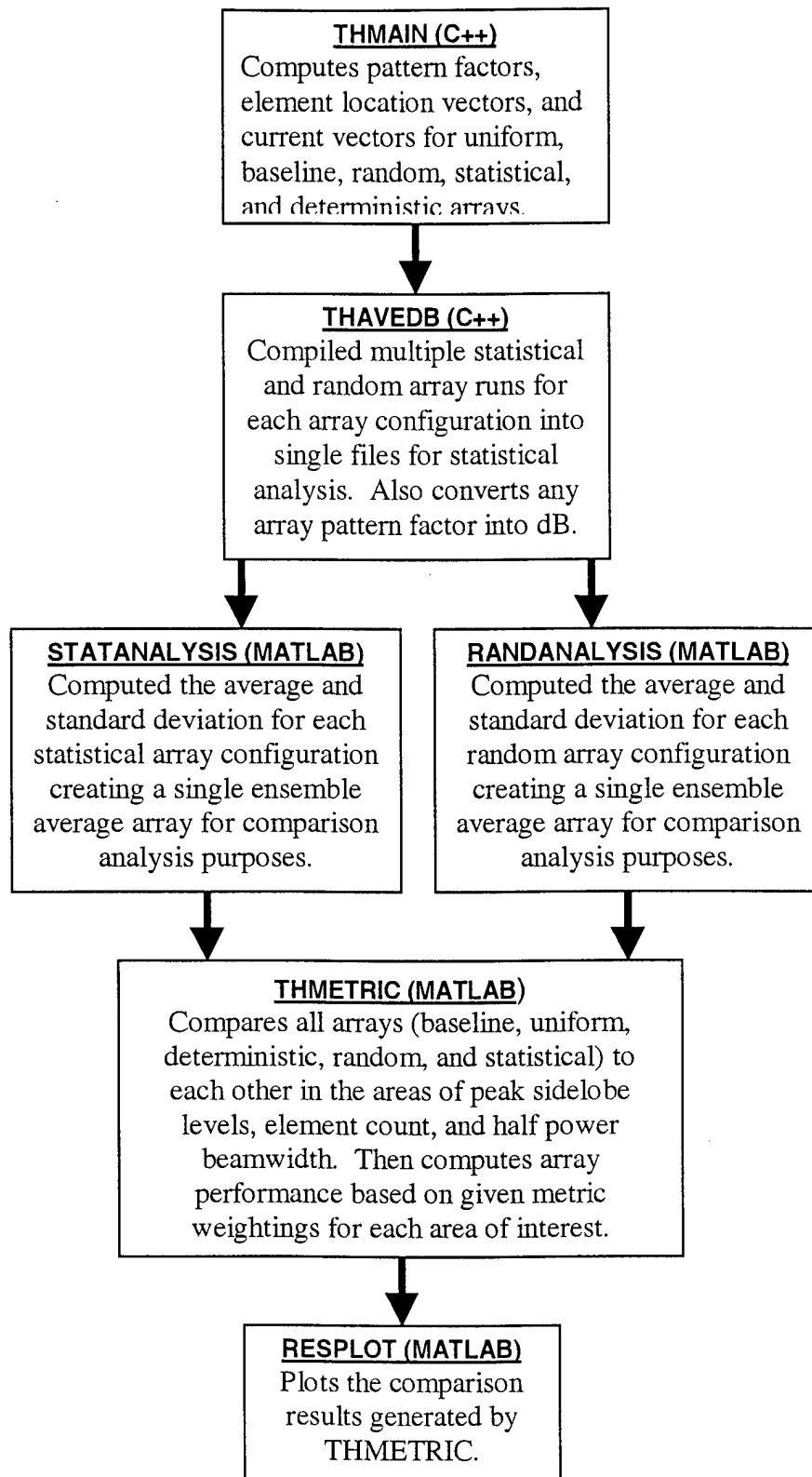


Figure 5.1 Process Of Data Generation And Analysis

5.2 Results

Due to the size of the arrays and the pattern factor sampling resolution requirements, the computational time was extensive. Along with the computational time, the volume of data generated and processed was overwhelming (15-20 GB). Table 5.1 shows a breakdown of the number of resolution samples required and used for the pattern factor generation.

Table 5.1 Pattern Factor Sampling

Array Area (m ²)	Required Samples for Sphere	Required for region of interest	Samples per degree	Theta samples	Phi Samples	Total # of Samples Used
4	321699	80425	4.96	201	402	80802
8	643398	160850	9.93	284	568	161312
12	965097	241274	14.89	347	694	240818
16	1286796	321699	19.86	401	802	321602
32	2573593	643398	39.72	567	1134	642978
100	8042477	2010619	124.11	1003	2006	2012018

There were multiple runs (each with a different set of element locations) for the pattern factors of the statistical and random arrays to allow for statistical analysis (see for run counts). The runs for the statistical and random arrays are compiled together and the ensemble average of each array configuration was calculated. The ensemble average is the arithmetic average of each θ and ϕ pair from each sample run. For example, look at Table 5.3. The Average row contains the values for each θ and ϕ pair for the ensemble average pattern factor for the array.

Table 5.2 Approach Run Counts

Area (m ²)	4	8	12	16
Statistical	37	14	29	21
Random	42	20	30	20
Random2	9	8	10	4

Table 5.3 Ensemble Average Pattern Factor Example

theta(deg)	0	0	0	0	1	1	1	...	90
phi (deg)	0	1	2	...	0	1	2	...	180
Run 1	1.00	0.25	0.10	0.50	0.00	0.10	0.15	..	1.00
Run 2	1.00	0.50	0.20	0.70	0.09	0.03	0.50	...	0.50
Run 3	1.00	0.25	0.16	0.80	0.11	0.13	0.18	...	0.70
Run 4	1.00	1.00	0.40	0.95	0.10	0.20	0.22	...	0.80
...
Average	1.00	0.50	0.22	0.74	0.08	0.12	0.26	...	0.75

These ensemble average pattern factors for the random or statistical arrays are then used for performance comparison purposes with the baseline, uniform, and deterministic arrays. Comparisons for each frequency and scan angle (for each planar cut) are then calculated.

There is an additional random array pattern in the comparisons. It is labeled “random”. The “random” pdf has twice the period of that in the original random, “random2”. It is included with this analysis to show the effects a second pdf on a random array that contains the same element count.

Additional runs of higher confidence levels (.999) for the 16m² array are included in the metric analysis. Additional single runs of statistical and random approaches applied to larger array sizes (25, 32, 64, and 100 m²). The results of these arrays are located in Appendix C.

5.2.1. Array Performance

The first figure in each series represents the performance of the different thinning approaches for a given array size in the areas of beamwidth and PSL. The boresight performance of an array was determined by the performance of each thinning approach over all frequencies (2-12 GHz) for $\theta_0=\phi_0=0^\circ$, in the areas of PSL and HPBW. The same applies to the performance in the xz and yz mainbeam scan positions with angles of $\theta_0=50^\circ, \phi_0=0^\circ$, and $\theta_0=50^\circ, \phi_0=90^\circ$ respectively. The second set of plots breaks down the overall performance for each array into the three beam positions. Finally, trend analysis plots for all approaches versus array size are provided for metrics emphasizing reduced element count, HPBW, PSL, and boresight (mainbeam at $\theta_0=\phi_0=0^\circ$).

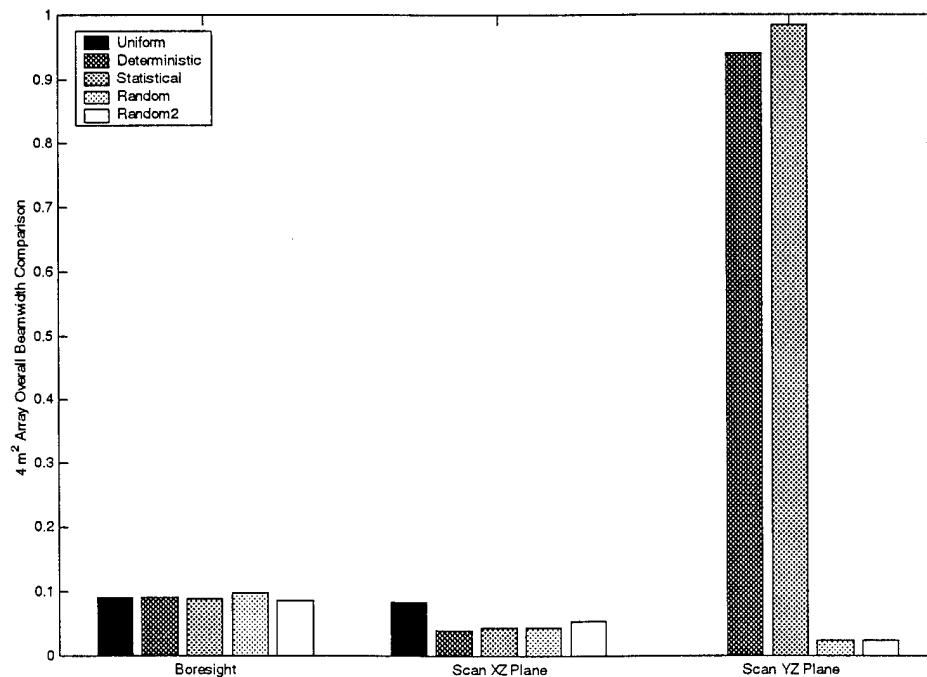


Figure 5.2 HPBW Comparison on 4m² Arrays

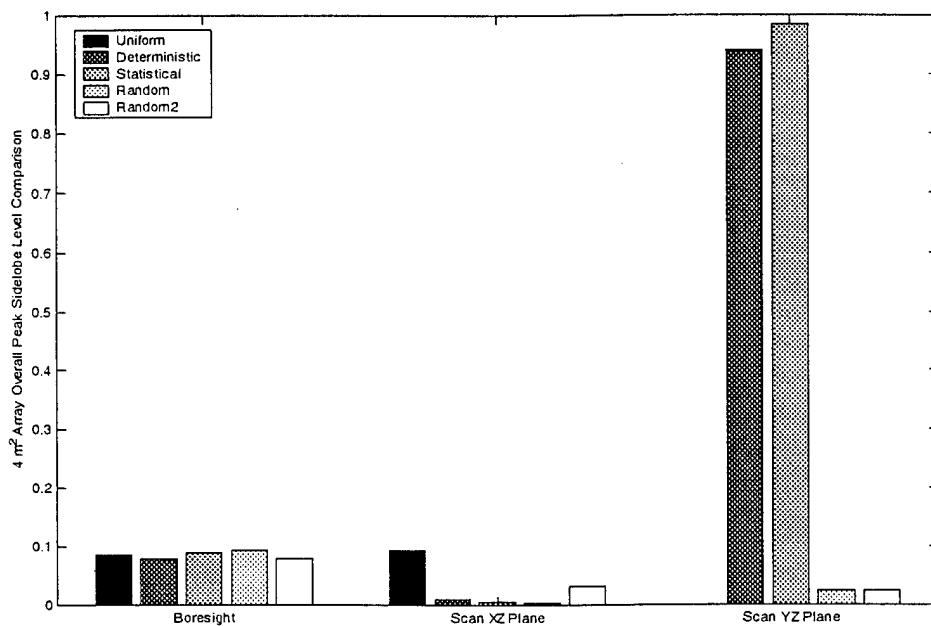


Figure 5.3 PSL Comparison on 4m² Arrays

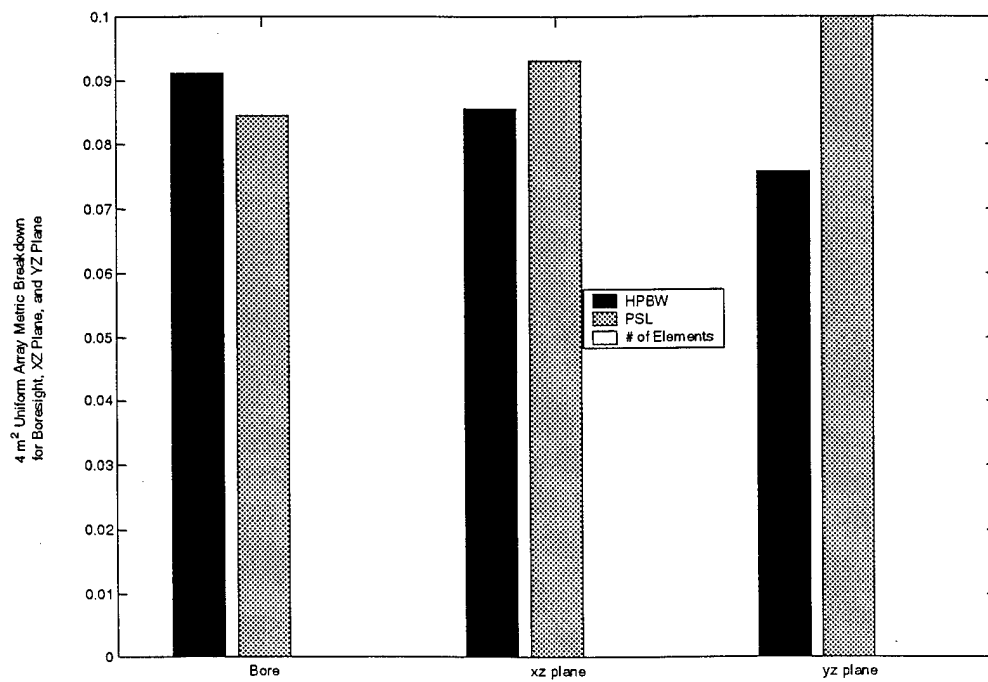


Figure 5.4 Uniform 4m² Array Metric Breakdown

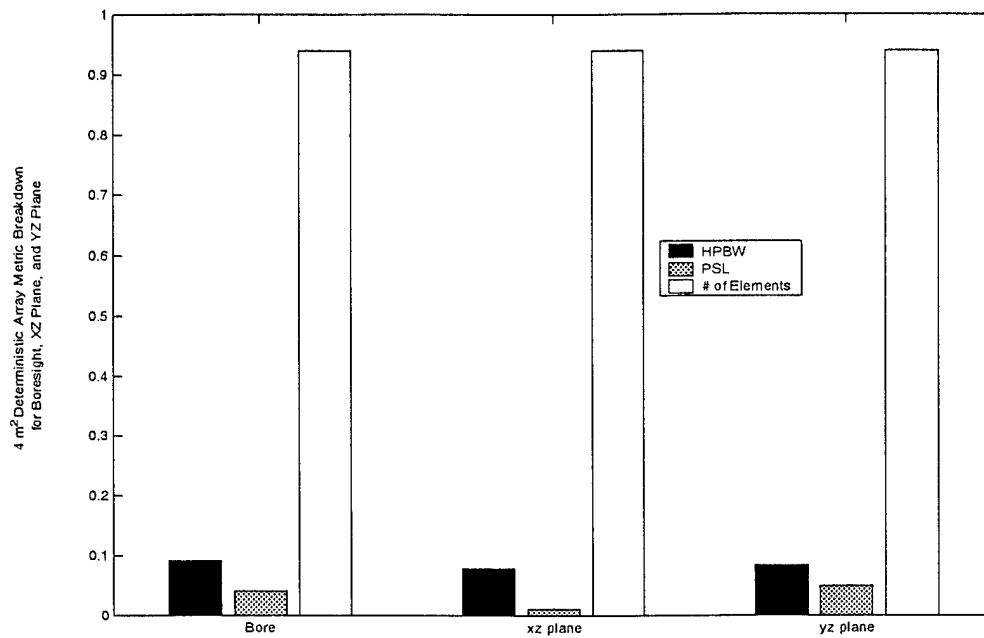


Figure 5.5 Deterministic 4m² Array Metric Breakdown

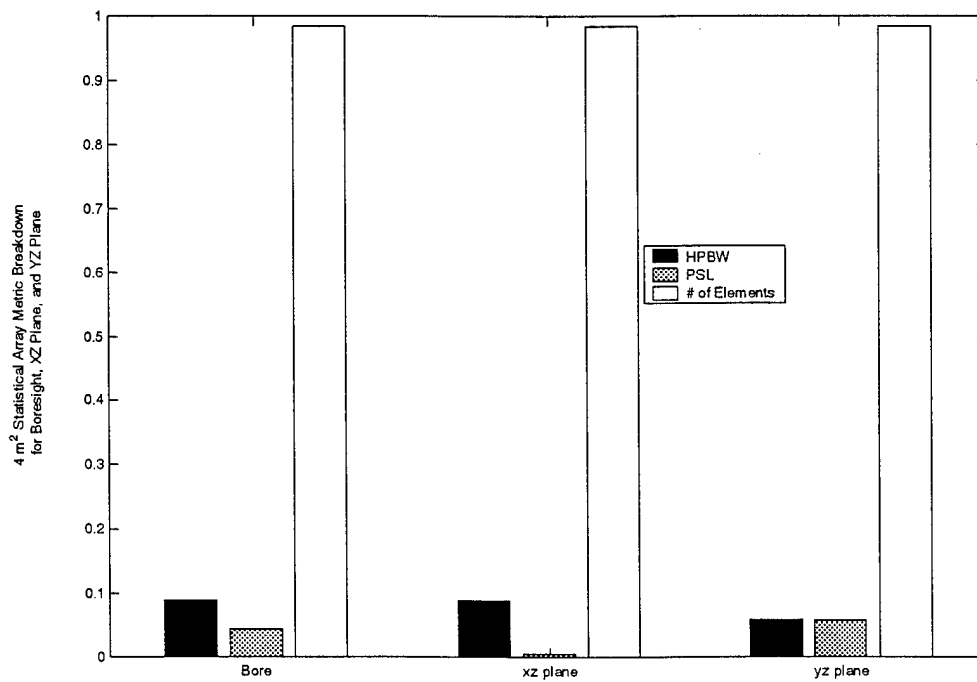


Figure 5.6 Statistic 4m² Array Metric Breakdown

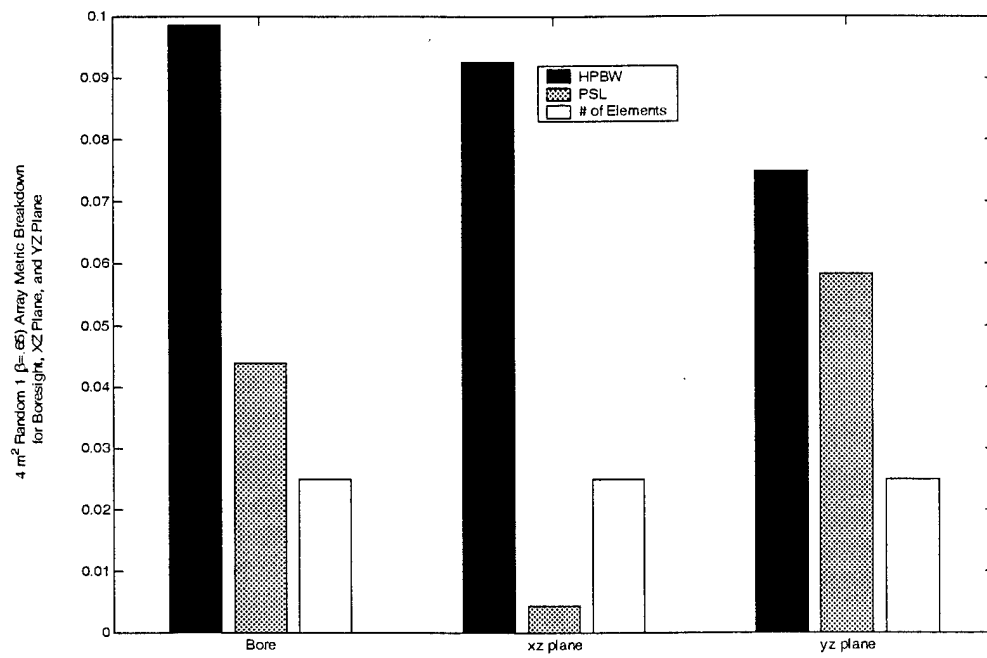


Figure 5.7 Random 4m² Array Metric Breakdown

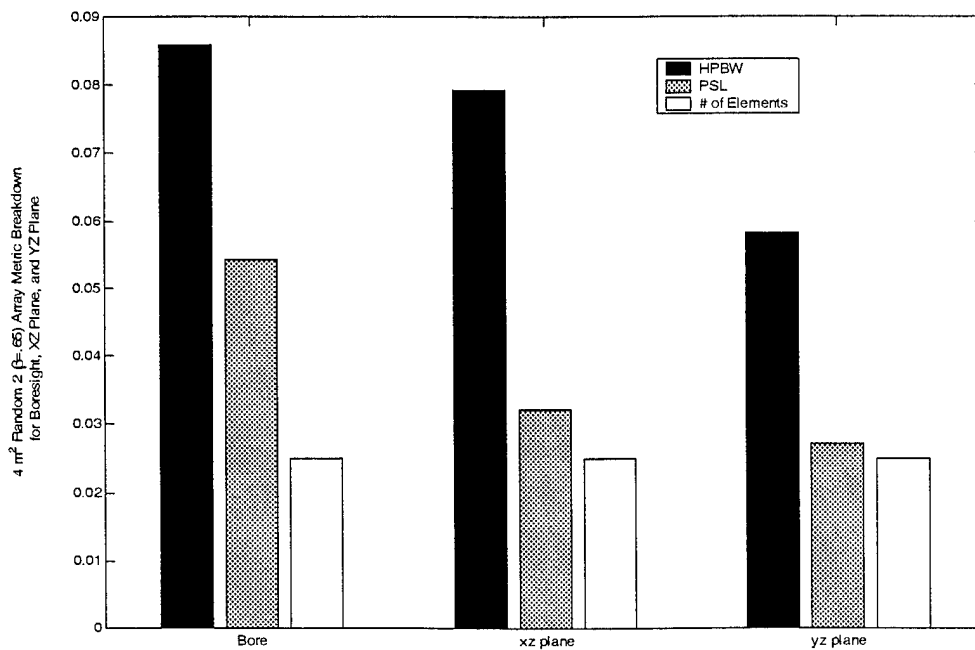


Figure 5.8 Random2 4m² Array Metric Breakdown

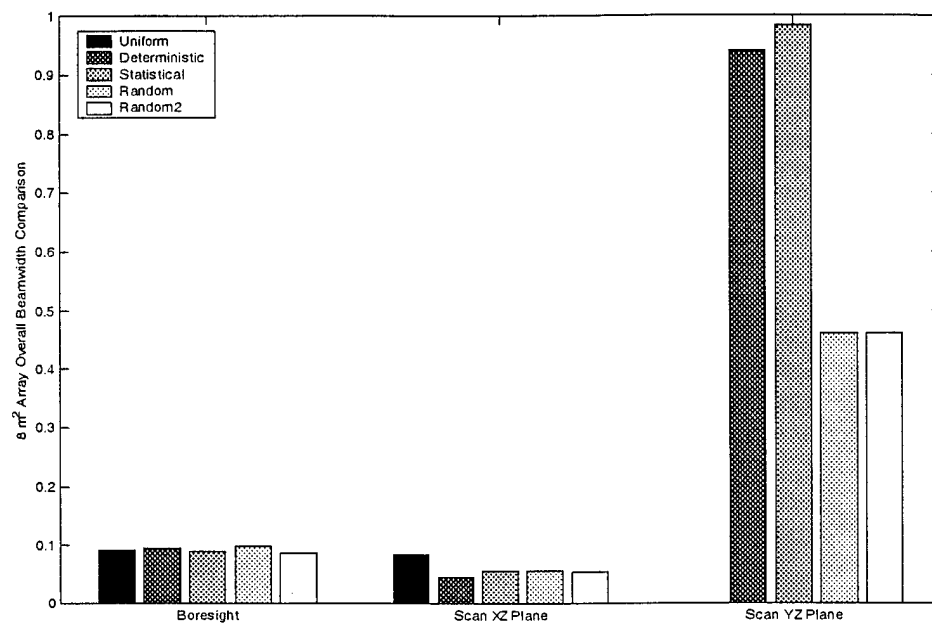


Figure 5.9 HPBW Comparison on 8m² Arrays

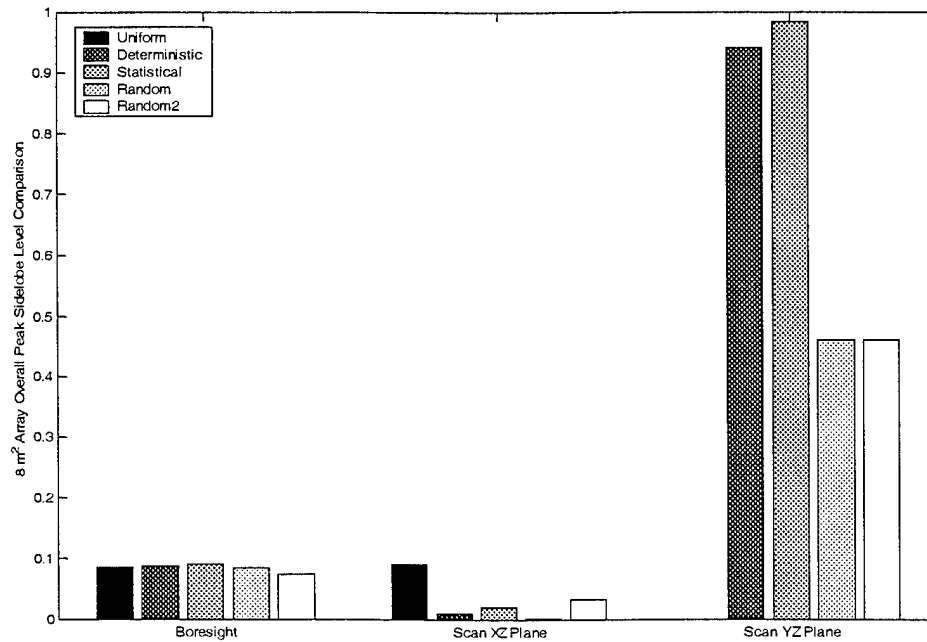


Figure 5.10 PSL Comparison on 8m² Arrays

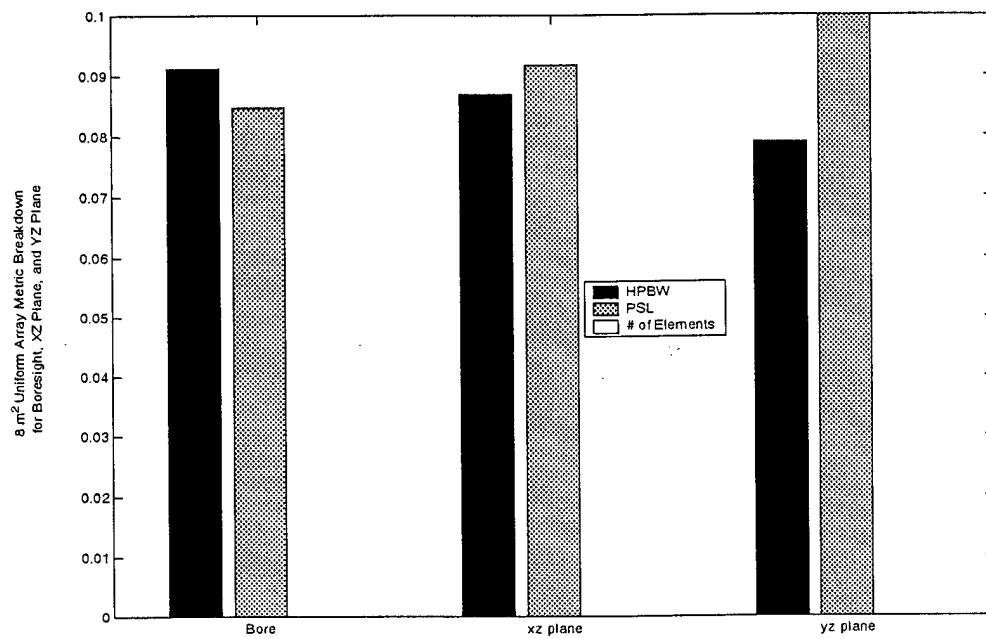


Figure 5.11 Uniform 8m² Array Metric Breakdown

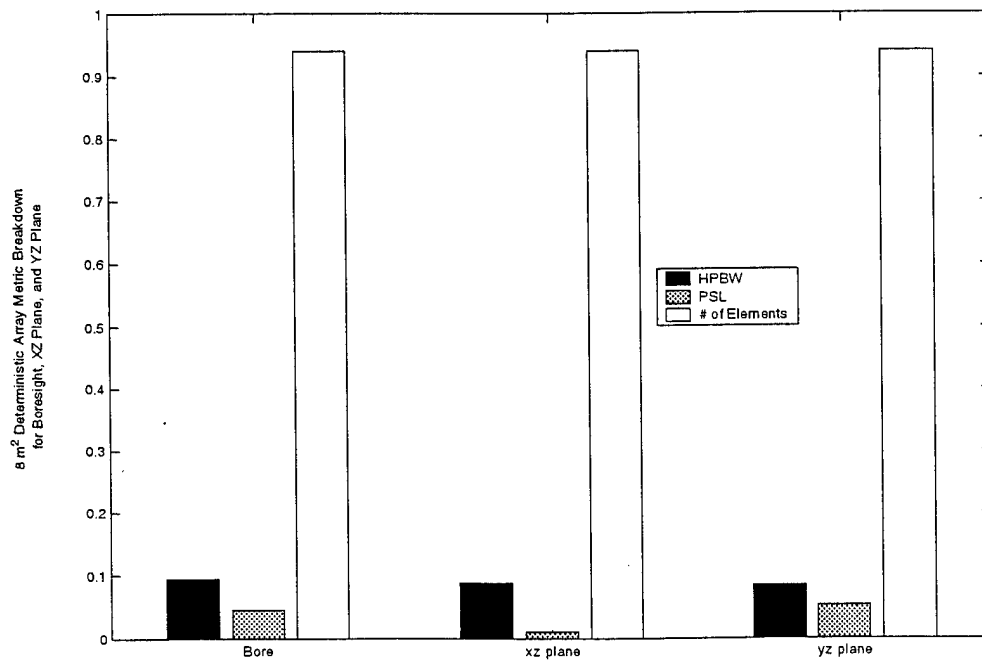


Figure 5.12 Deterministic 8m² Array Metric Breakdown

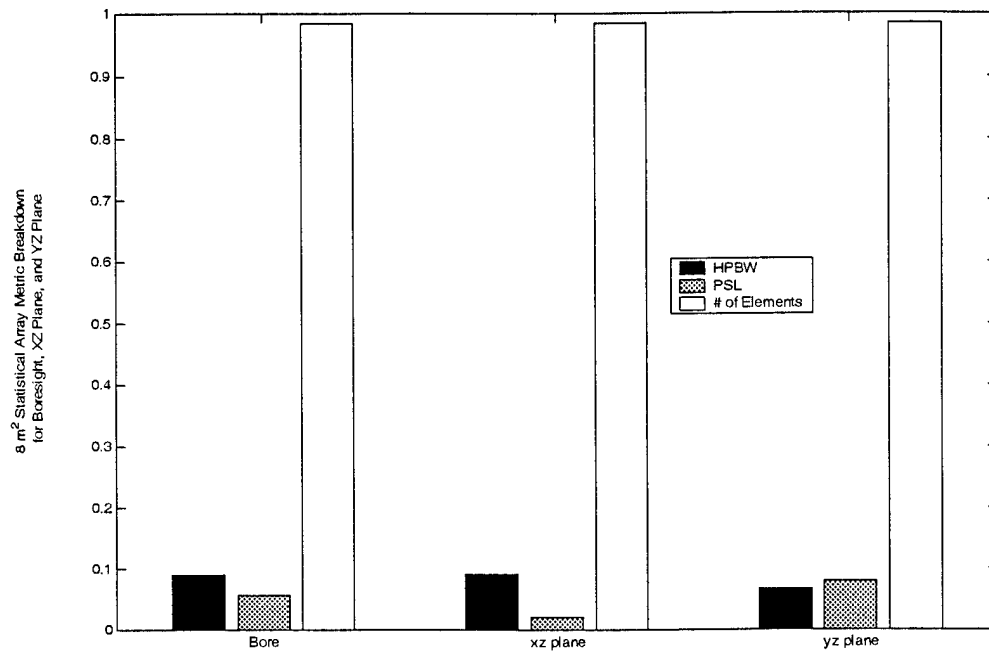


Figure 5.13 Statistic 8m² Array Metric Breakdown

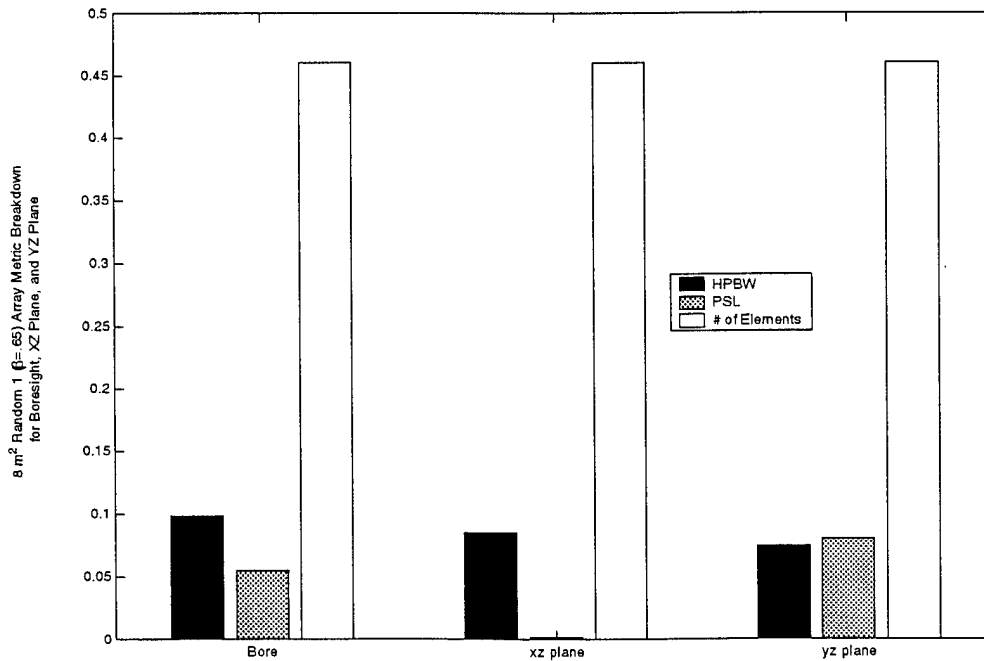


Figure 5.14 Random 8m² Array Metric Breakdown

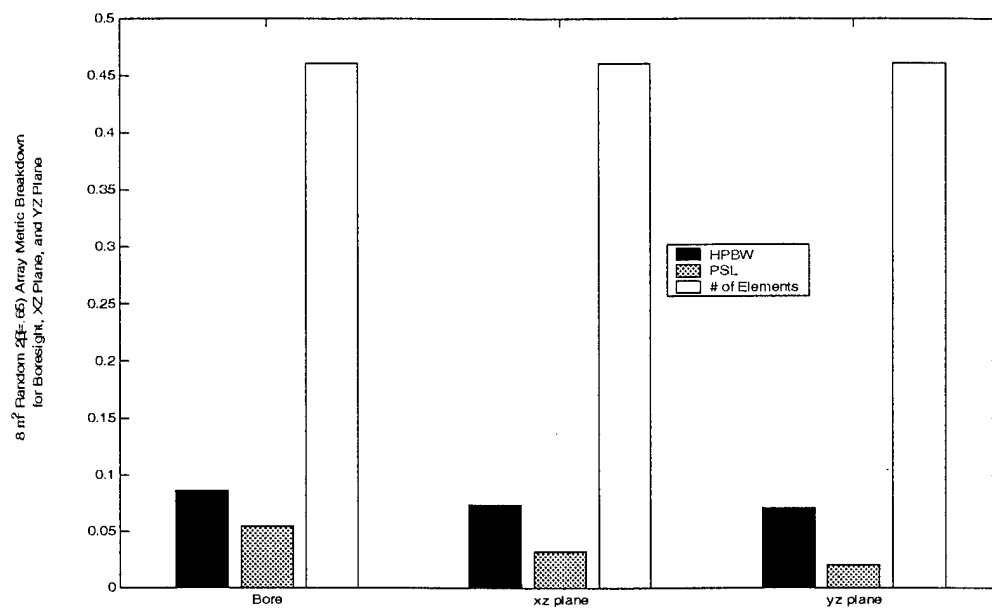


Figure 5.15 Random2 8m² Array Metric Breakdown

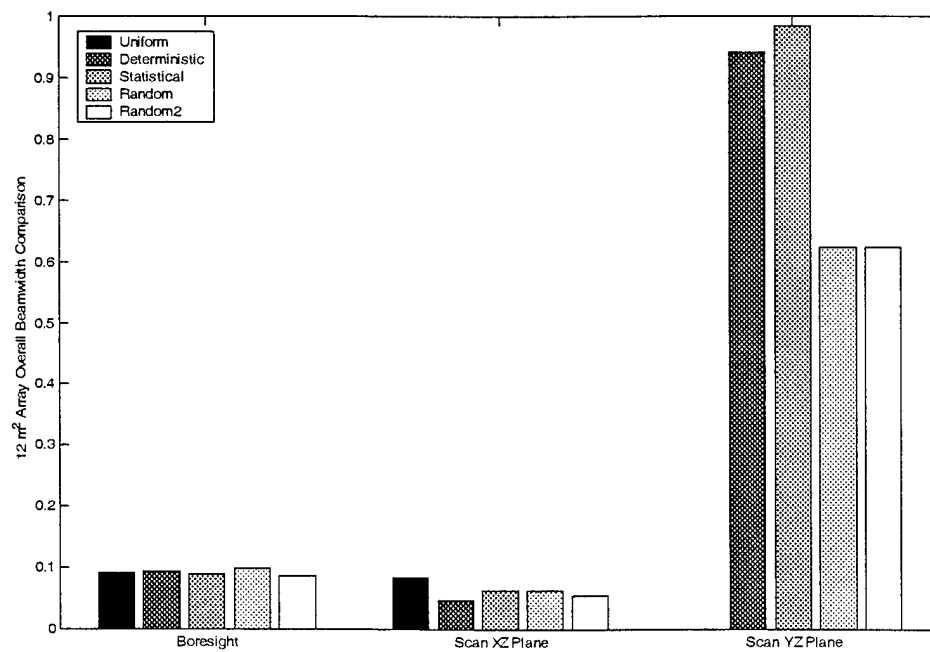


Figure 5.16 HPBW Comparison on 12m² Arrays

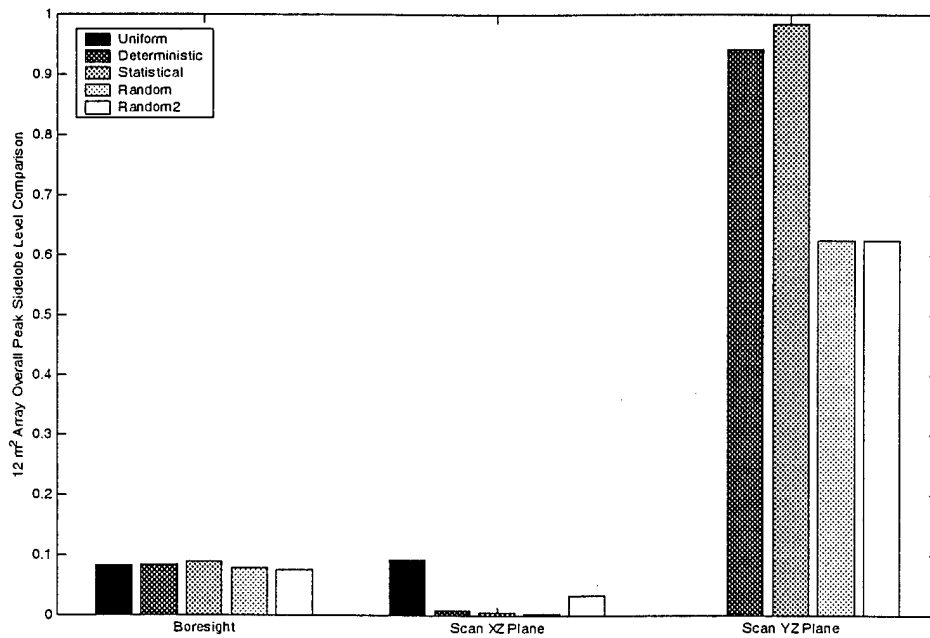


Figure 5.17 PSL Comparison on 12m² Arrays

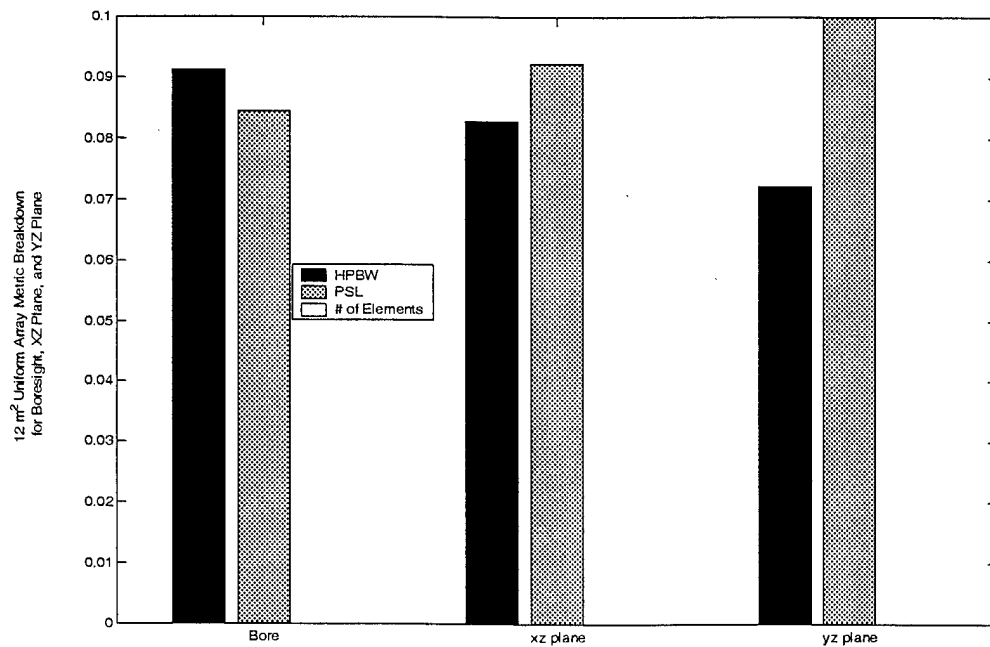


Figure 5.18 Uniform 12m² Array Metric Breakdown

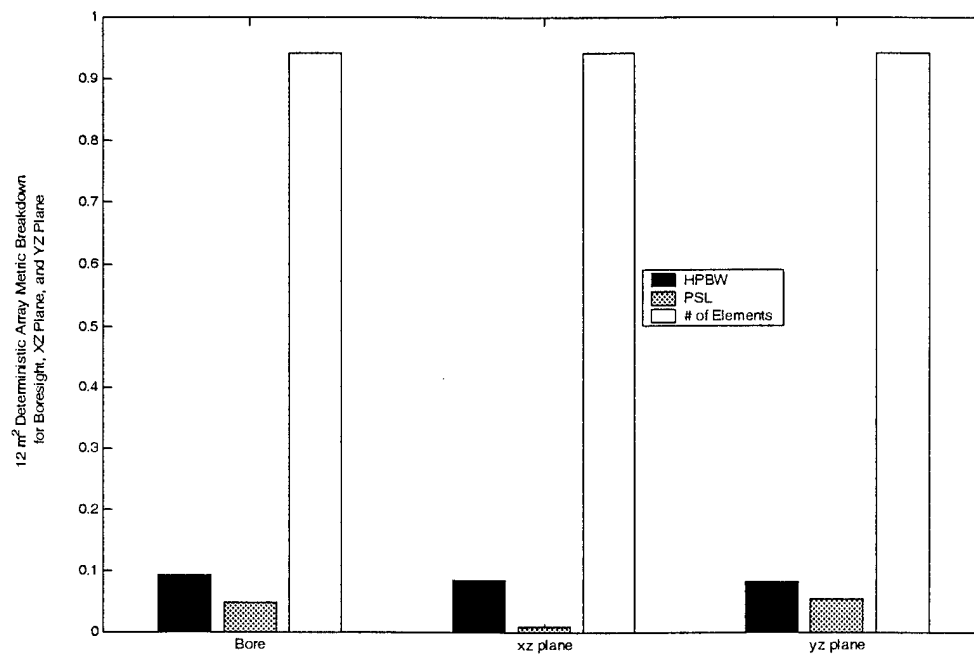


Figure 5.19 Deterministic 12m² Array Metric Breakdown

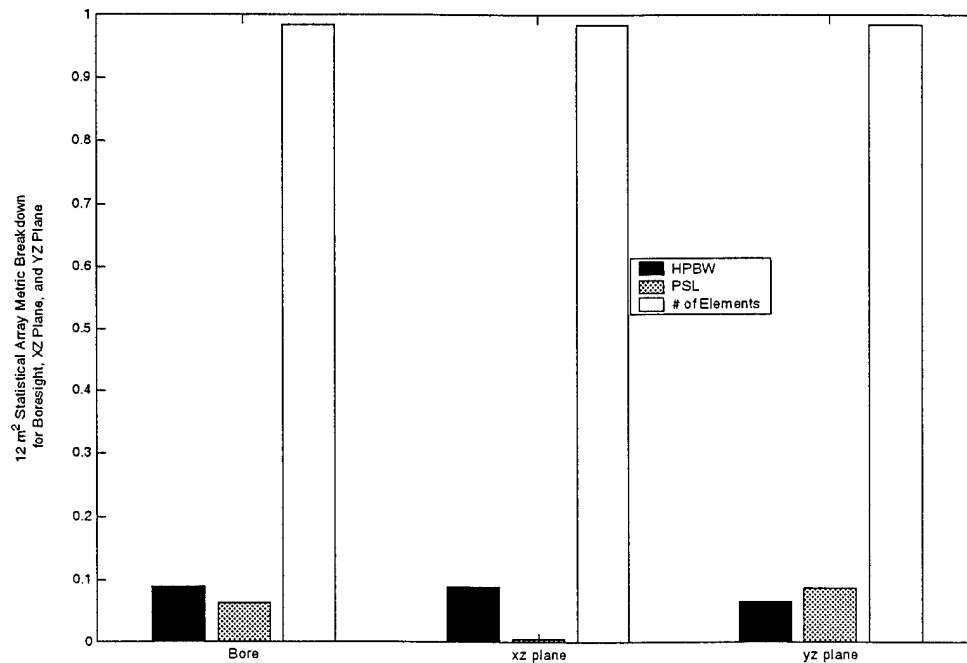


Figure 5.20 Statistic 12m² Array Metric Breakdown

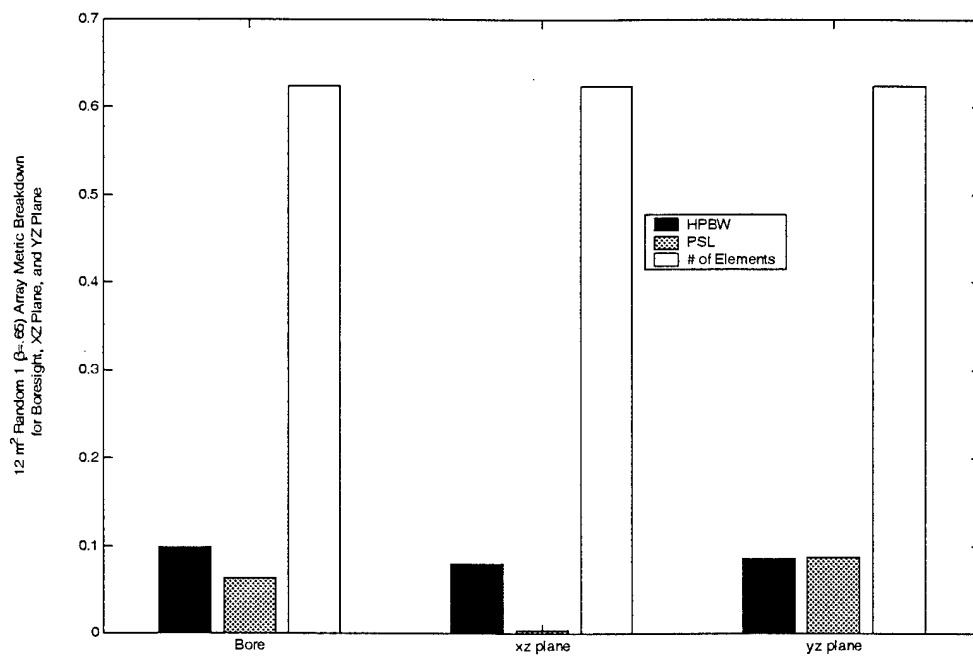


Figure 5.21 Random 12m² Array Metric Breakdown

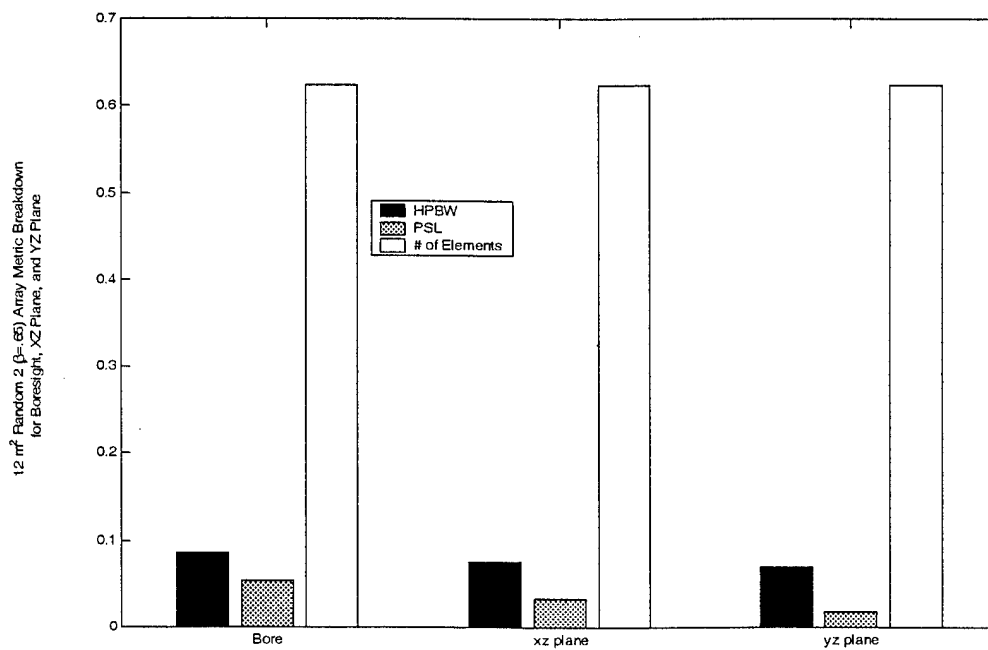


Figure 5.22 Random2 12m² Array Metric Breakdown

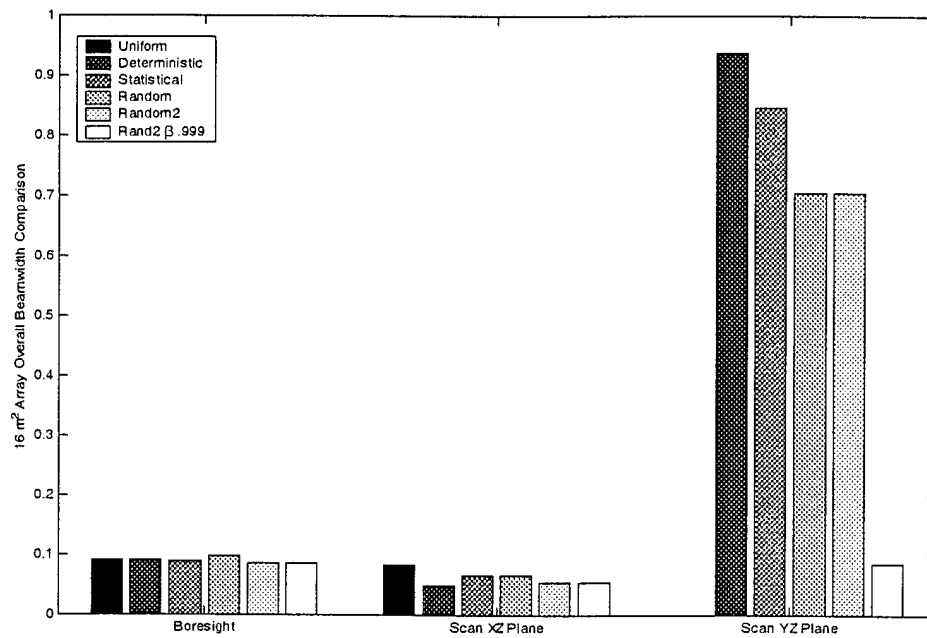


Figure 5.23 HPBW Comparison on 16m² Arrays

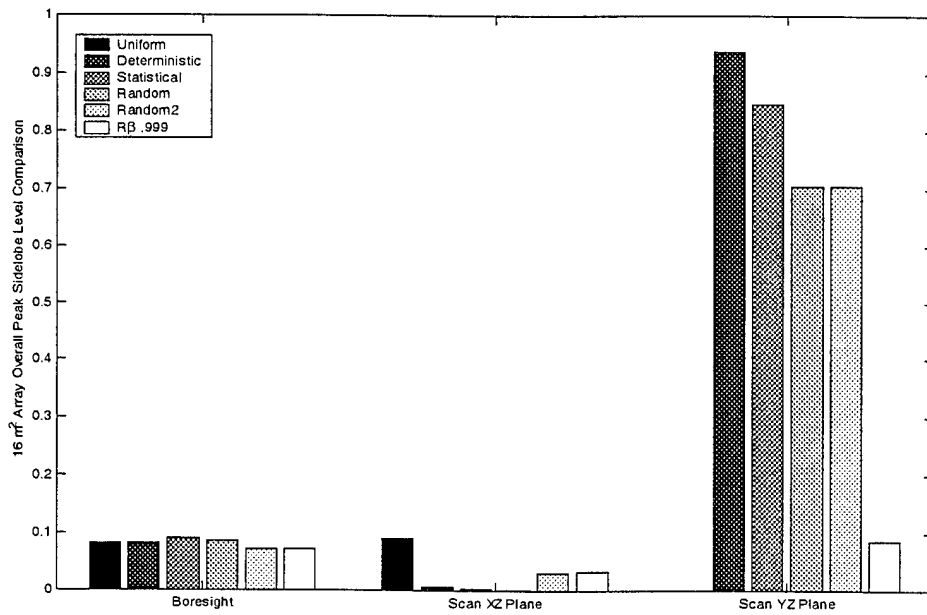


Figure 5.24 PSL Comparison on 16m² Arrays

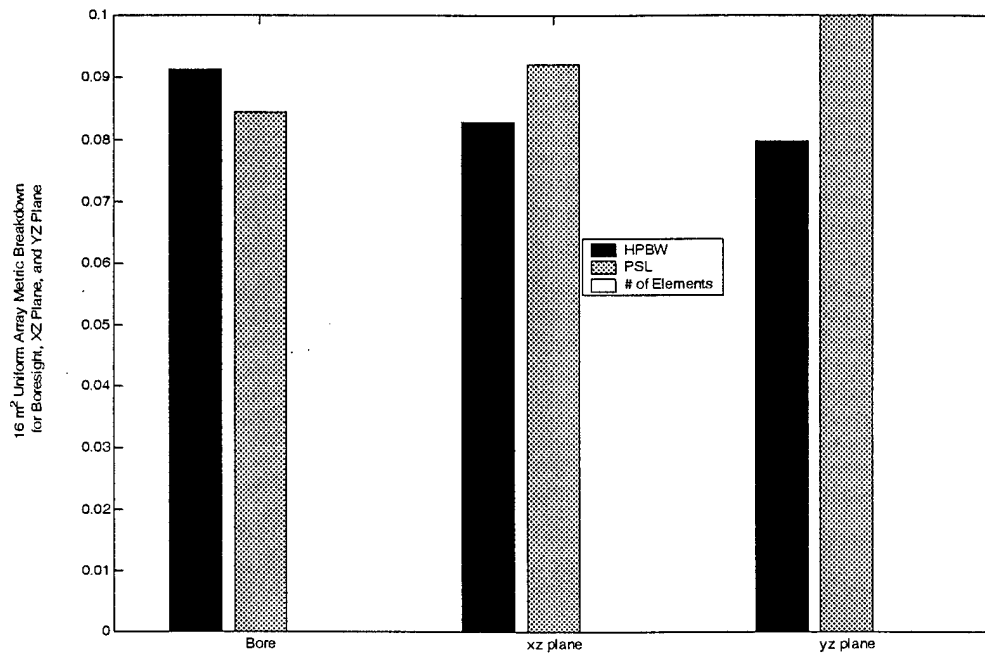


Figure 5.25 Uniform 16m² Array Metric Breakdown

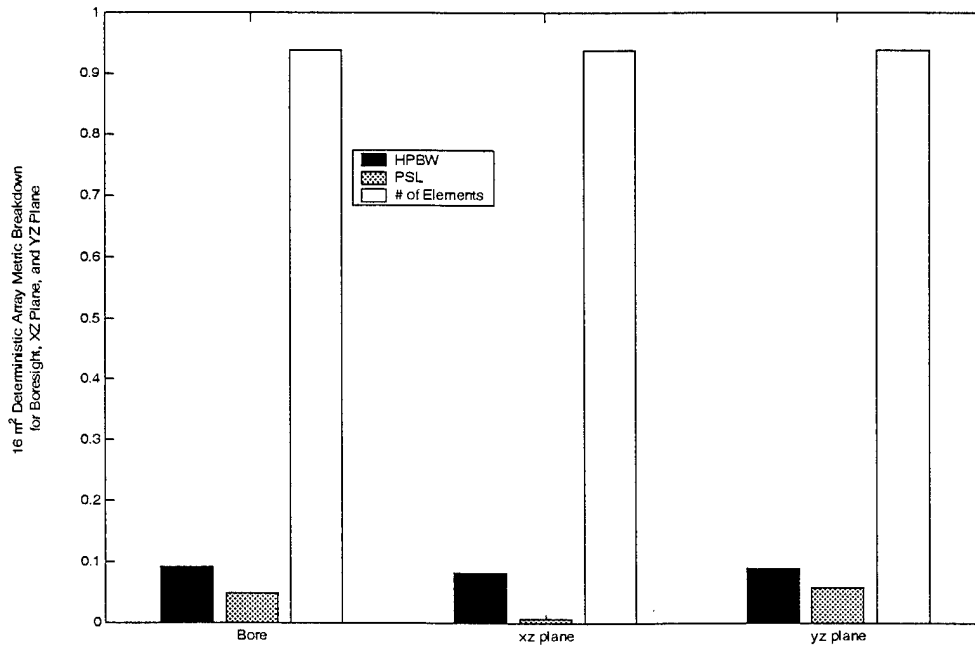


Figure 5.26 Deterministic 16m² Array Metric Breakdown

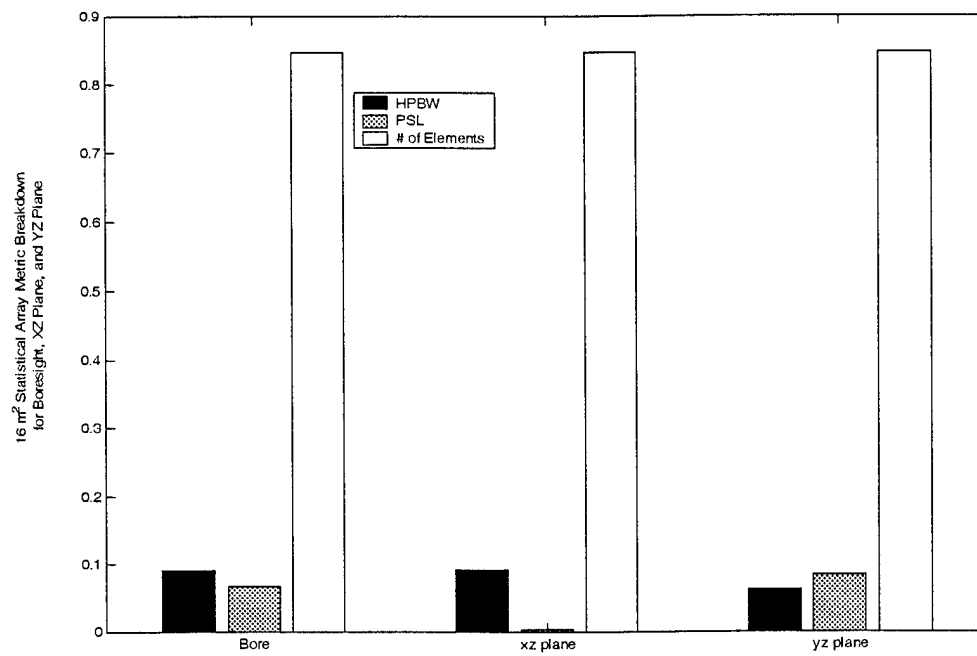


Figure 5.27 Statistic 16m² Array Metric Breakdown

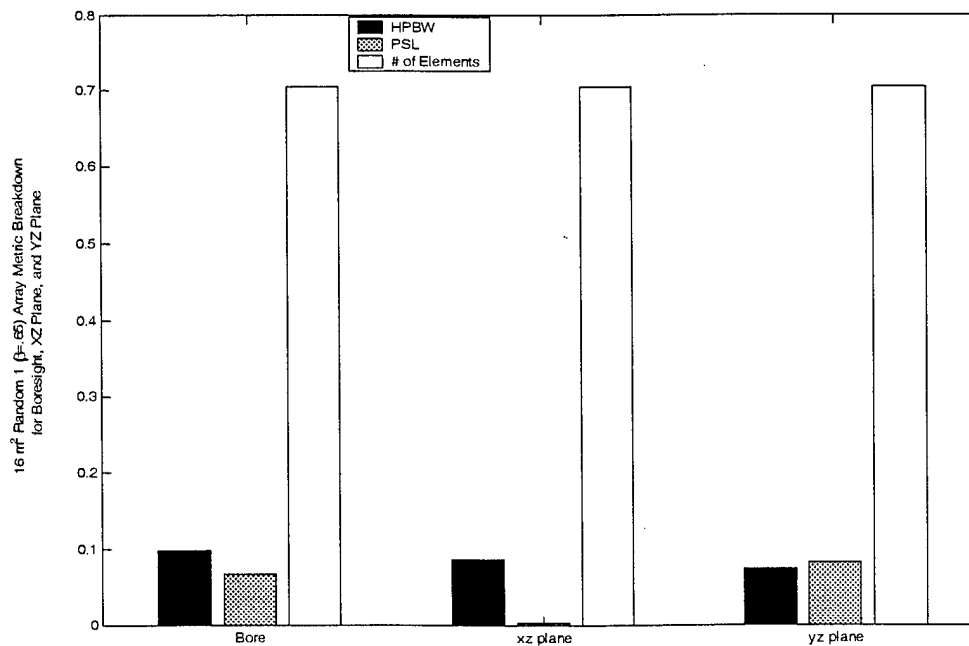


Figure 5.28 Random 16m² Array Metric Breakdown

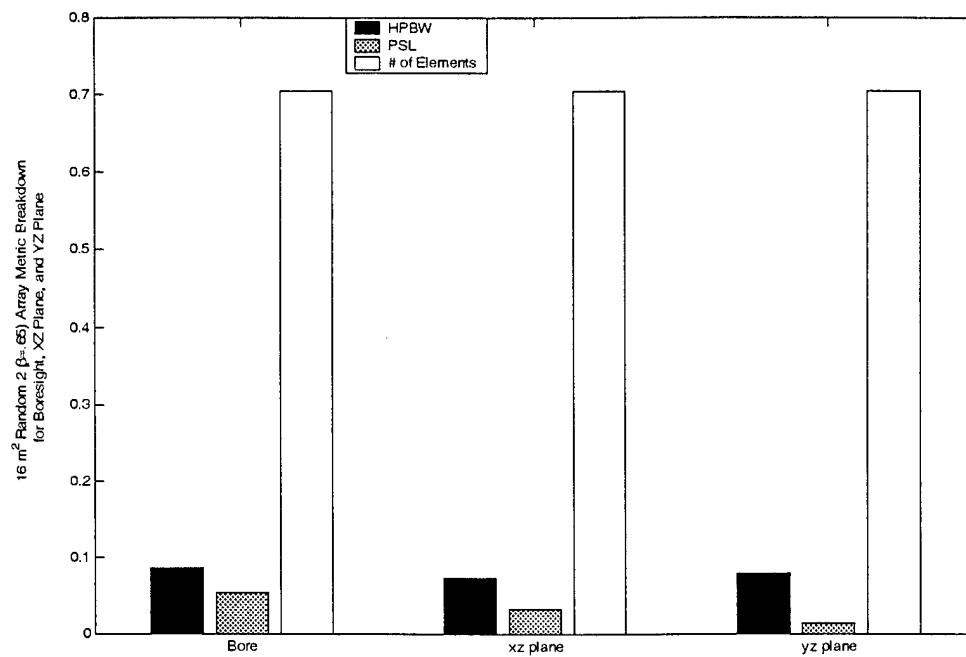


Figure 5.29 Random2 16m² Array Metric Breakdown

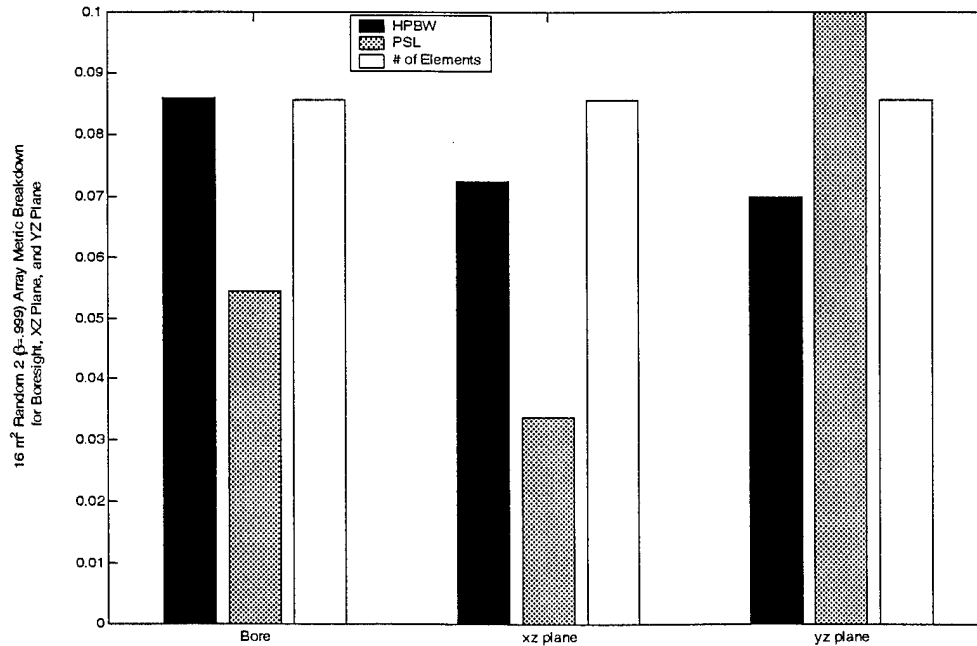


Figure 5.30 Random2 16m² Array ($\beta=.999$) Metric Breakdown

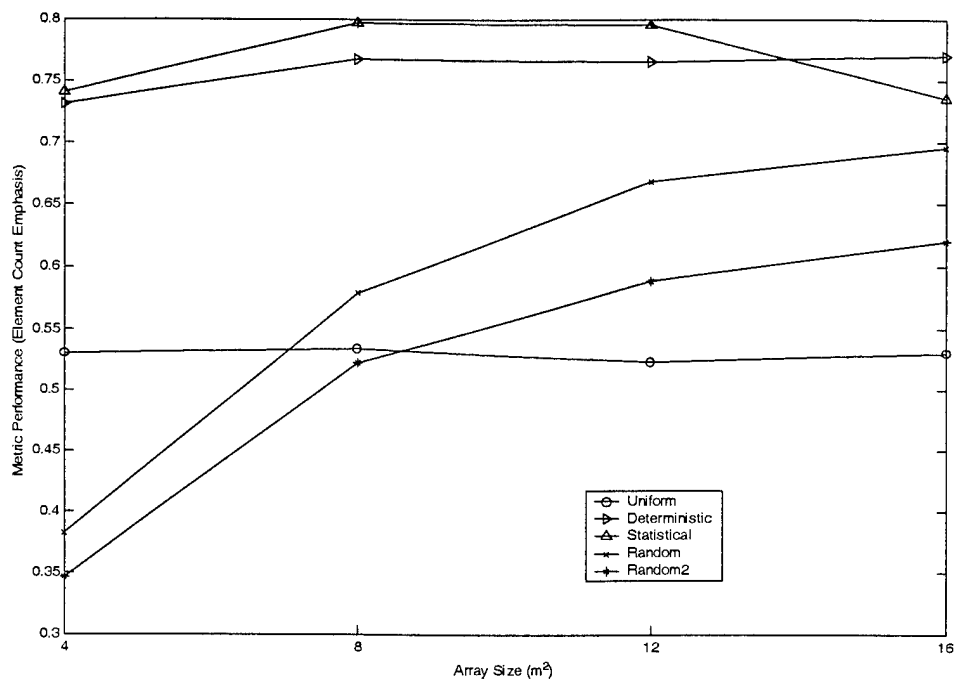


Figure 5.31 Element Count Trend For Each Array vs. Array Size

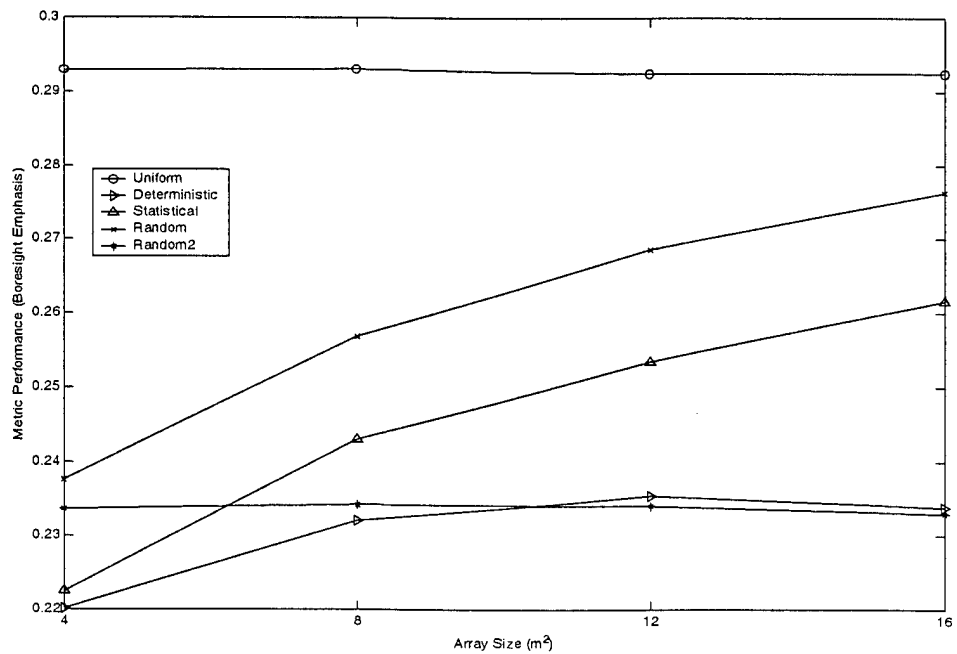


Figure 5.32 Boresight Trend For Each Array vs. Array Size

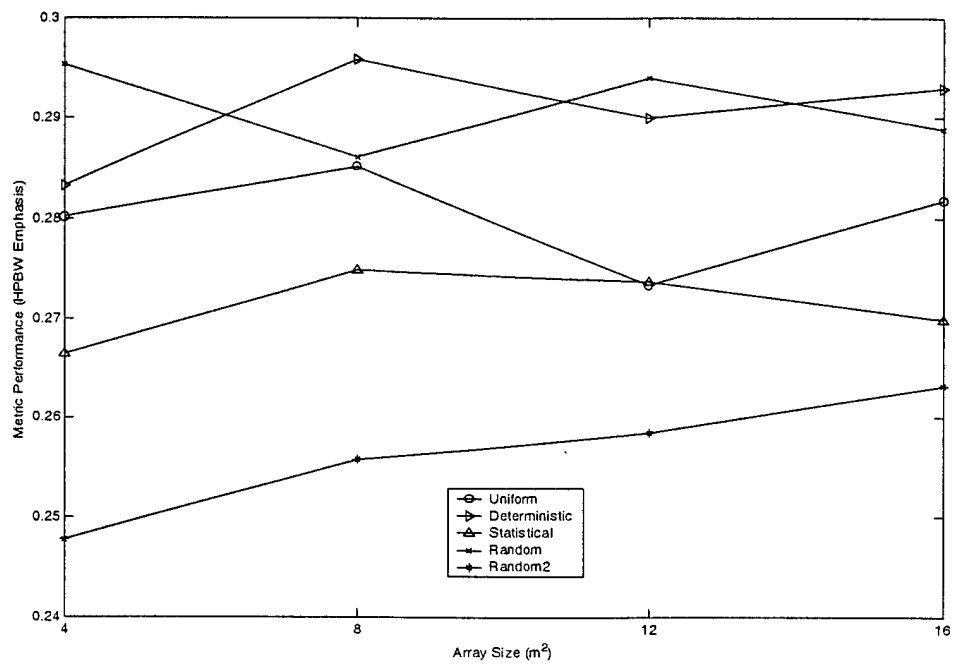


Figure 5.33 HPBW Trend For Each Array vs. Array Size

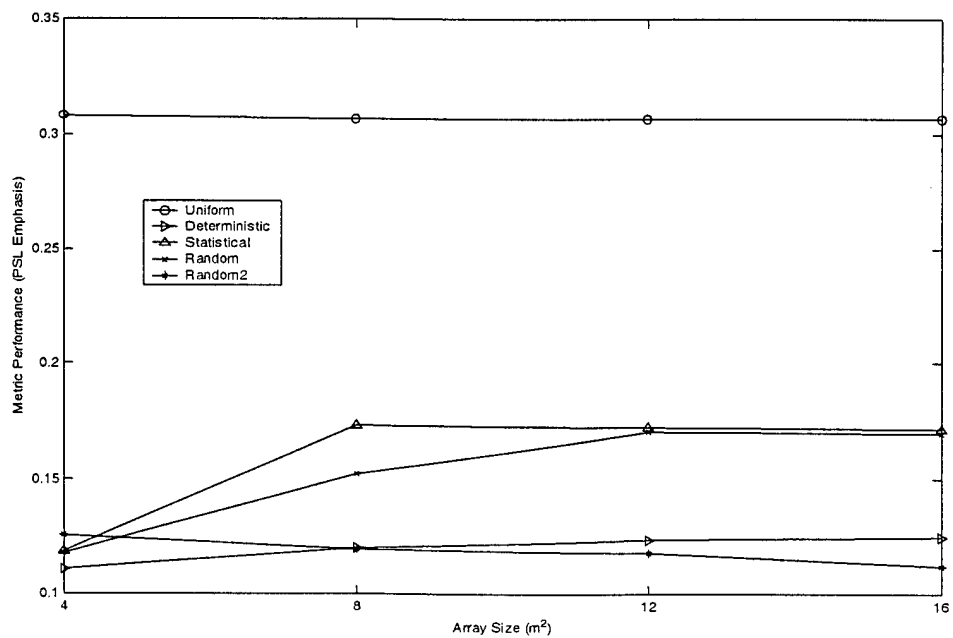


Figure 5.34 PSL Trend For Each Array vs. Array Size

5.2.2. Element Counts

The resulting element counts are found in Table 5.4. Table 5.5 contains the statistical and random array element statistics. The advantage of the element reduction of the random array is not apparent in the 4 and 8 m² arrays. The statistical and deterministic arrays outperform the random array in the area of element reduction.

Table 5.4 Non Statistical Array Element Counts

	Area			
	4	8	12	16
Baseline	25600	51076	76729	102400
Uniform	25600	51076	76729	102400
Deterministic	441	961	1369	1681

Table 5.5 Random and Statistical Array Element Statistics

		Area			
	Statistic	4	8	12	16
Statistical Array Element Count	Average	389.00	787.00	1202.14	1571.67
	Variance	618.67	849.23	1461.98	4092.13
	Stdev	24.87	29.14	38.24	63.97
	Max	459	847	1271	1683
	Min	337	729	1139	1445
	Median	385	784	1193	1575
Random Array Element Count	Average	24961.71	27553.60	28897.47	30273.70
	Variance	5.97	4.04	4.95	3.91
	Stdev	2.44	2.01	2.22	1.98
	Max	24964	27556	28900	30276
	Min	24954	27550	28892	30268
	Median	24962	27554	28898	30274

5.3 Analysis

5.3.1. Statistical Array

From Figure 5.31, for the reduced element count emphasis, the statistical and deterministic thinning approaches out performs the random approaches for all sized arrays. The main reason for this is obviously due to the extremely low element count. The statistical and deterministic thinning approaches have the highest thinning ratios at these sized arrays (see Table 5.6). However, the performance of the statistical array in the area of scanning was poor. Looking at all the statistical pattern factor plots in Appendix B (and C), there is a major lobe present at $\theta=30^\circ$ that will limit its scan capability and prevent it from meeting the $\pm 50^\circ$ scan requirement. This is expected since the interelement spacing is periodic (2λ). Taking the interelement spacing and using a combination of Equations (2.7) and (2.8) to get

$$d = \frac{\lambda}{1 + |\sin \theta_0|} \quad (5.1)$$

which for $d=2\lambda$ results in $\theta_0=30^\circ$. Otherwise, the metrics in Figures 5.11 through 5.14 show that it performs competitively with the random and uniform arrays.

5.3.2. Random Array

The random arrays performed as expected. Due to the small sizes of the arrays, the number of elements was high with respect to the other approaches. However, as can

be seen in Table 5.6, as the array size increases the thinning ratio is also increasing, which means improved performance with larger array sizes for reduced element metrics. This is also evident in Figure 5.31. In this figure, the metrics for both random approaches are increasing, while the statistical begins to decrease. The thinning ratio for the random approaches is only going to increase. However, the statistical approach remains constant, allowing the random arrays to exceed the performance of the statistical array as the array size increases. In Figure 5.33, it is apparent that as the array size increases the HPBW performance also increases for the random arrays. It also shows that the random outperforms the random2 in HPBW. This is due to the array having a larger effective aperture than the random2 array since the array has element clusters at the edges of the array, instead of only at the center.

5.3.3. Deterministic Array

The deterministic approach performed the well in the HPBW and element reduction metrics. However, it did not perform as well in the PSL and boresight metrics. In the PSL and boresight metrics, it stayed level while the random and statistical approaches were on the rise. For the most part though, the difference between the deterministic within 5% of the random and statistical approaches.

Table 5.6 Resulting array Percent Thinning

	4	8	12	16
Uniform	0%	0%	0%	0%
Deterministic	98%	98%	98%	98%
Statistical	98%	98%	98%	98%
Random	2%	46%	62%	70%

6 Conclusions and Recommendations

6.1 Conclusions

For the array sizes looked at, the deterministic and statistical arrays are ideal according to the metrics. However, looking at the PSL of the deterministic, and the limited scan capability of the statistic arrays, these approaches do not meet the desired performance requirements. The random array doesn't perform exceedingly well at these sized arrays either. However, the trends show that as the array sizes increase the HPBW, PSL, and element reduction performance of the random array continually increases. It is not apparent at the largest size ($16m^2$) that the random array outperforms the other two aperiodic approaches. However, looking at the larger array sizes with a higher beta (see Appendix C), it can be seen that the PSL, HPBW, element count (see Table 4.5), and boresight performance continues to improve as the array size increases. However, since only boresight data is available at the 12 GHz frequency, overall performance of the larger arrays can not be determined without further data generation. However, based on the trends on the boresight, for larger arrays, the random approach is the ideal aperiodic approach out of the thinning approaches studied in this thesis.

6.2 Recommendations

There are two possible recommendations that can be derived from the results in Chapter 5. First, based on the metrics, the use of deterministic thinning approach is optimal. However, that will not meet the PSL requirements. The second recommendation, based on looking at pattern factor results such as in Appendices B and

C, the random array would be more suitable, especially if the array is actually going to be larger than the 16m^2 . Looking at Appendix C, the larger random arrays, have better beamwidth and peak sidelobe performance than the statistical, while maintaining scanning capability. For large aperture SBR's, random array thinning should be feasible assuming there is capable and practical supporting architecture available to operate a randomly thinned array. Further research would be required to prove the feasibility of random arrays for even larger arrays. Use of the Major Shared Computer Resource Center is recommended due to the mass amounts of data storage and computational time required for larger arrays.

6.3 Future Topics

There are some topic recommendations for further study. One area is array geometry. This involves looking at the effects of aperiodic element distributions for circular, three-dimensional, and conformal array applications. Other areas of further research include application feasibility in multibeam phased arrays and satellite communications systems. Further analysis needs to be done on other aperiodic approaches, in particular deterministic, and combinations of approaches.

Another area that needs to be looked into is the effective footprint of SBR's. At LEO and MEO, the footprint of the radar is in hundreds, if not thousands (depending on aperture size) of kilometers in diameter.

APPENDIX A: C++ Flowcharts

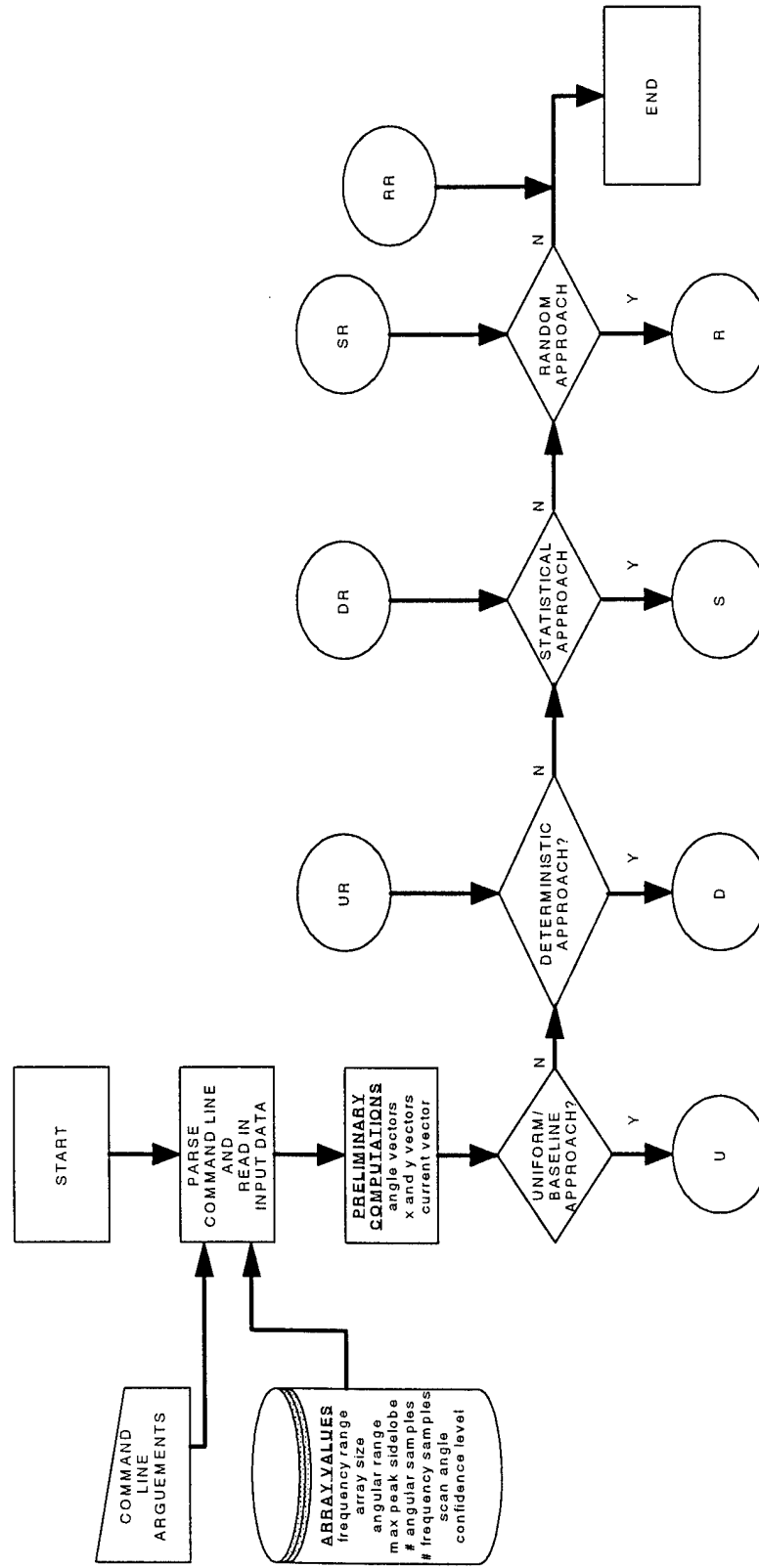


Figure A.1 Program Flowchart of Main

BLANK PAGE

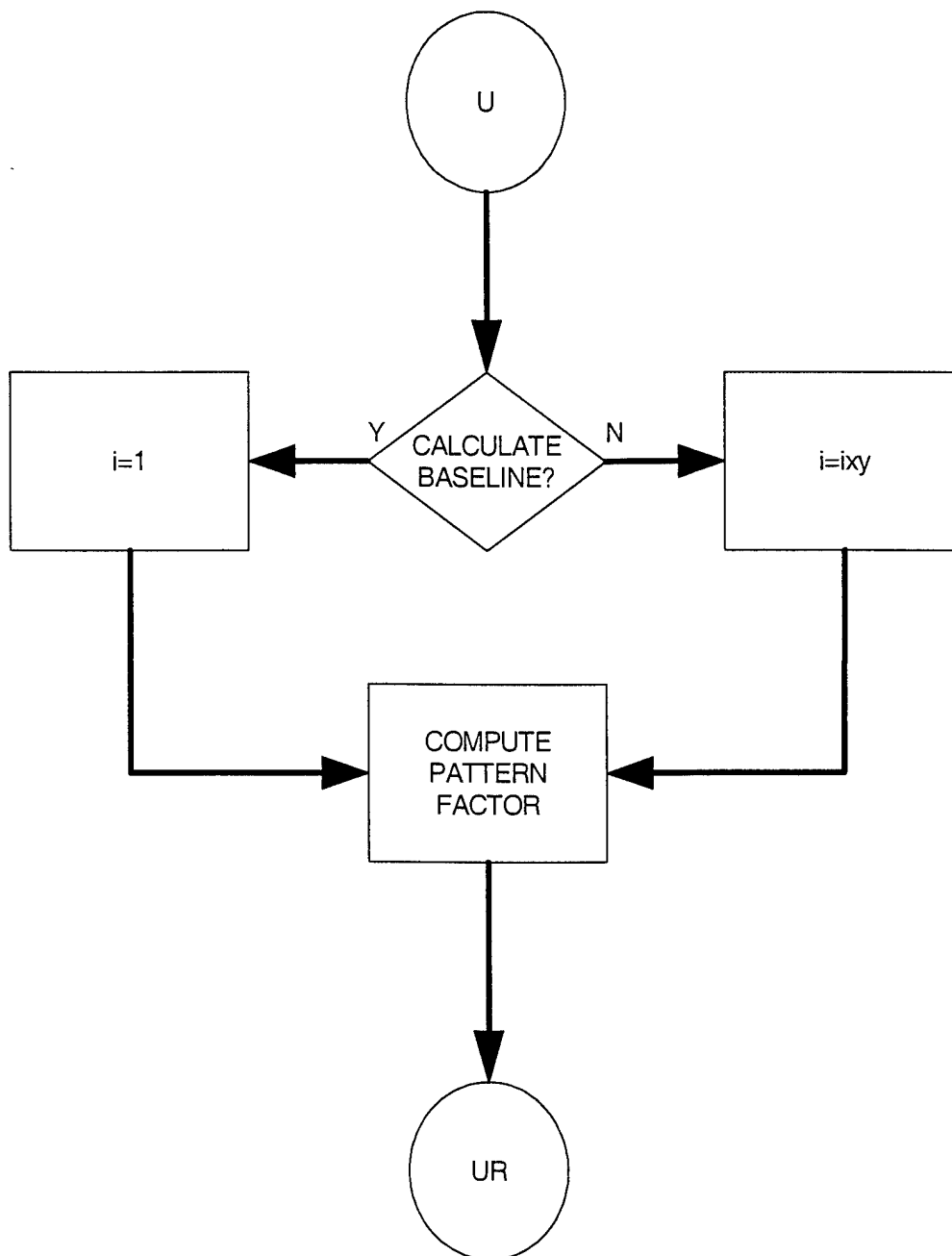


Figure A.2 Program Flowchart of Uniform/Baseline Routine

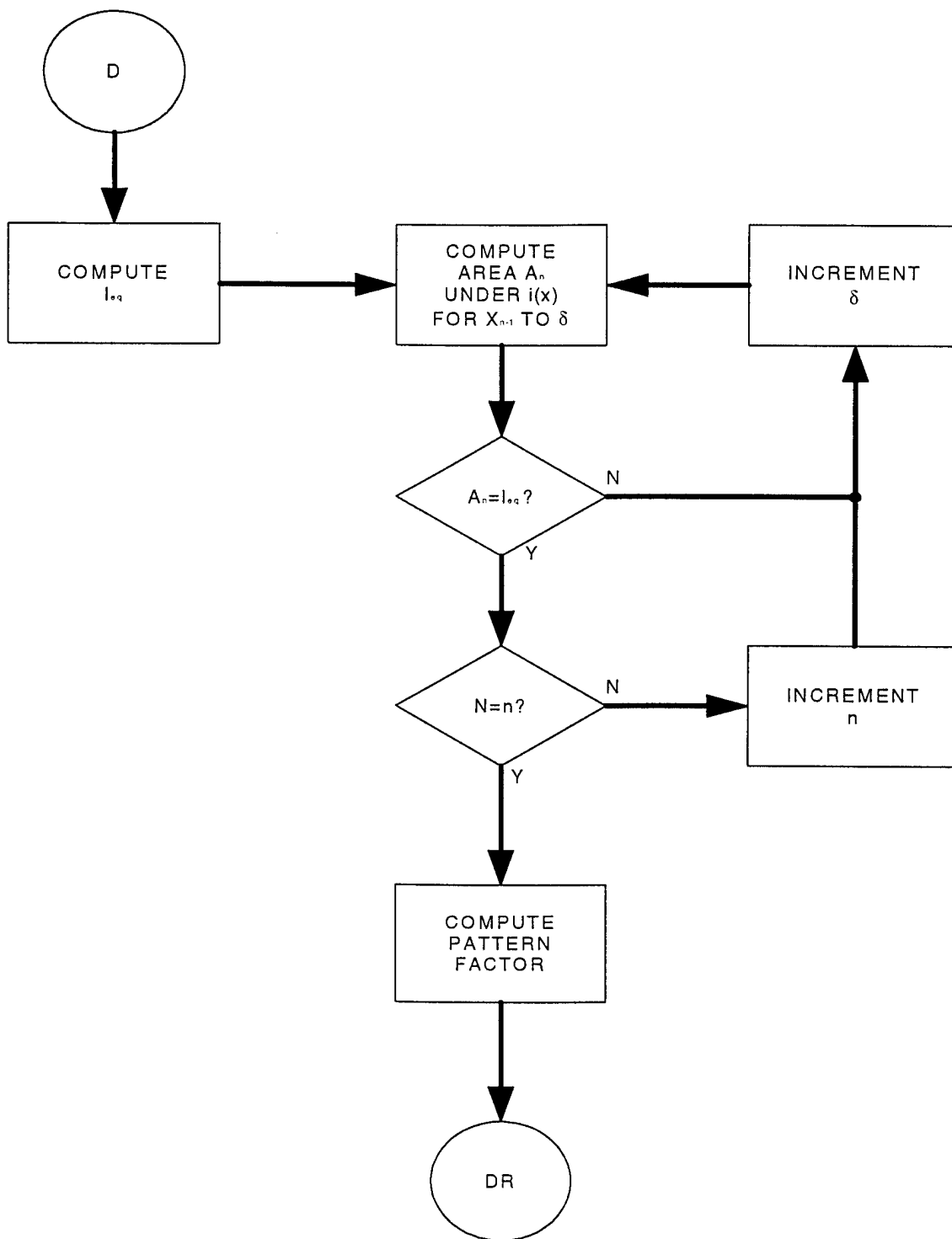


Figure A.3 Program Flowchart for Deterministic Routine

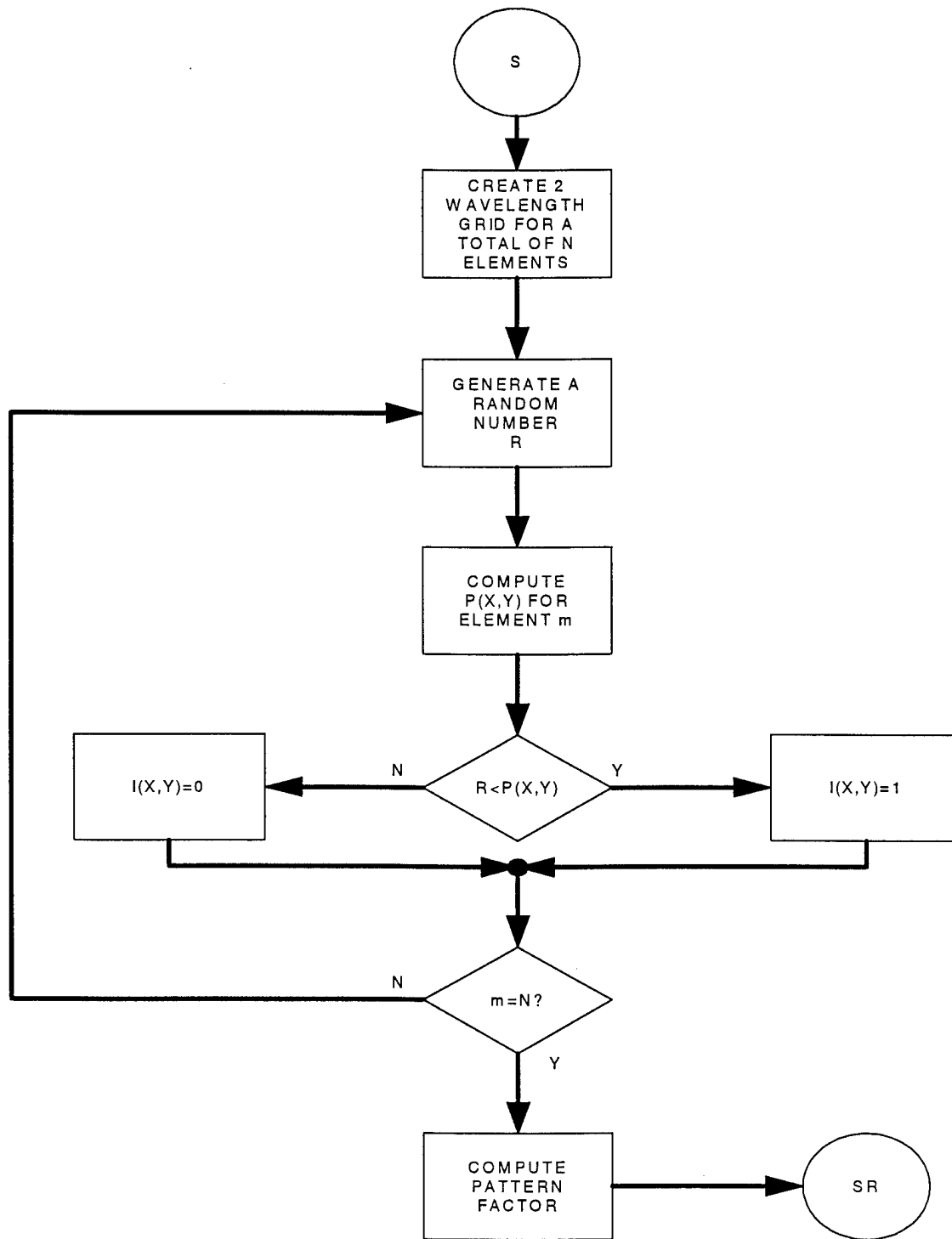


Figure A.4 Program Flowchart for Statistical Routine

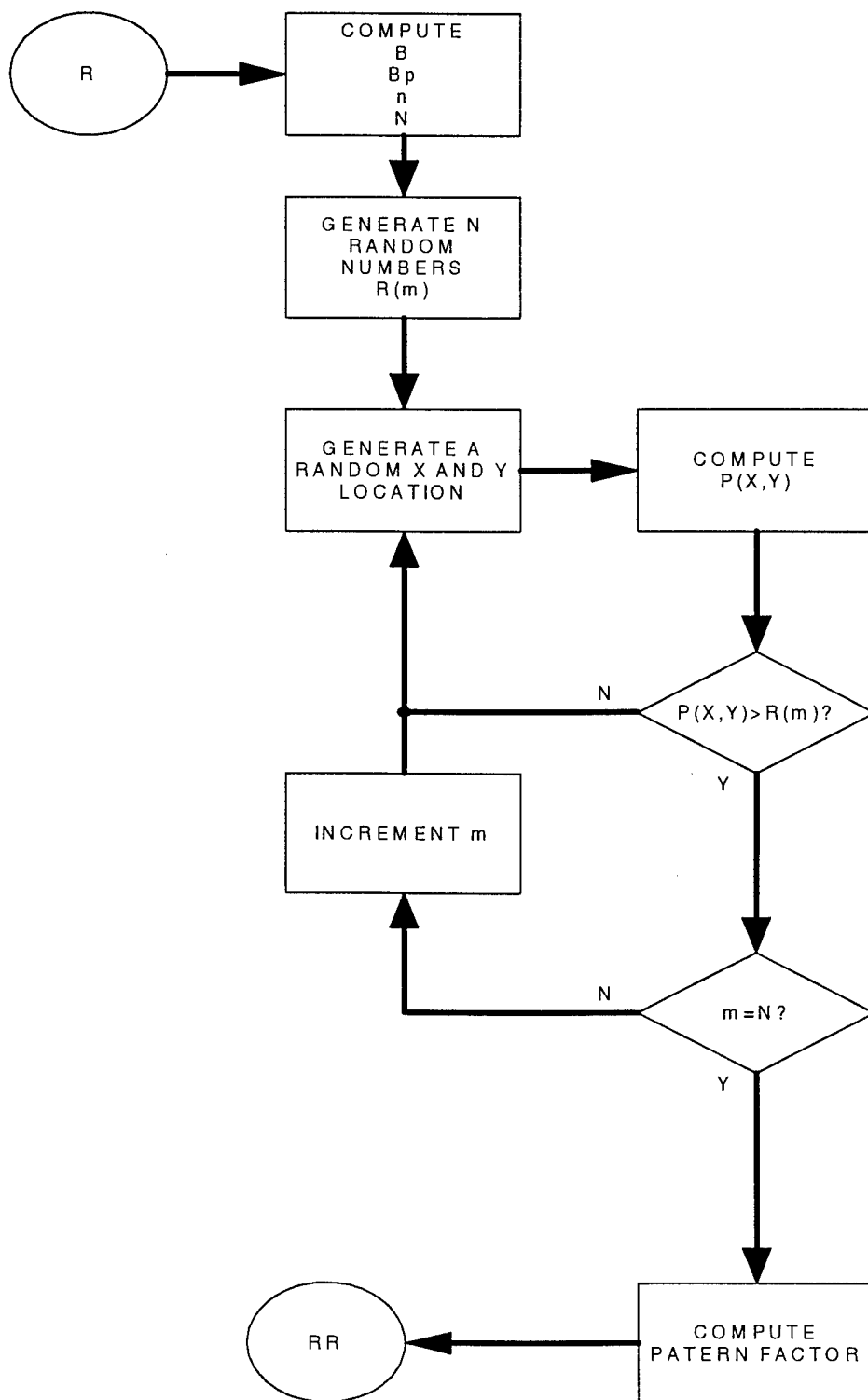


Figure A.5 Program Flowchart for Random Routine

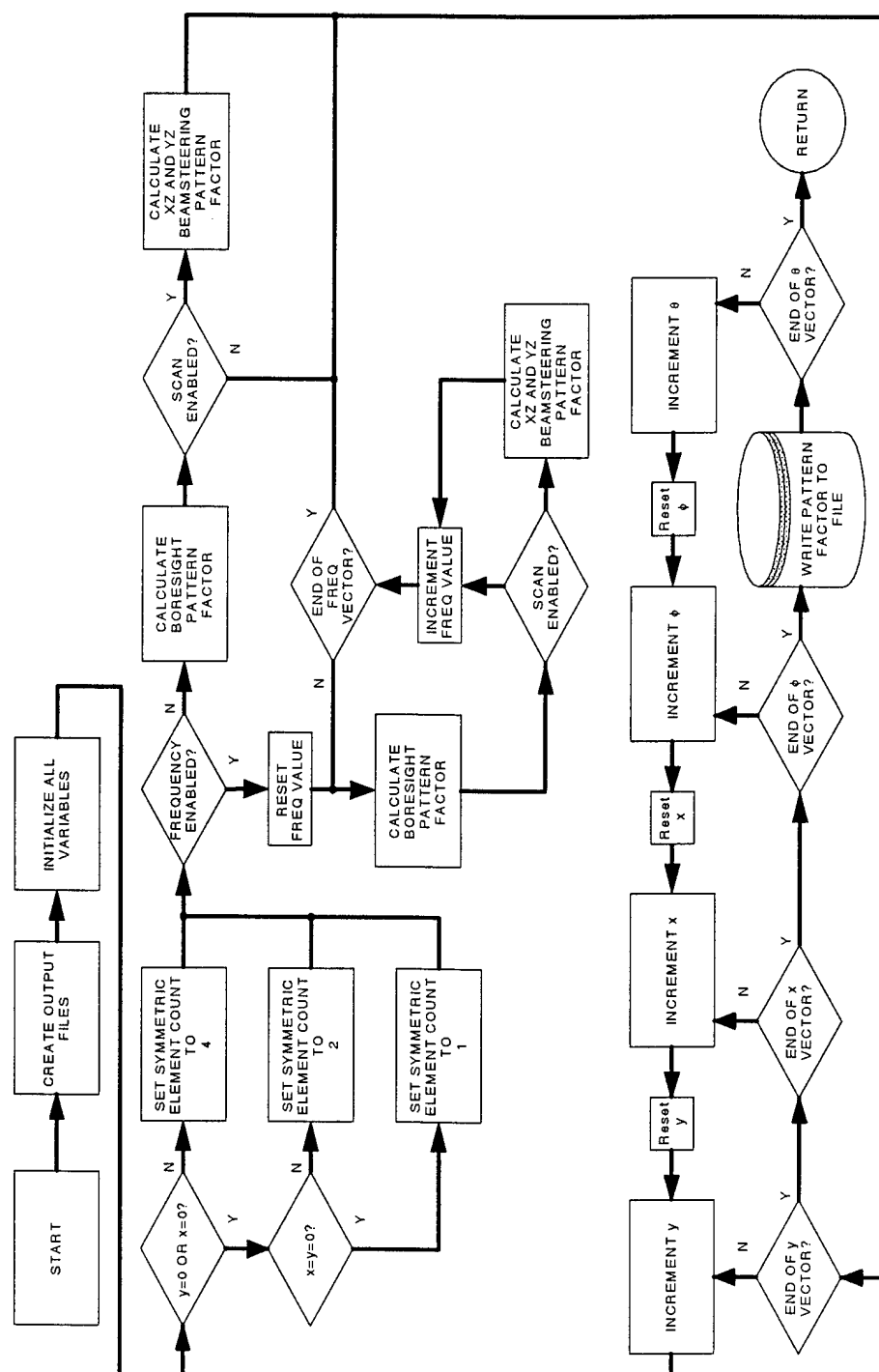


Figure A.6 Program Flowchart of Pattern Factor Generation Routine

APPENDIX B: Boresight Pattern Factors

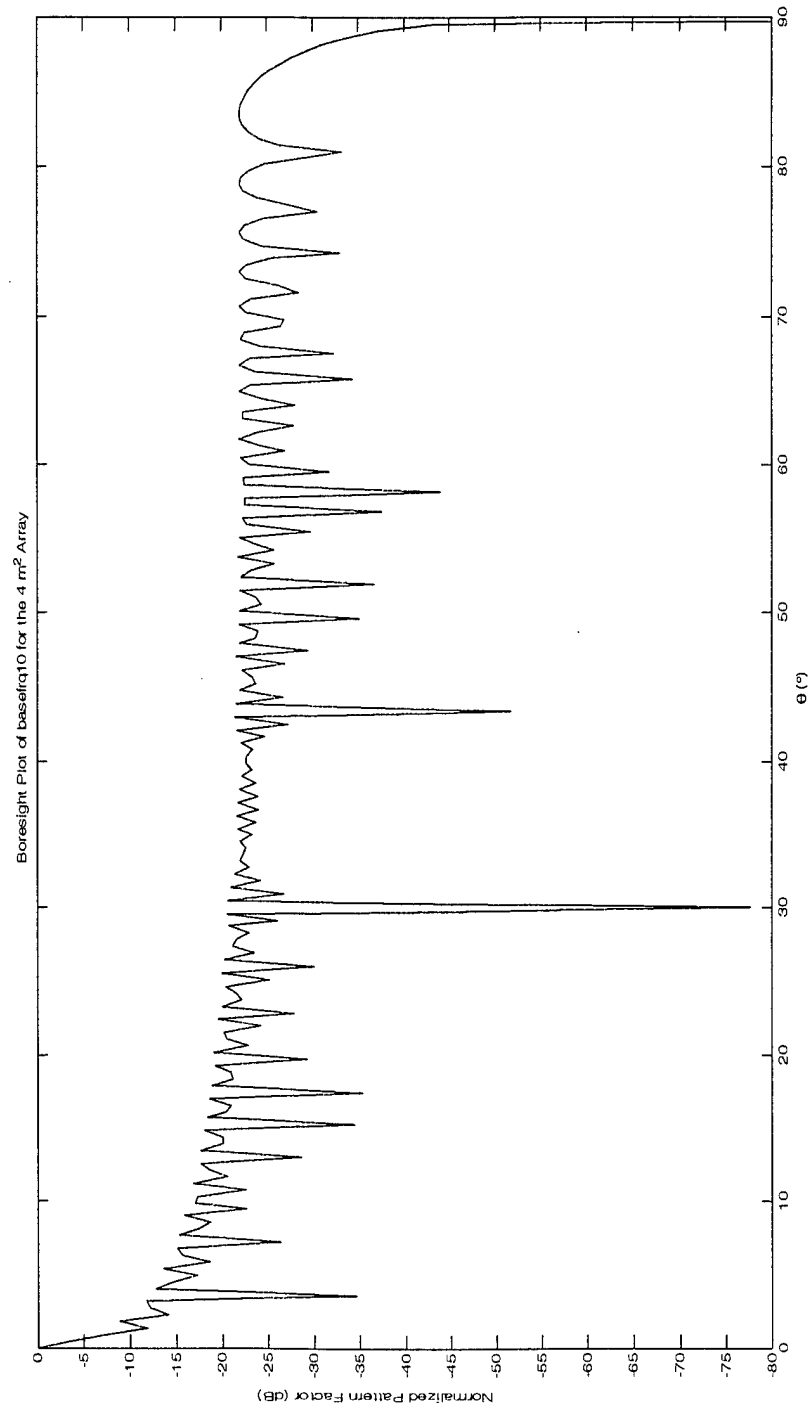


Figure B.1 Baseline 4m² Array

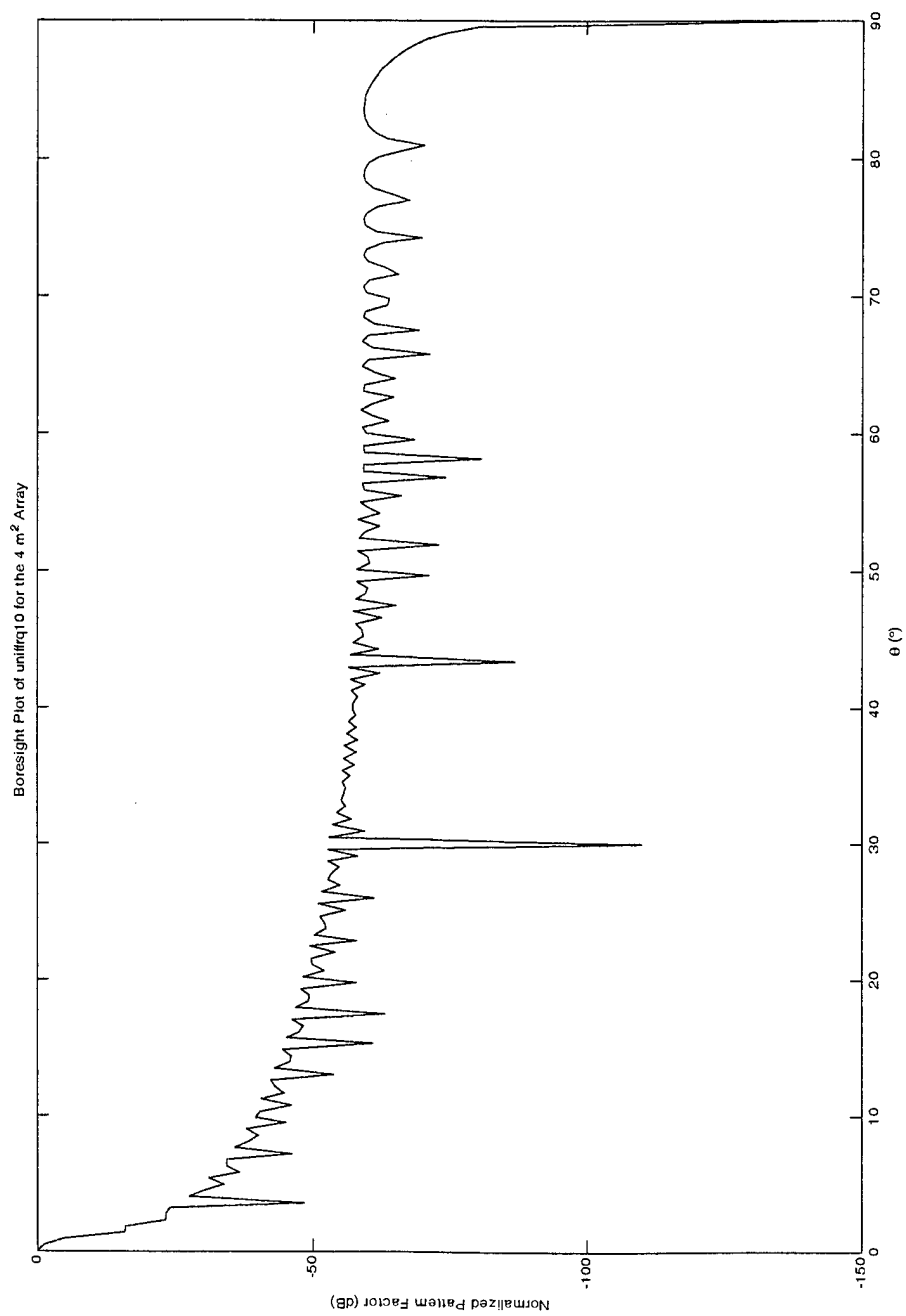


Figure B.2 Uniform 4m² Array

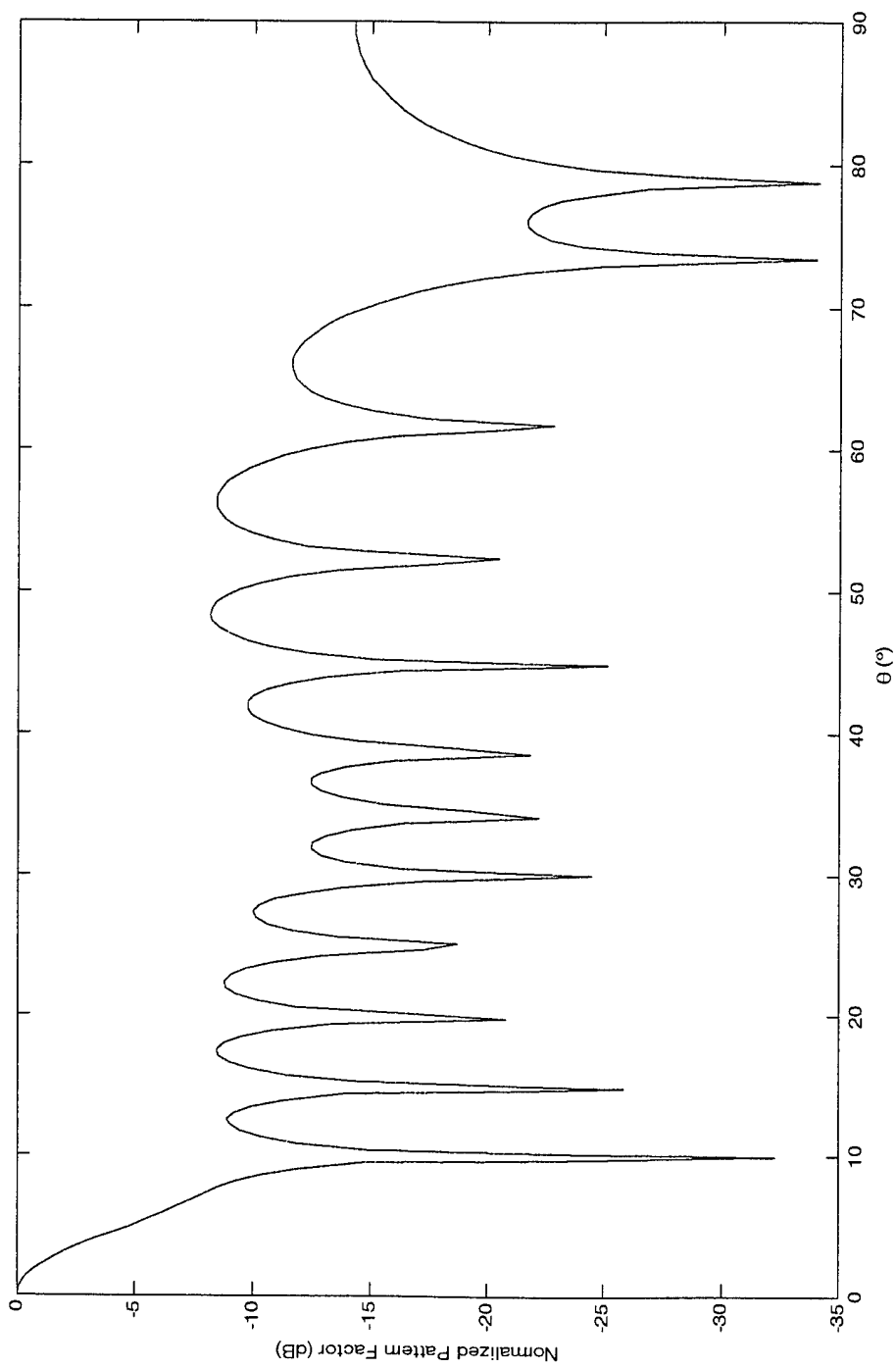


Figure B.3 Deterministic 4m² Array

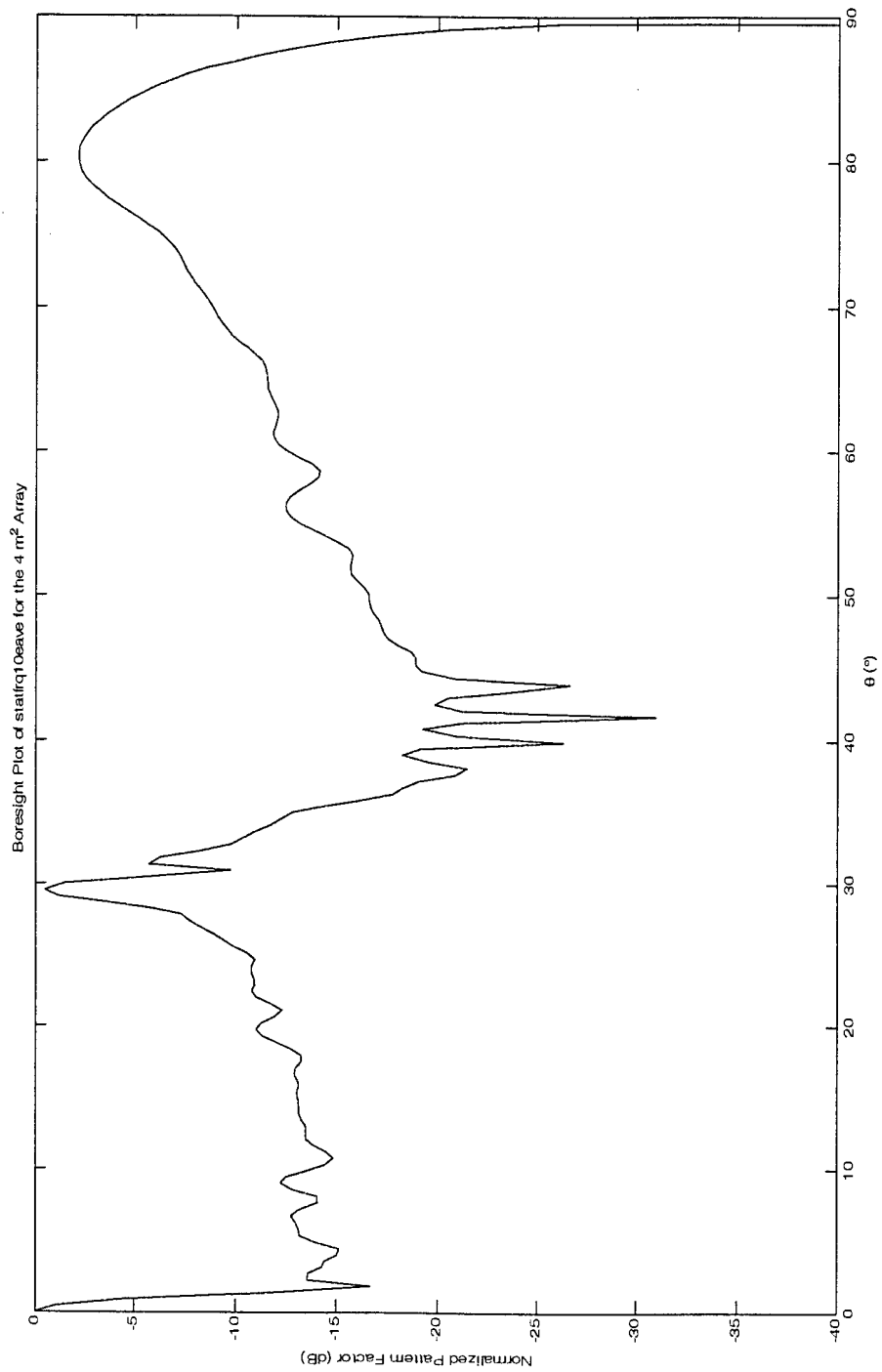


Figure B.4 Statistical 4m² Array

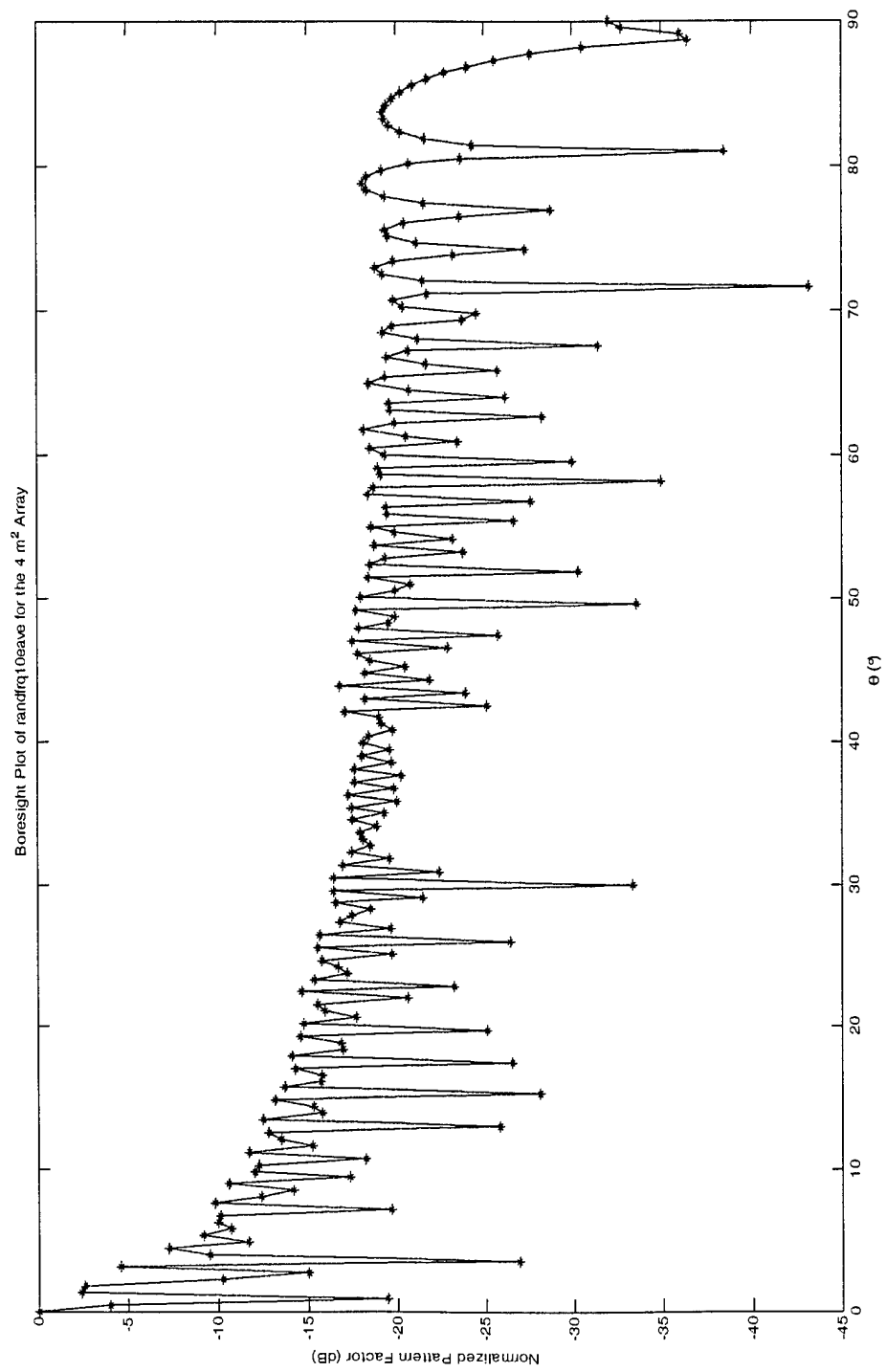


Figure B.5 Random 4m² Array

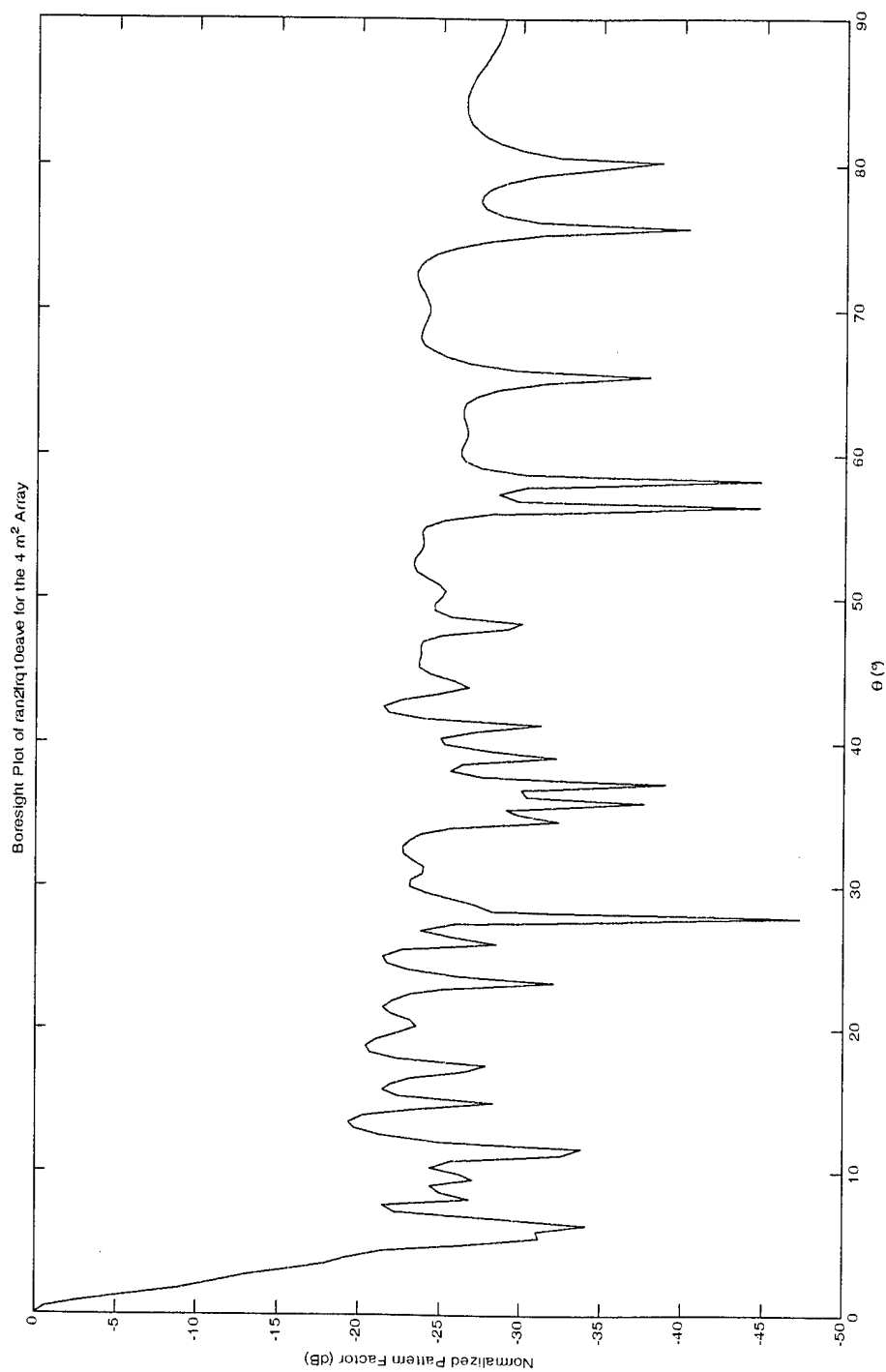


Figure B.6 Random2 4m² Array

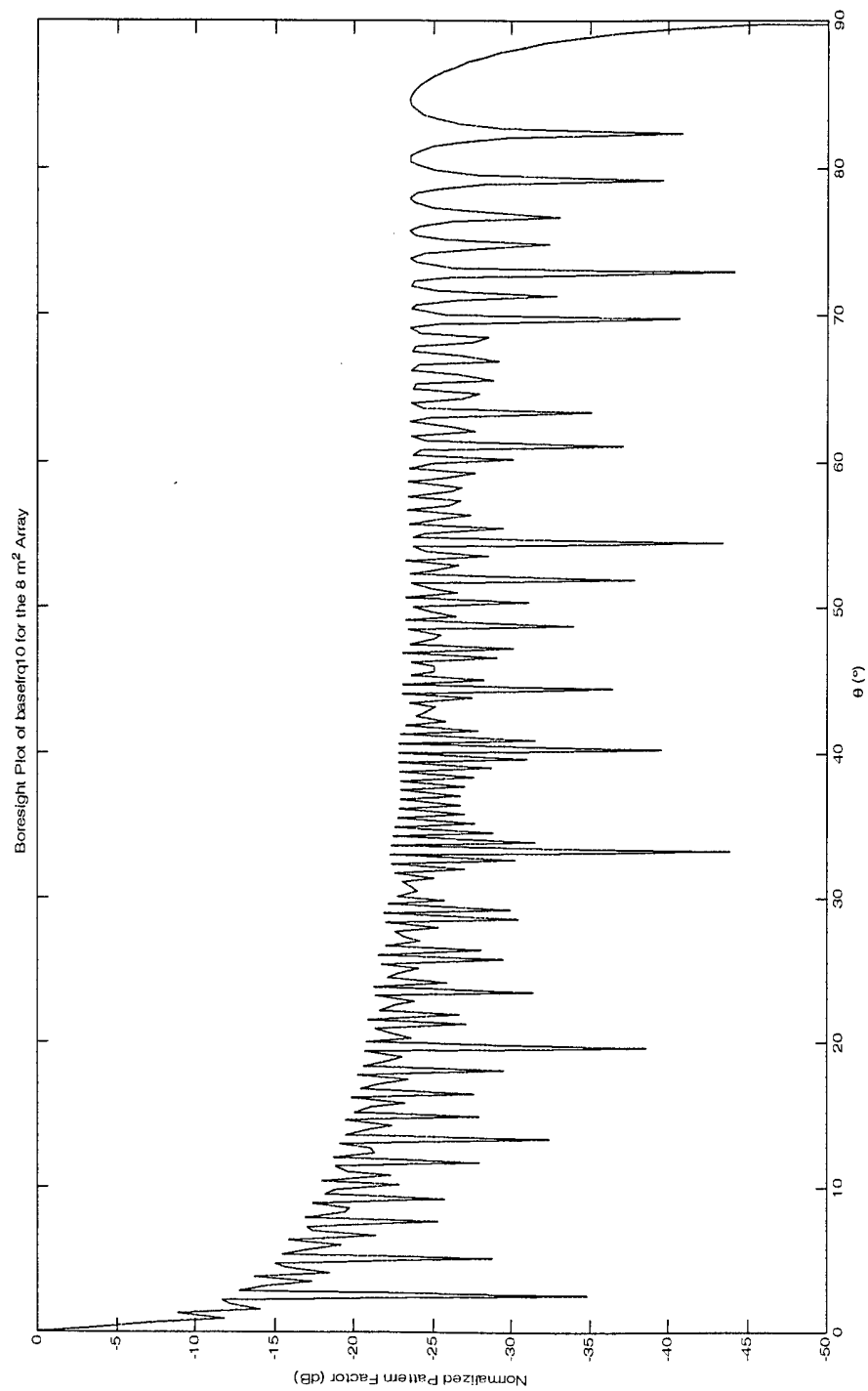


Figure B.7 Baseline 8m² Array

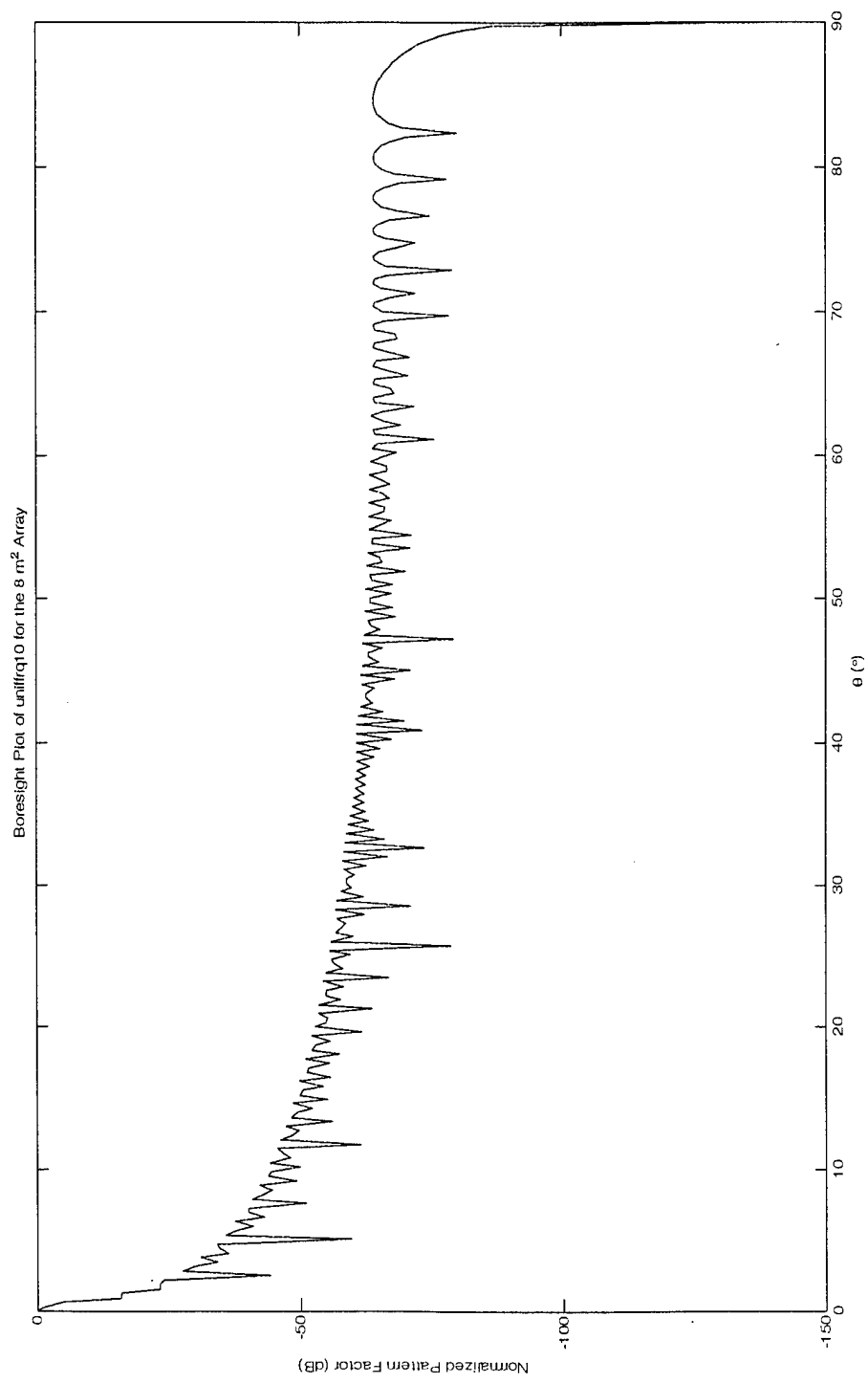


Figure B.8 Uniform 8m² Array

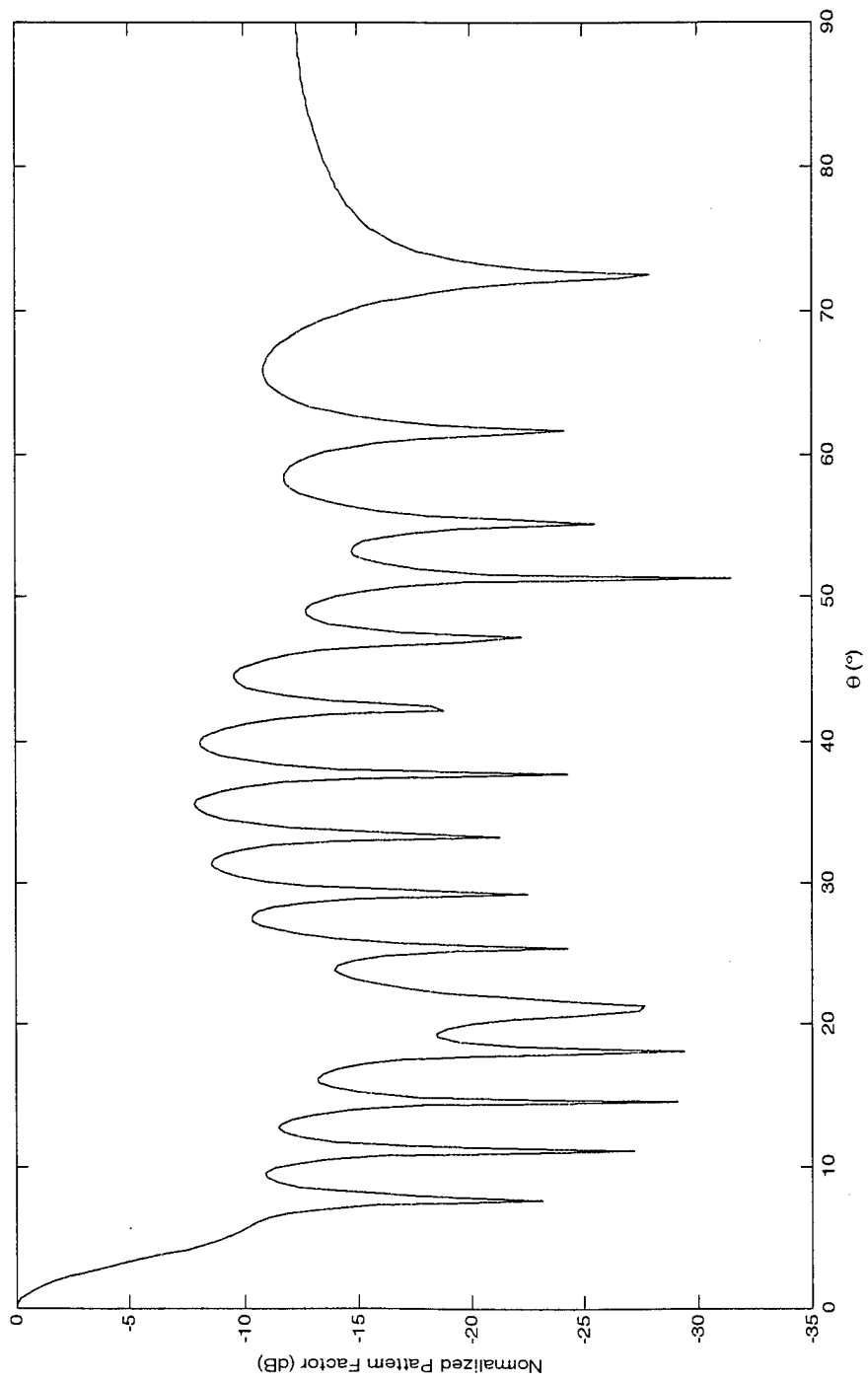


Figure B.9 Deterministic 8m² Array

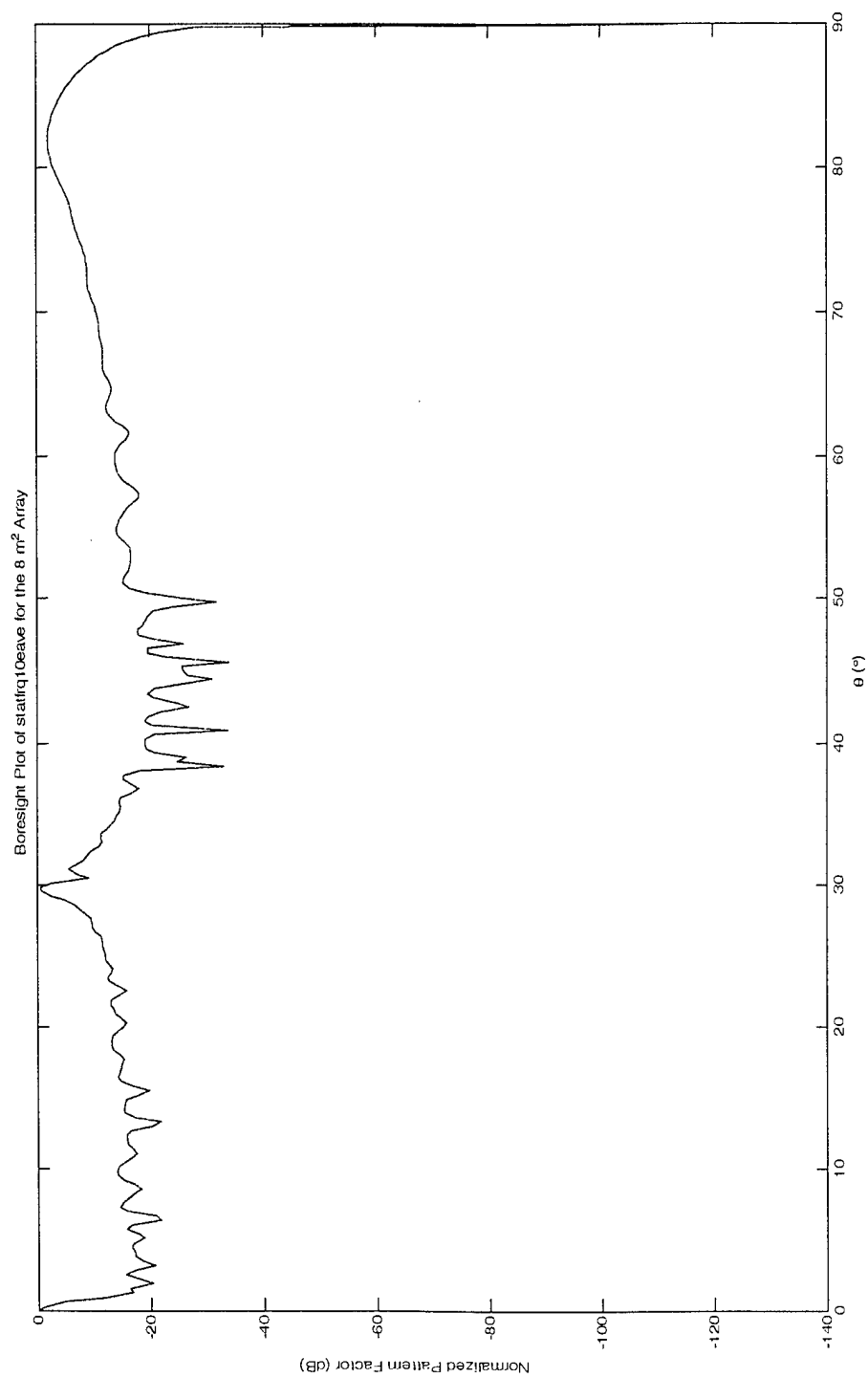


Figure B.10 Statistical 8m² Array

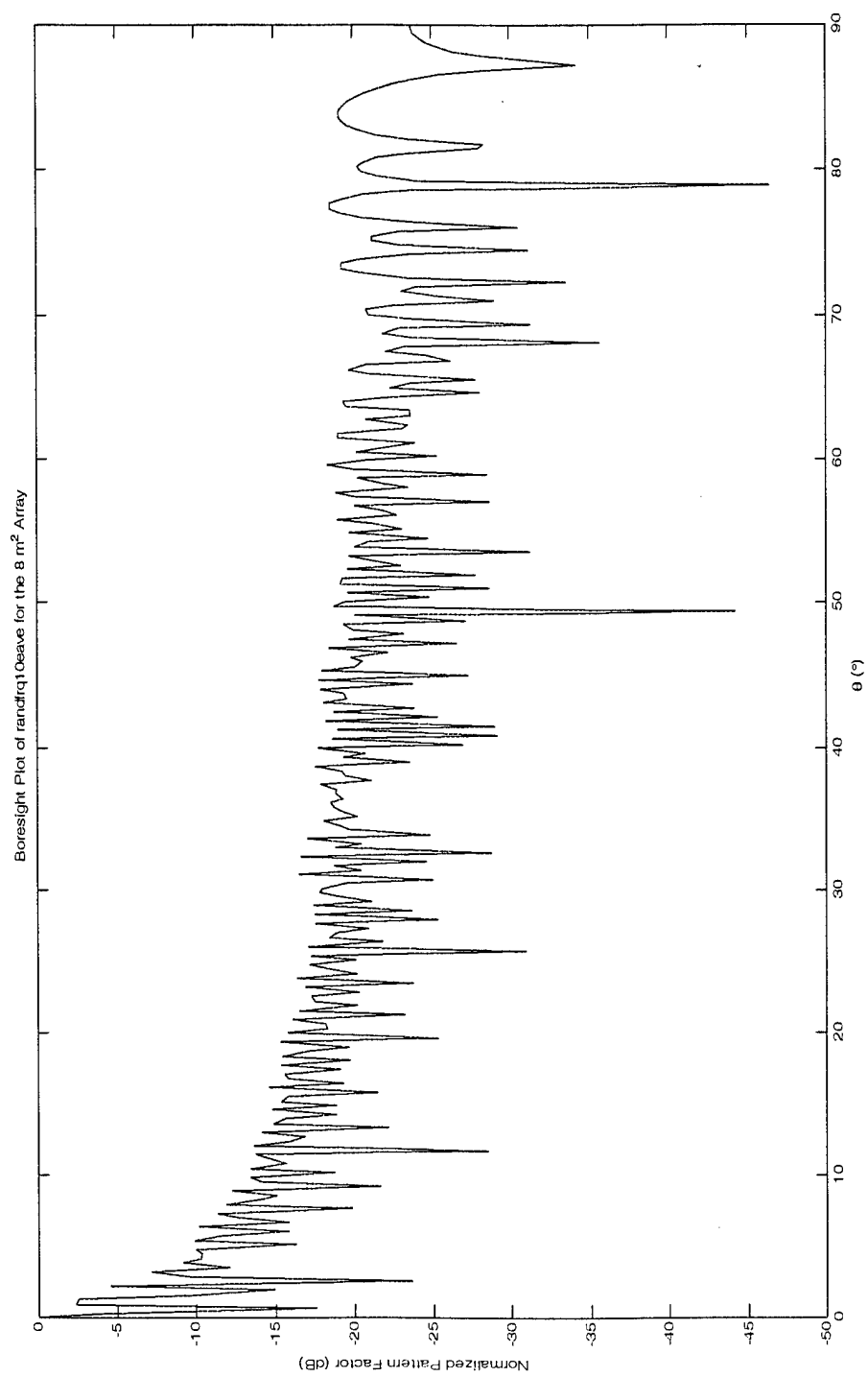


Figure B.11 Random 8m² Array

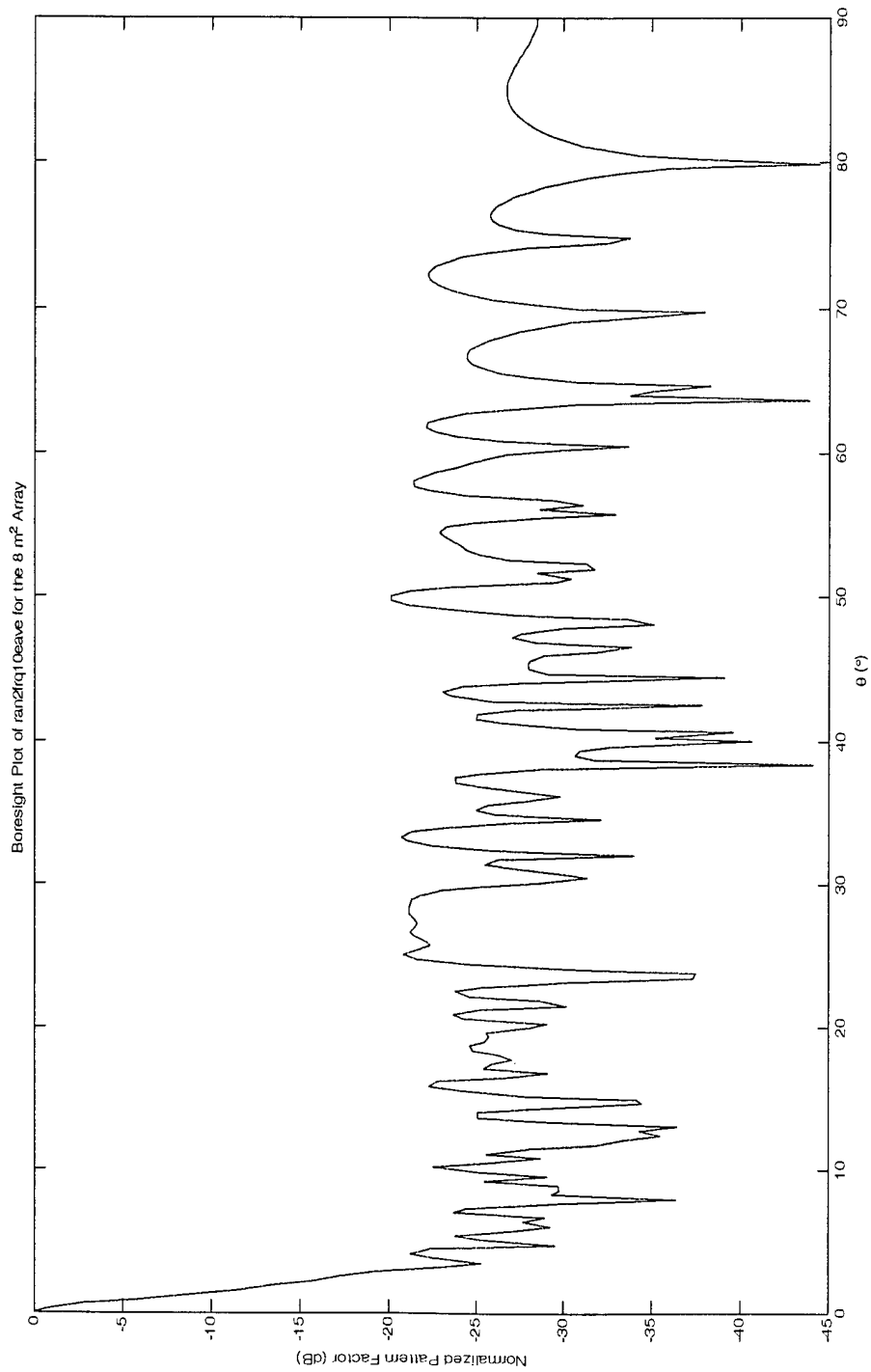


Figure B.12 Random2 8m² Array

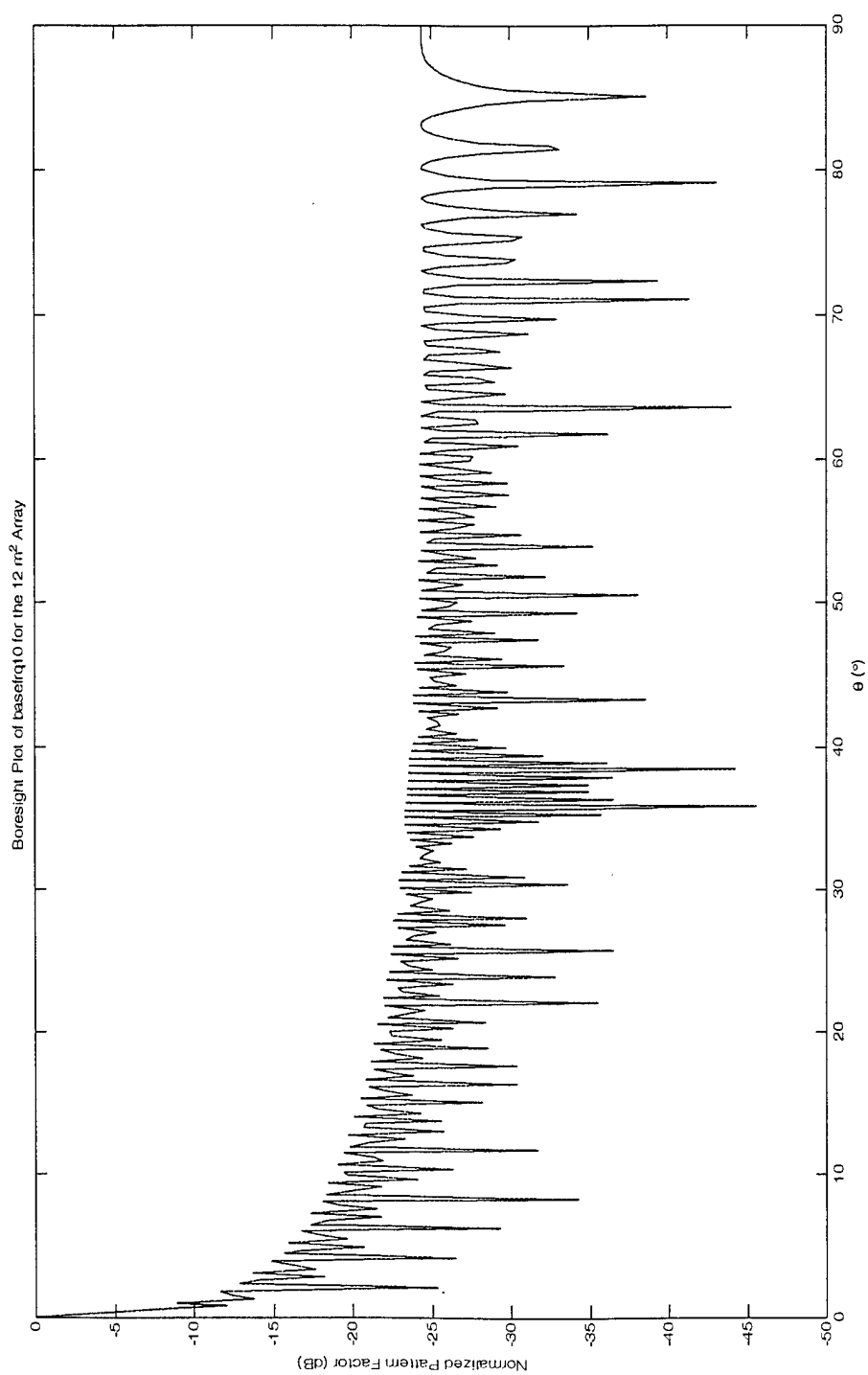


Figure B.13 Baseline 12m² Array

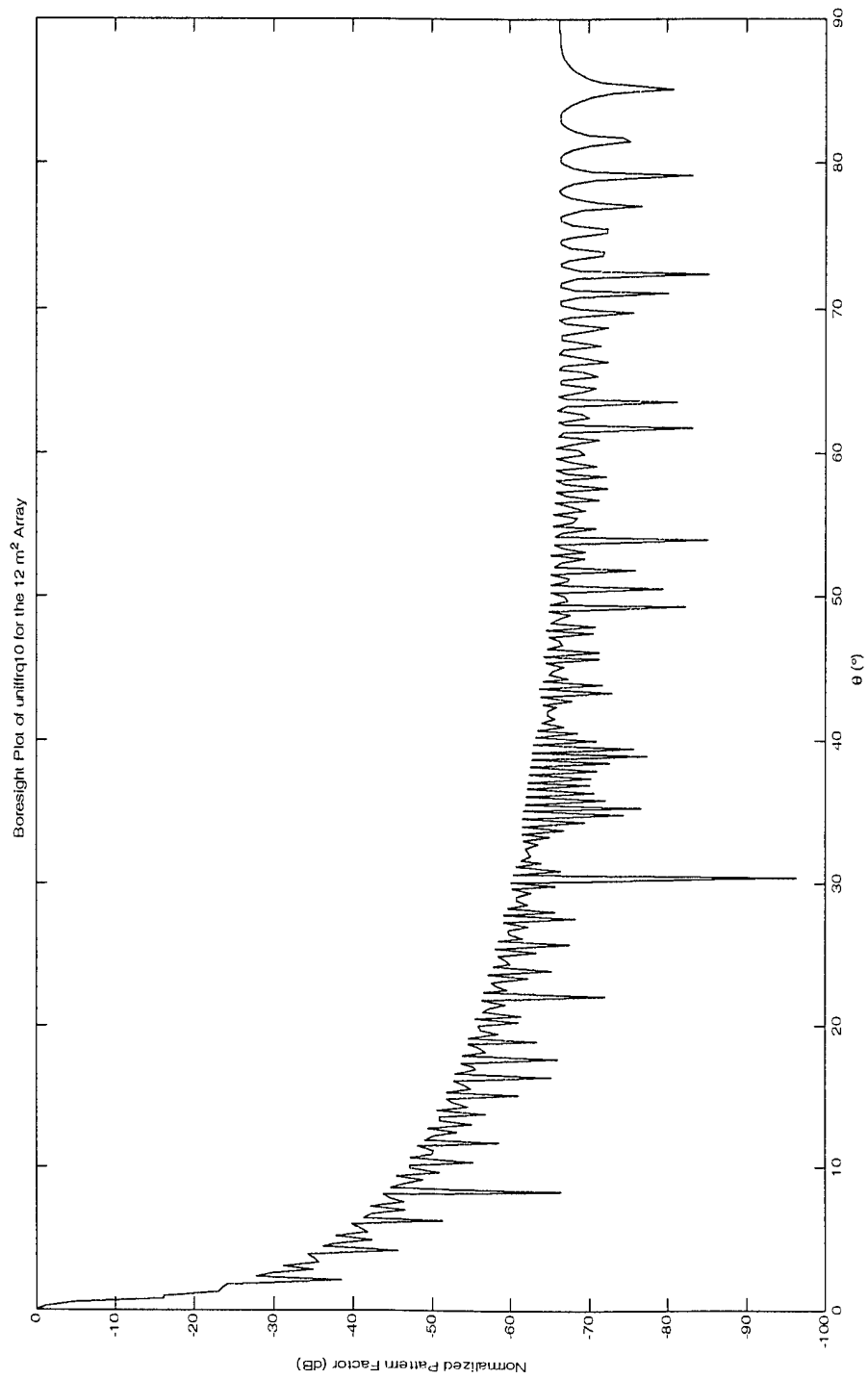


Figure B.14 Uniform 12m² Array

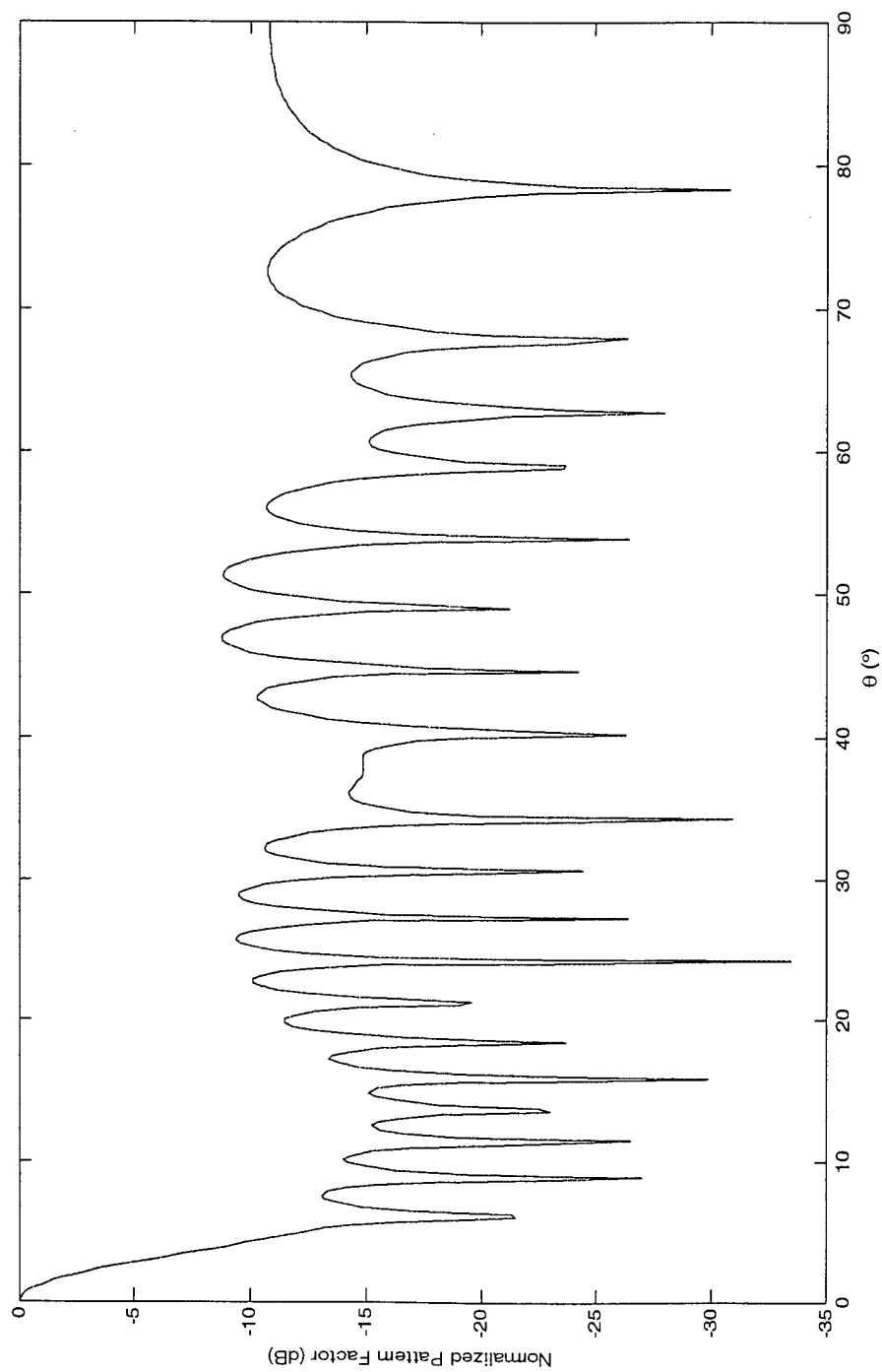


Figure B.15 Deterministic 12m² Array

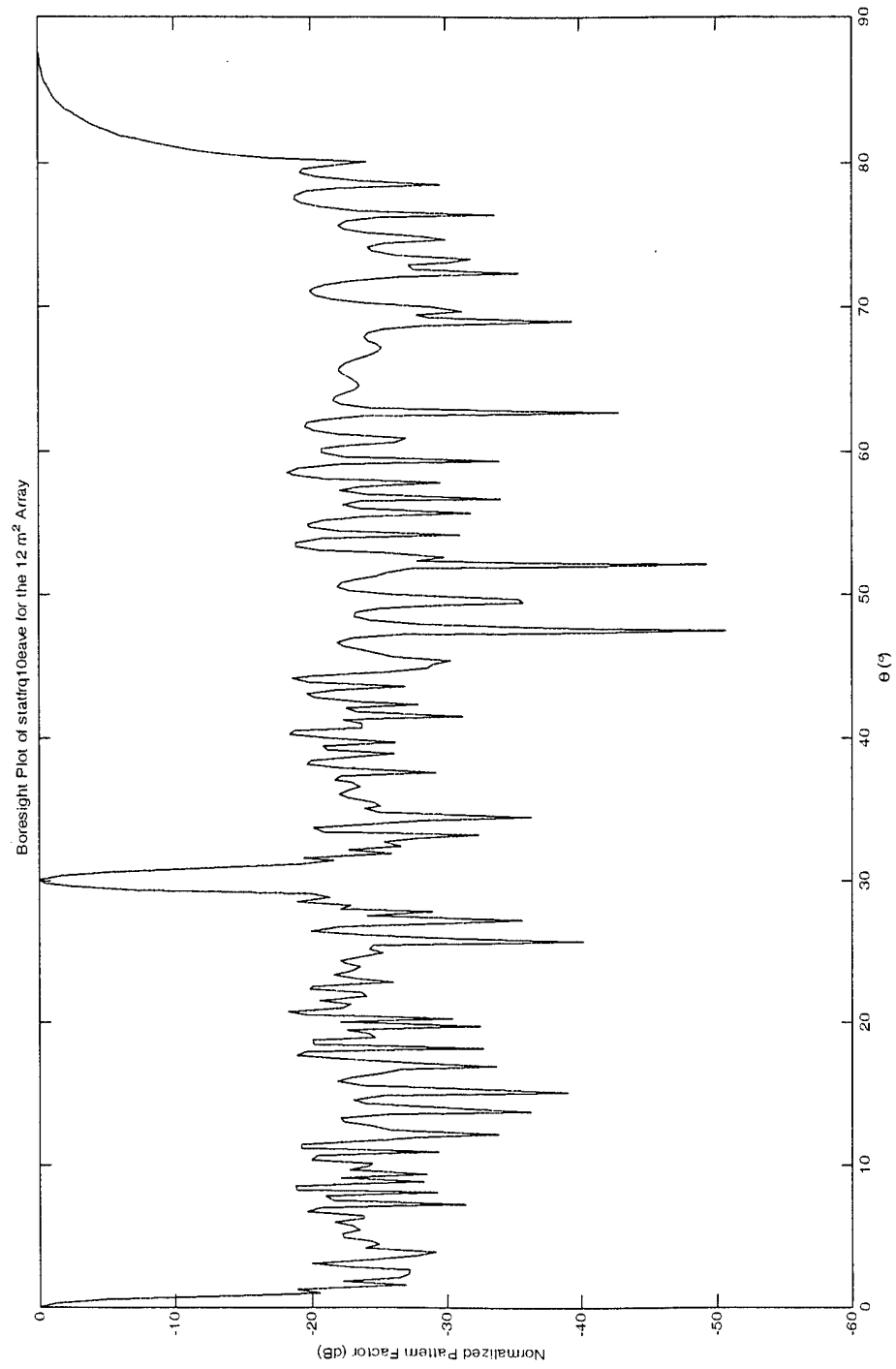


Figure B.16 Statistical 12m² Array

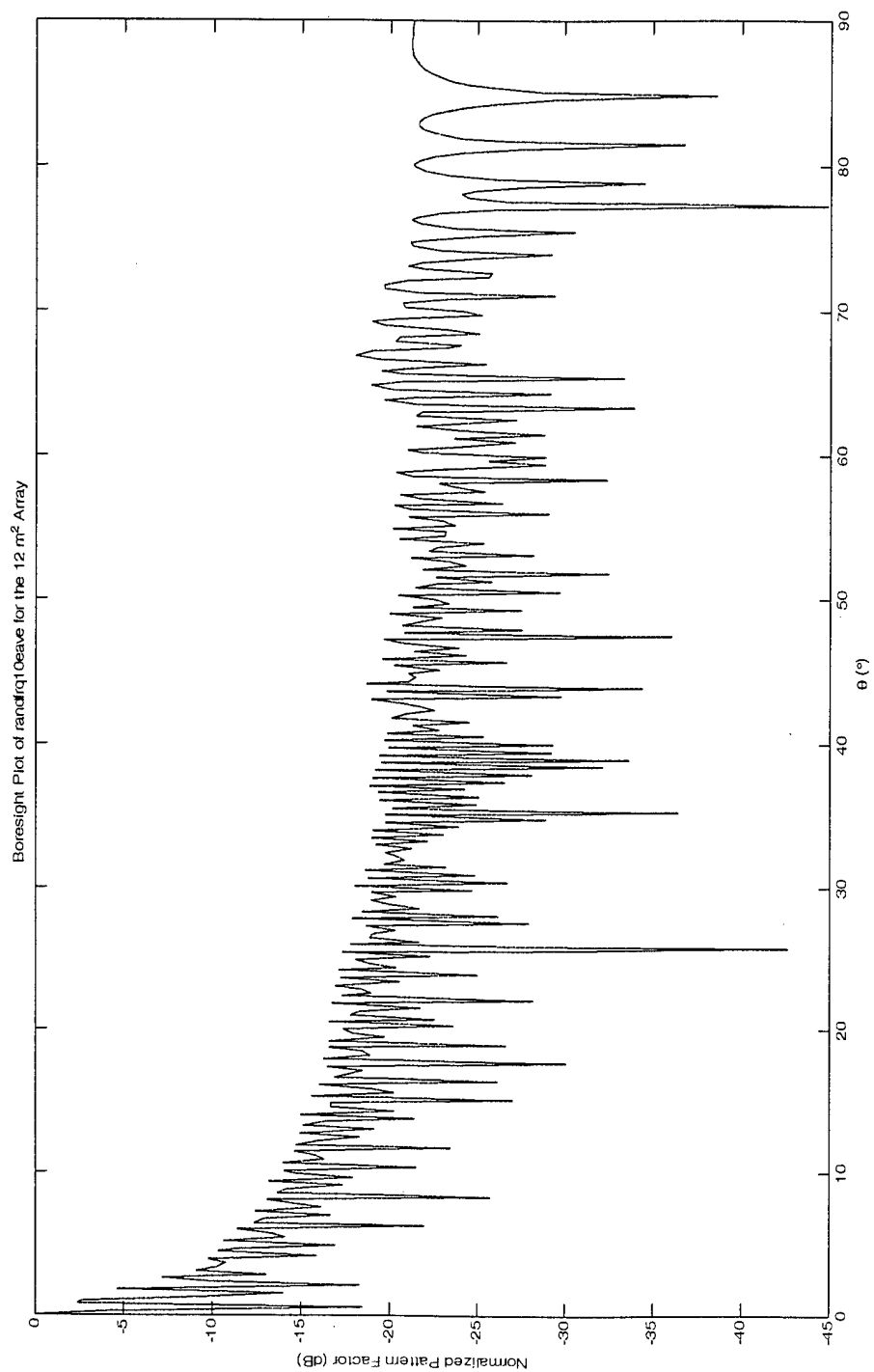


Figure B.17 Random 12m² Array

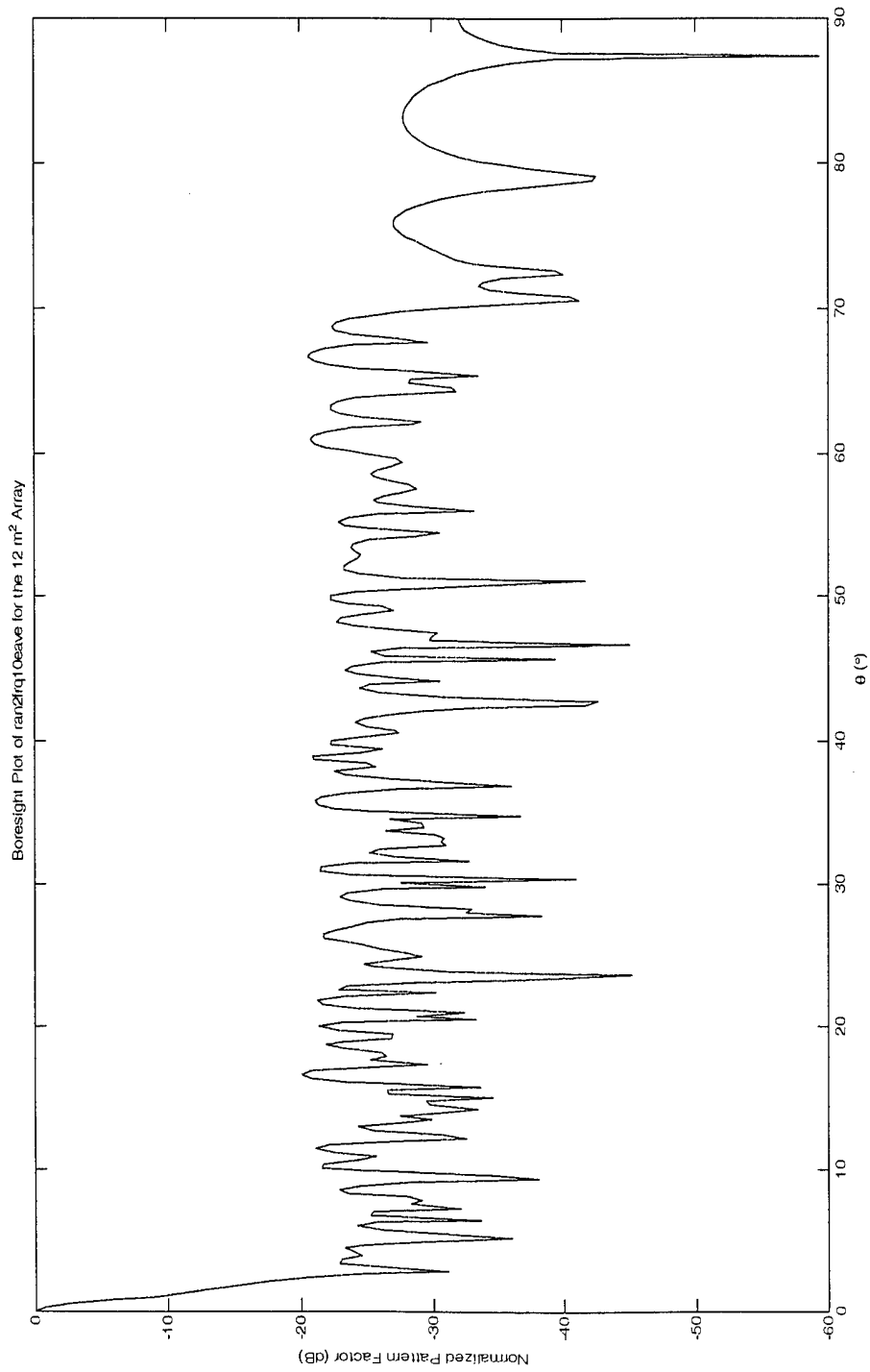


Figure B.18 Random2 12m² Array

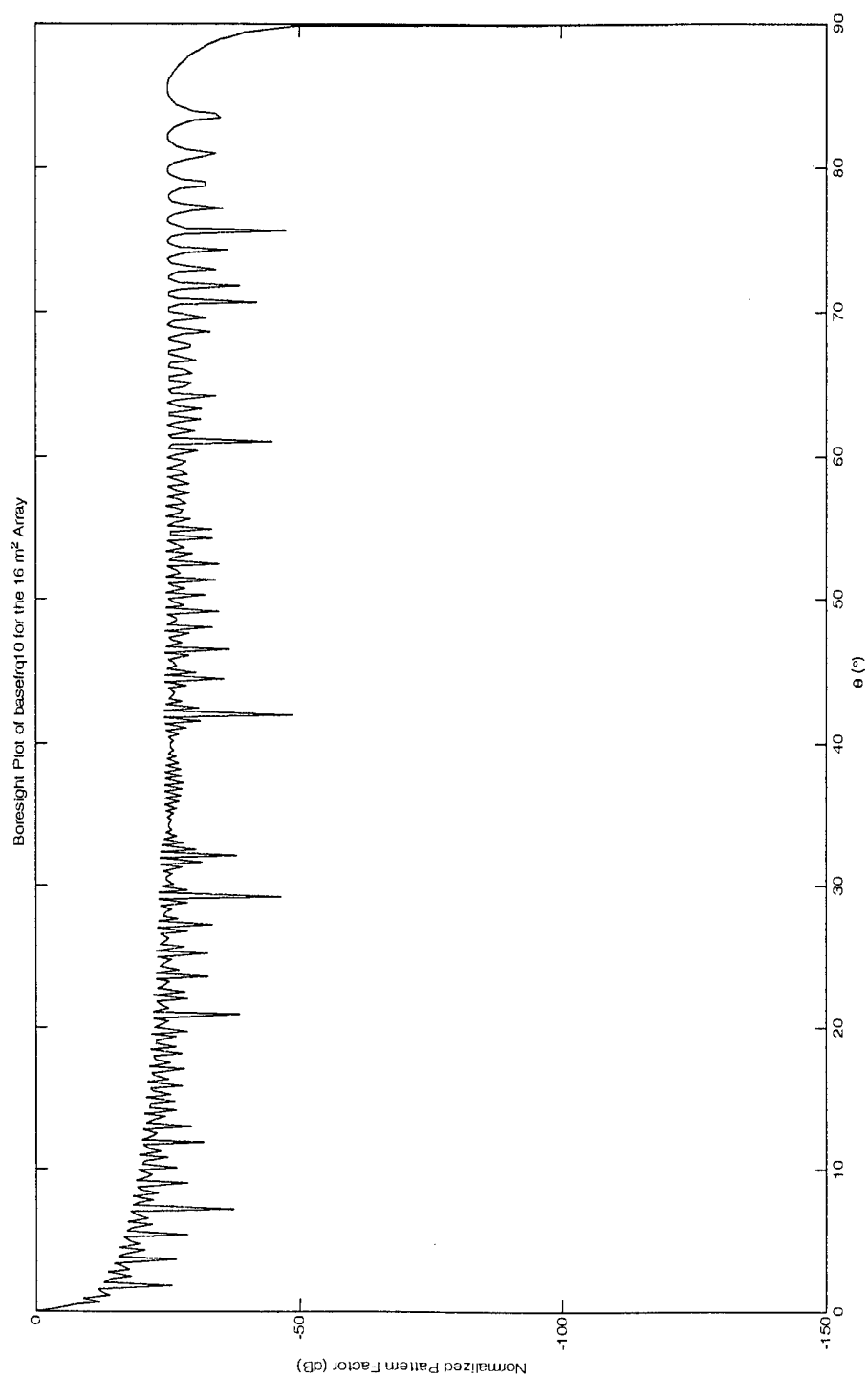


Figure B.19 Baseline 16m² Array

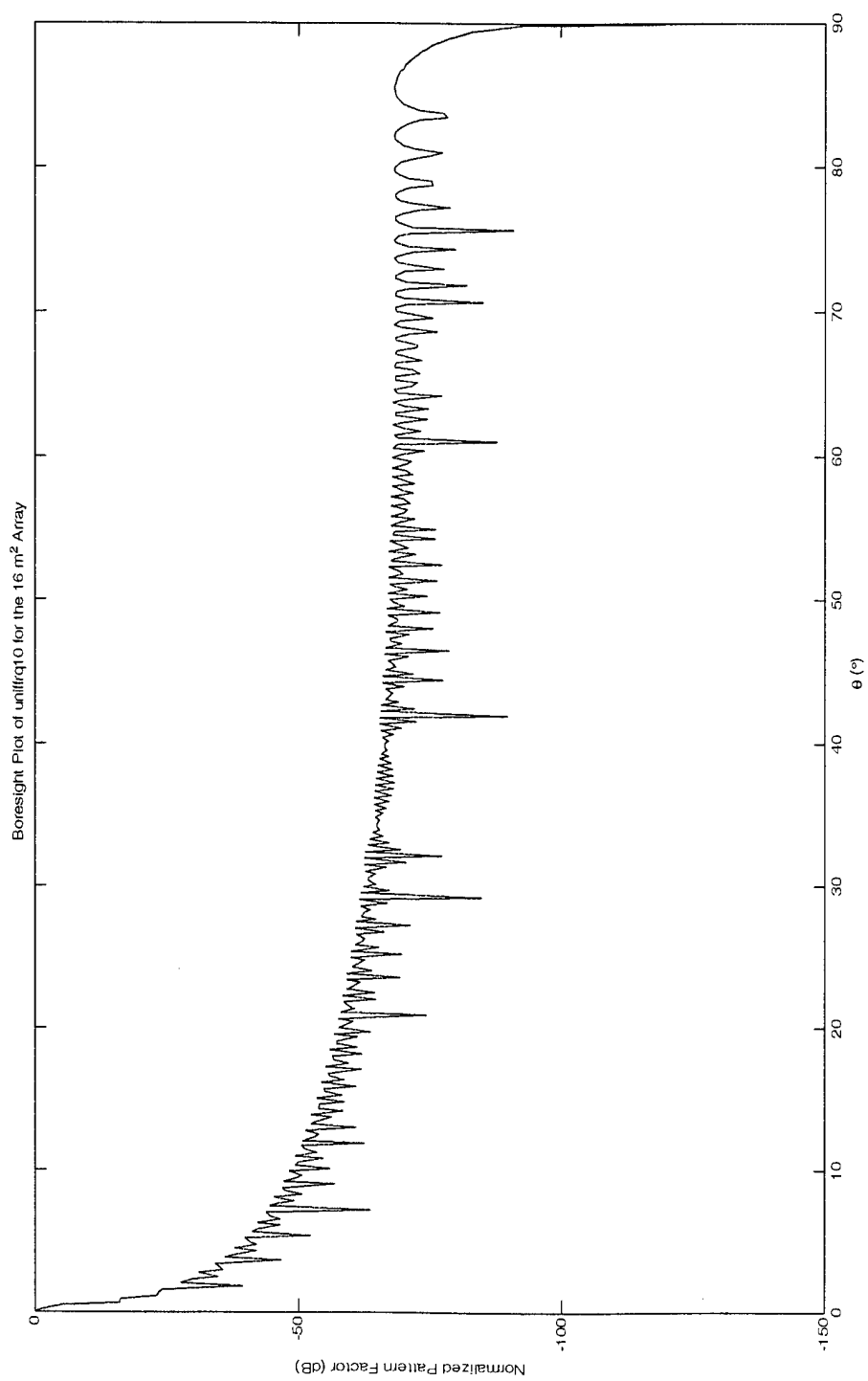


Figure B.20 Uniform 16m² Array

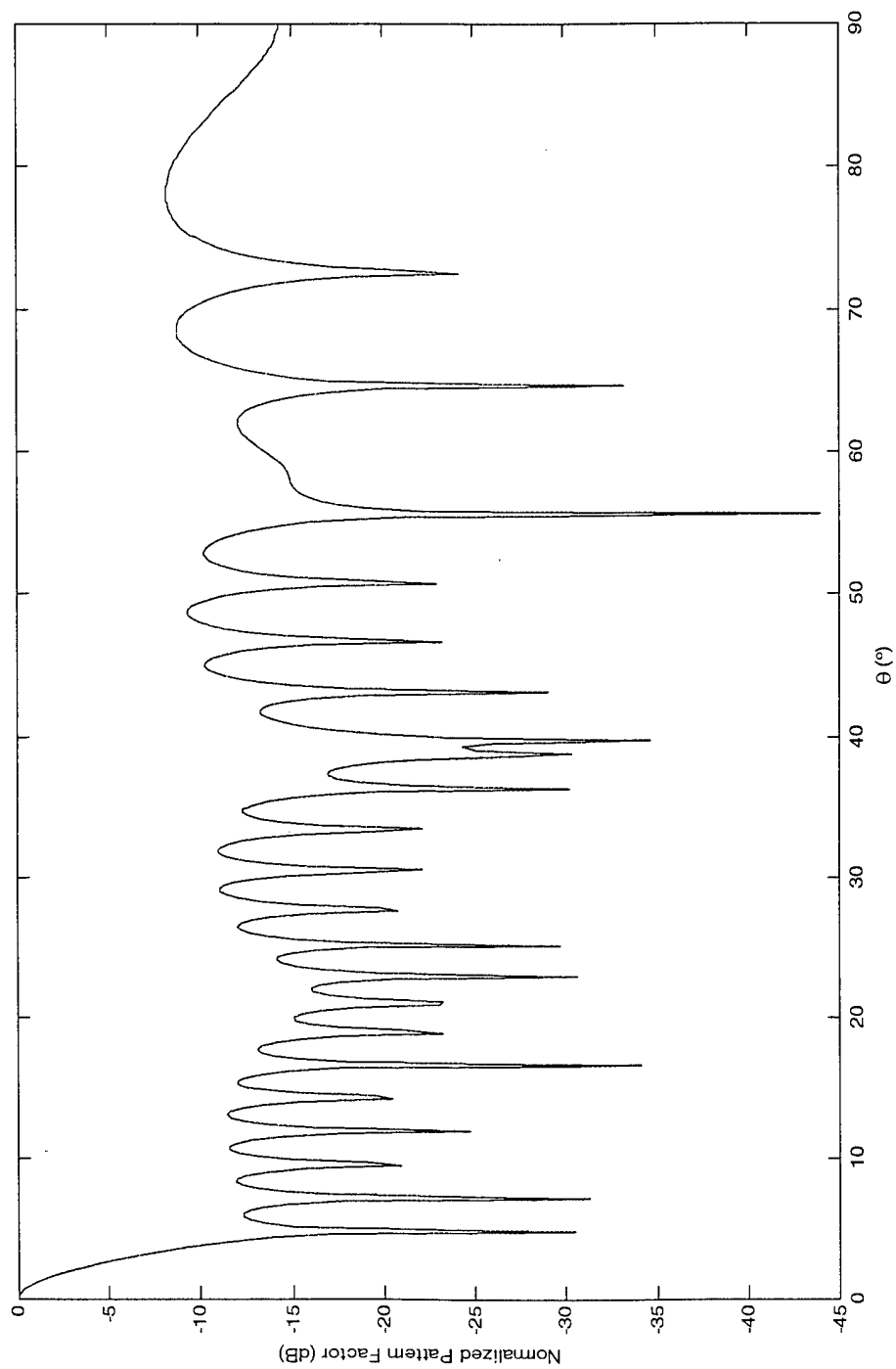


Figure B.21 Deterministic 16m^2 Array

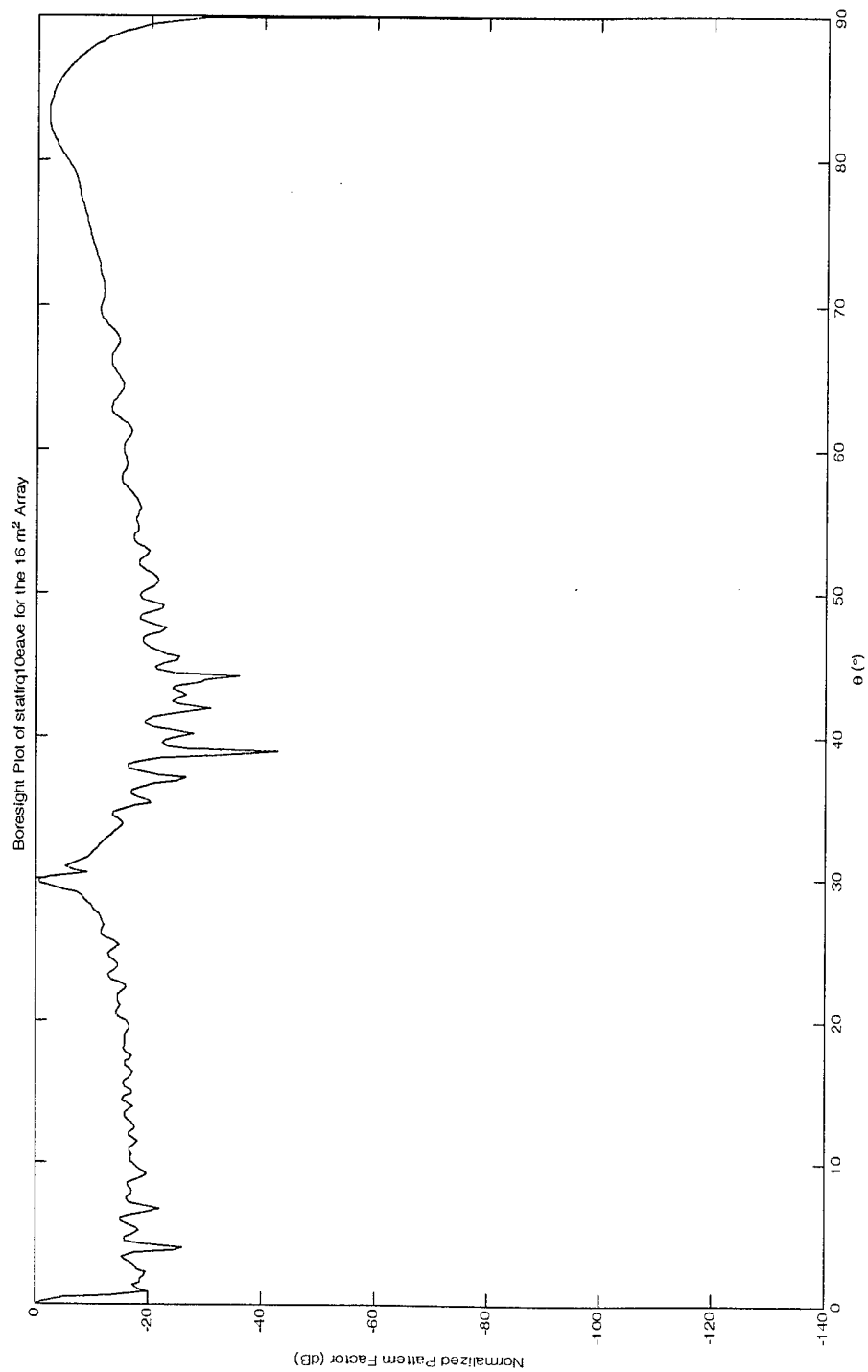


Figure B.22 Statistical 16m² Array

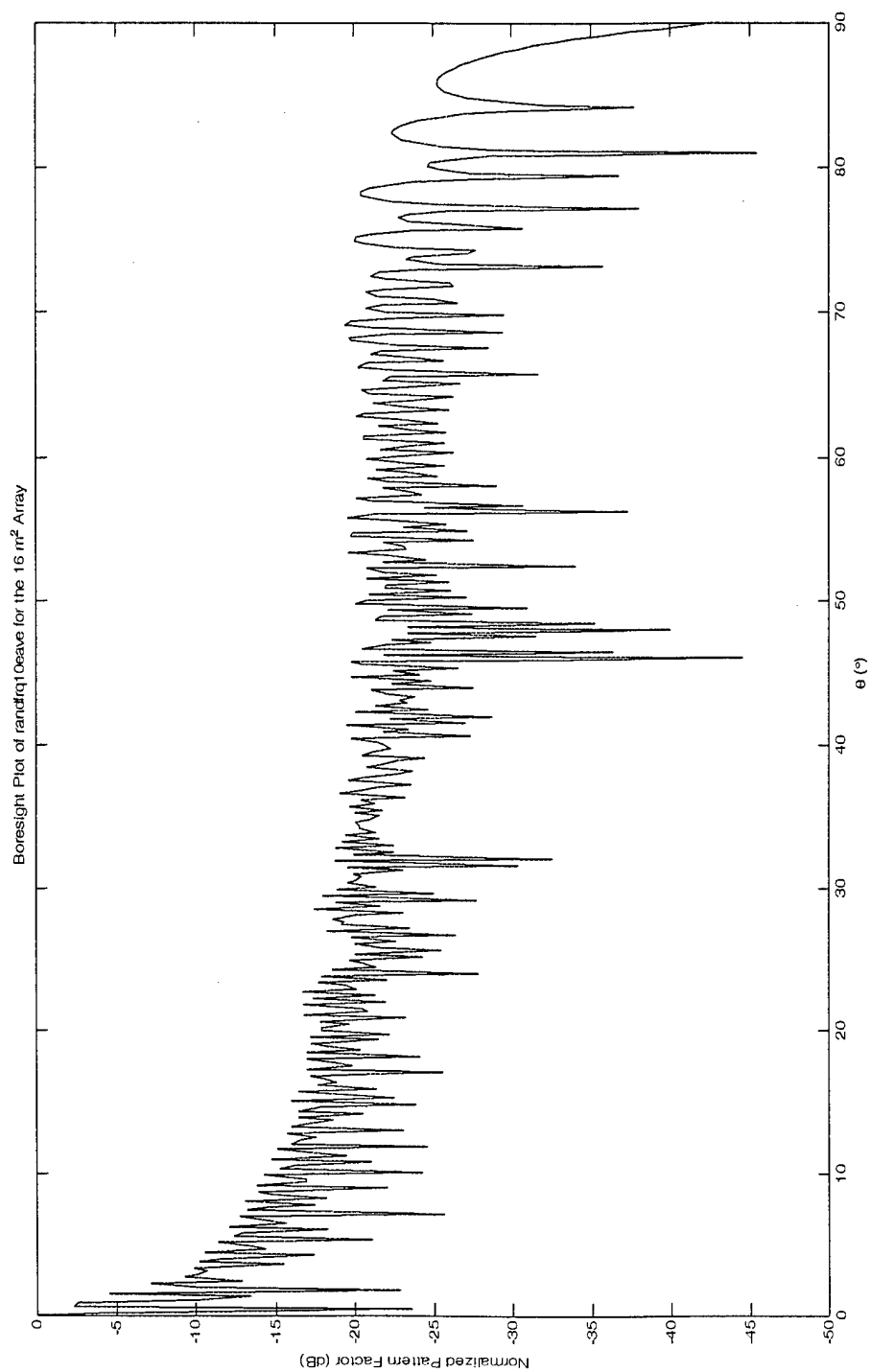


Figure B.23 Random 16m² Array

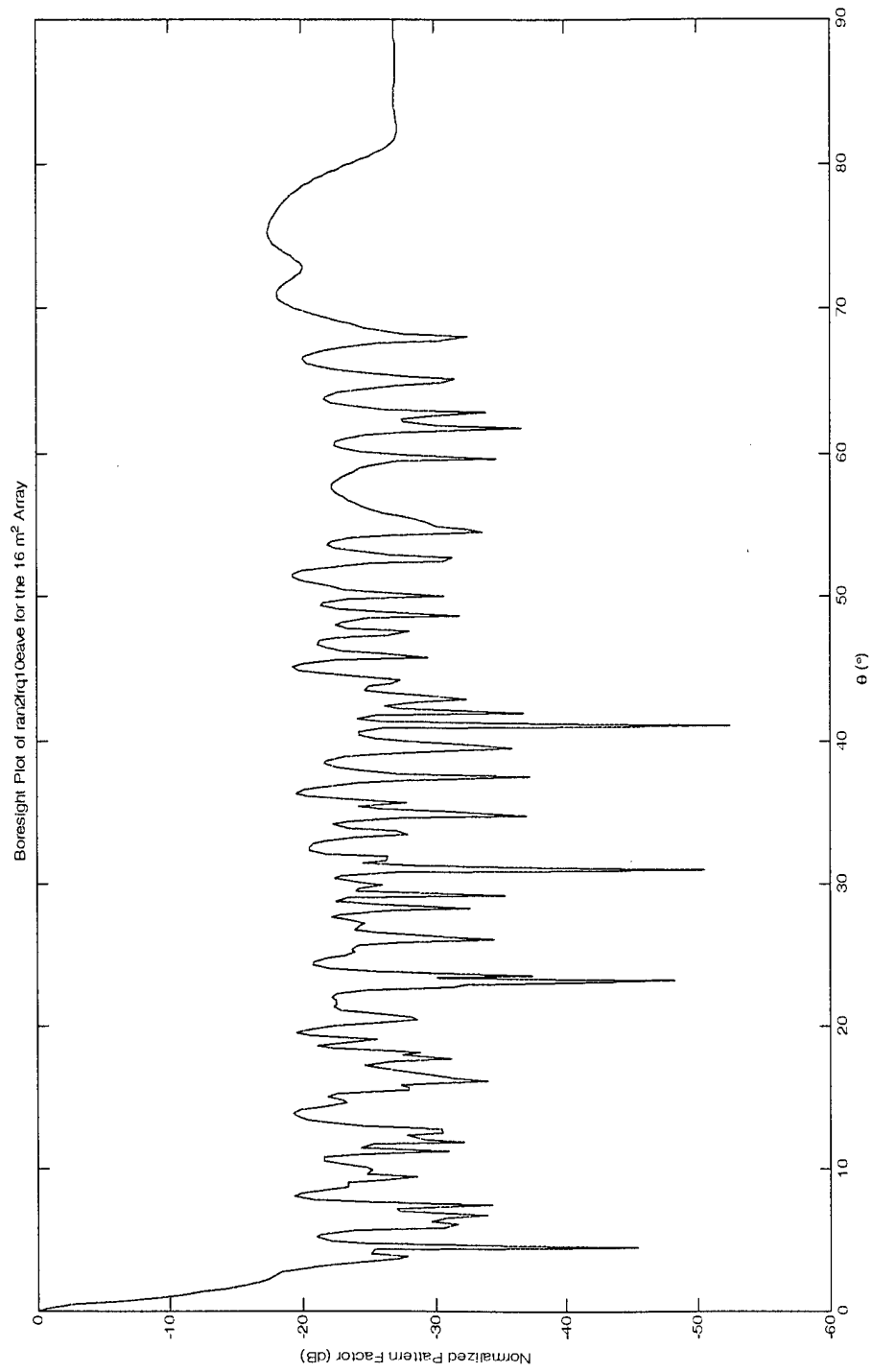


Figure B.24 Random2 16m² Array

APPENDIX C: Boresight Plots of Larger Arrays with Higher β Values

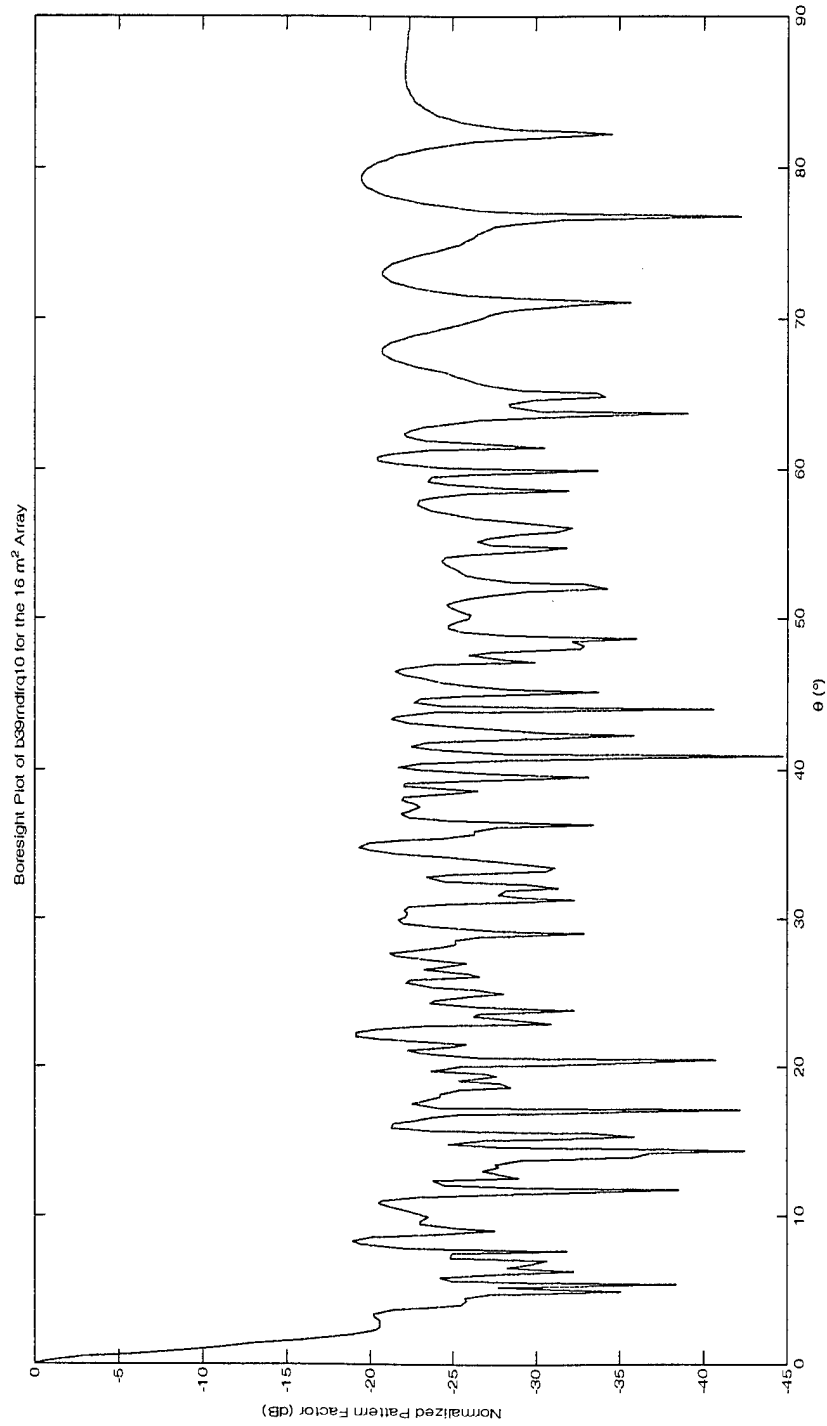


Figure C.1 Random2 $\beta=.999$ 16m² Array

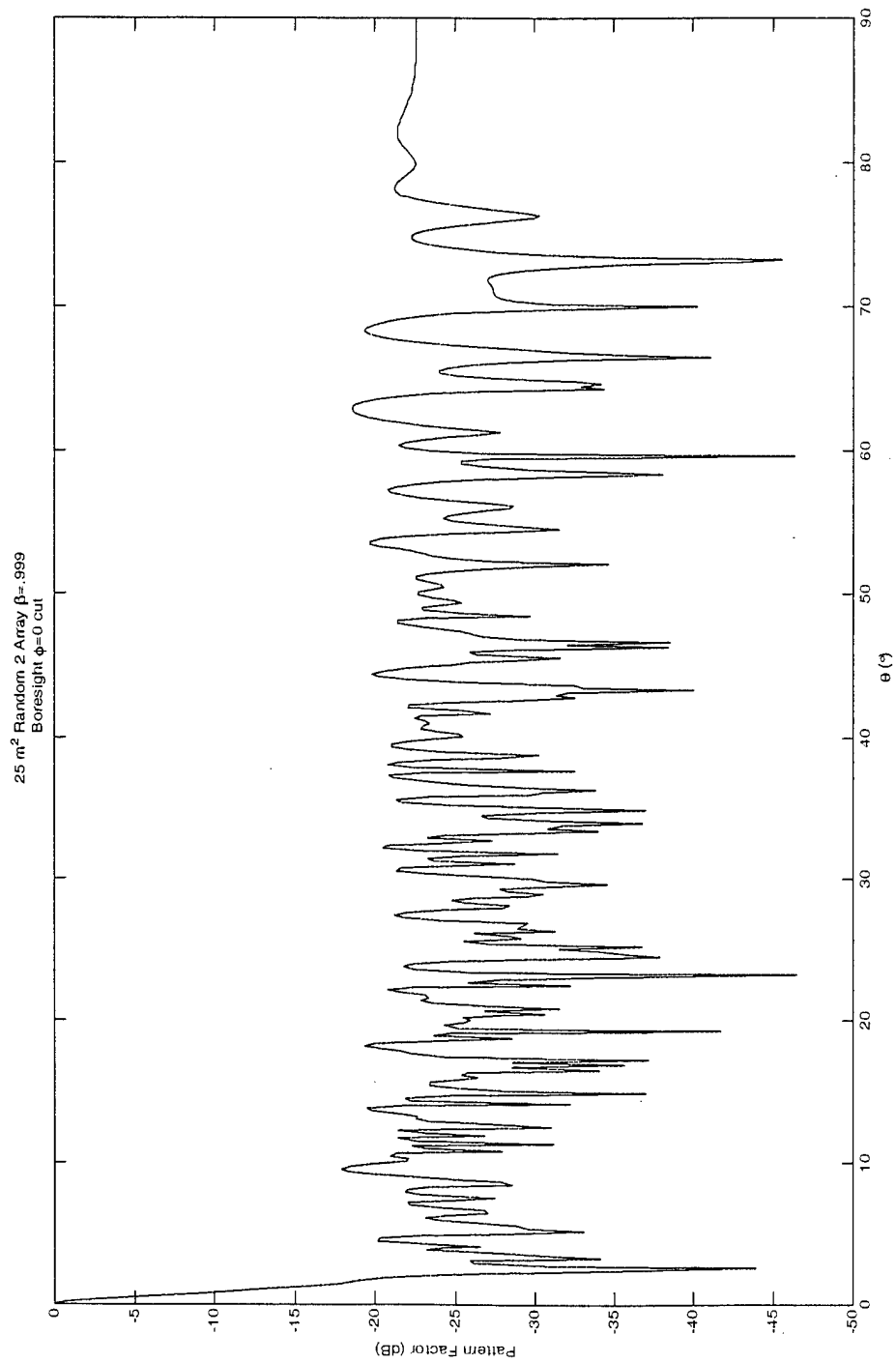


Figure C.2 Random2 $\beta=.999$ 25m² Array

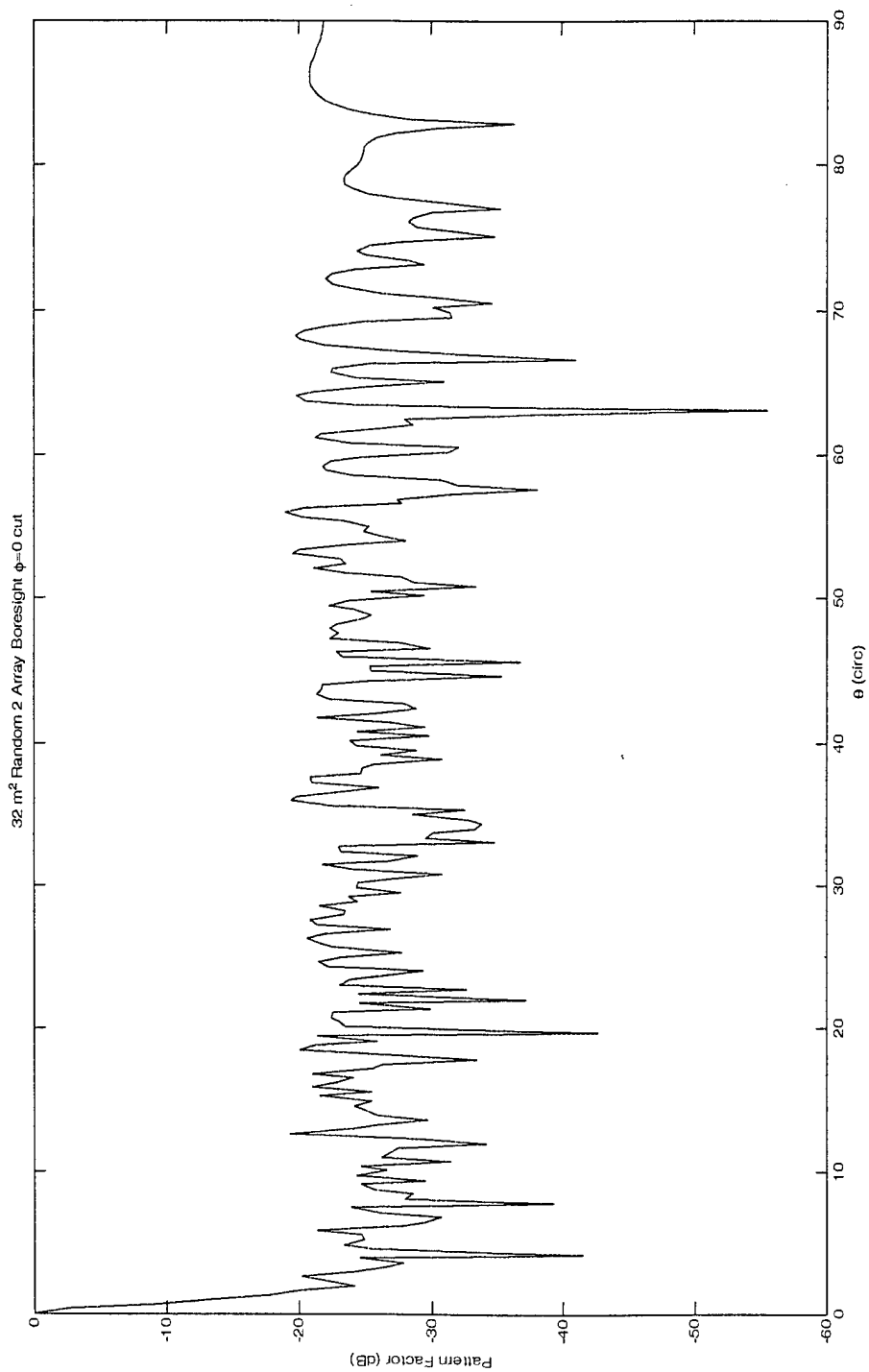


Figure C.3 Random2 $\beta=.999$ 32m² Array

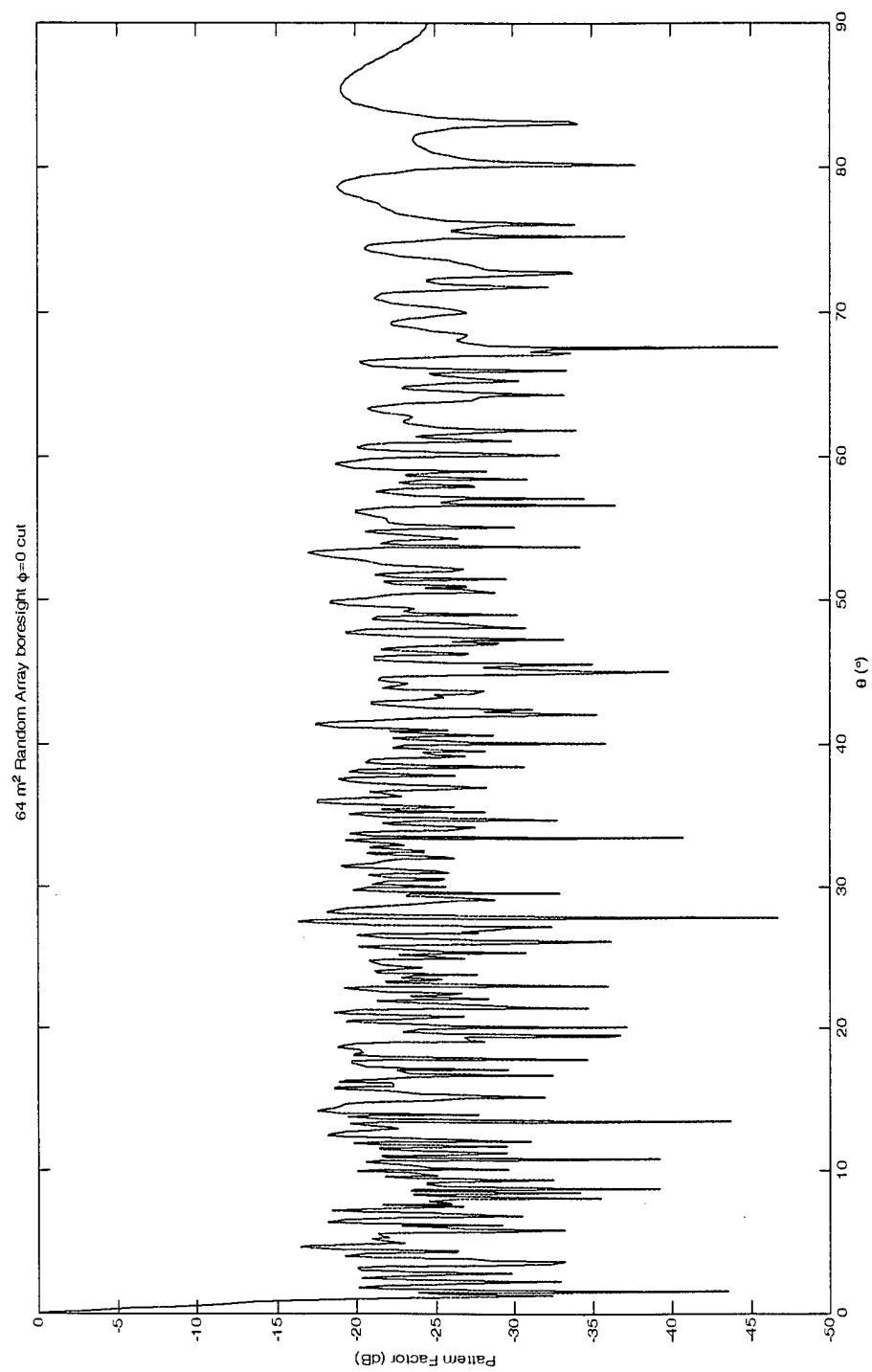


Figure C.4 Random2 $\beta=.999$ 64m² Array

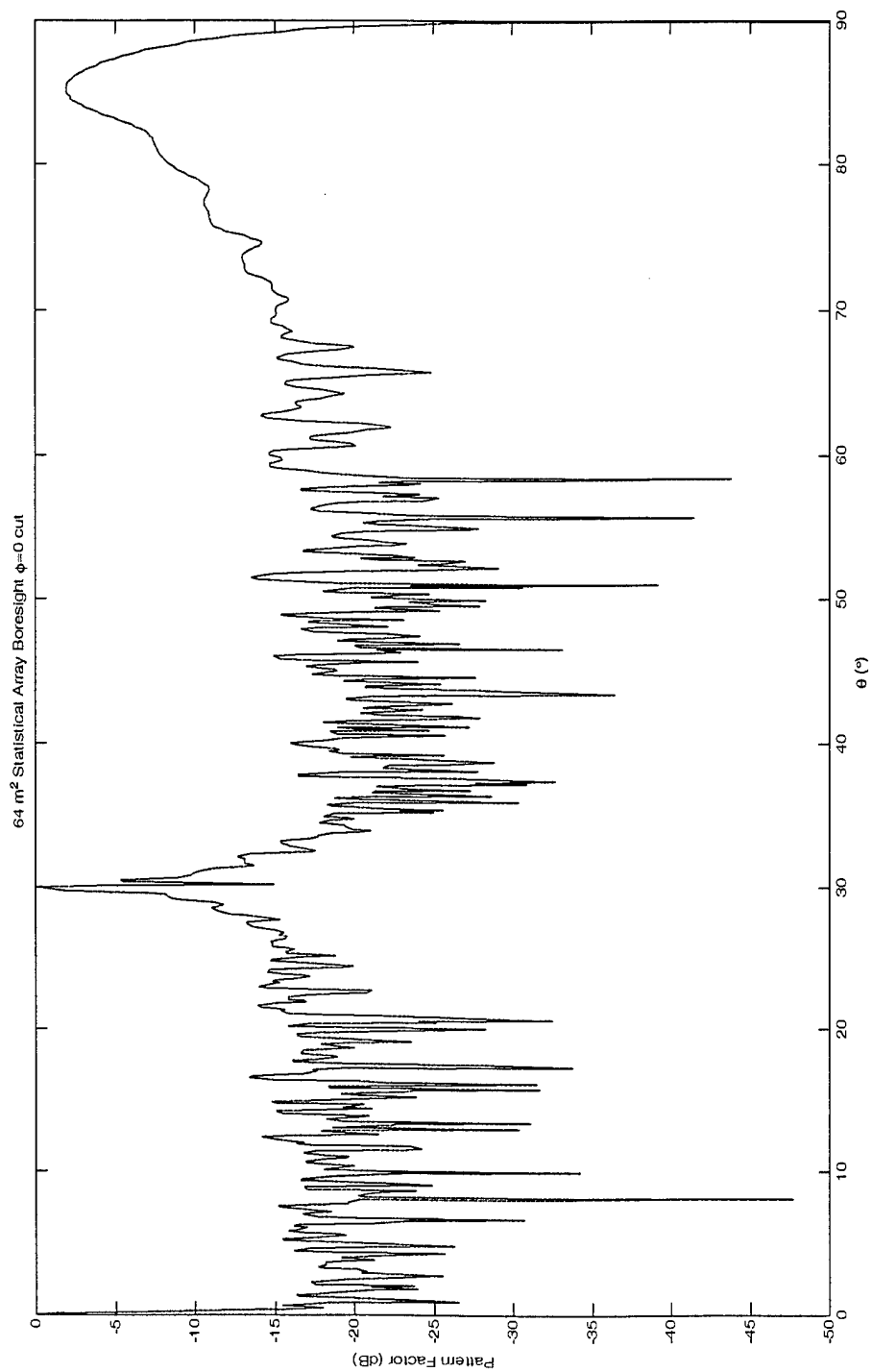


Figure C.5 Statistical 64m² Array

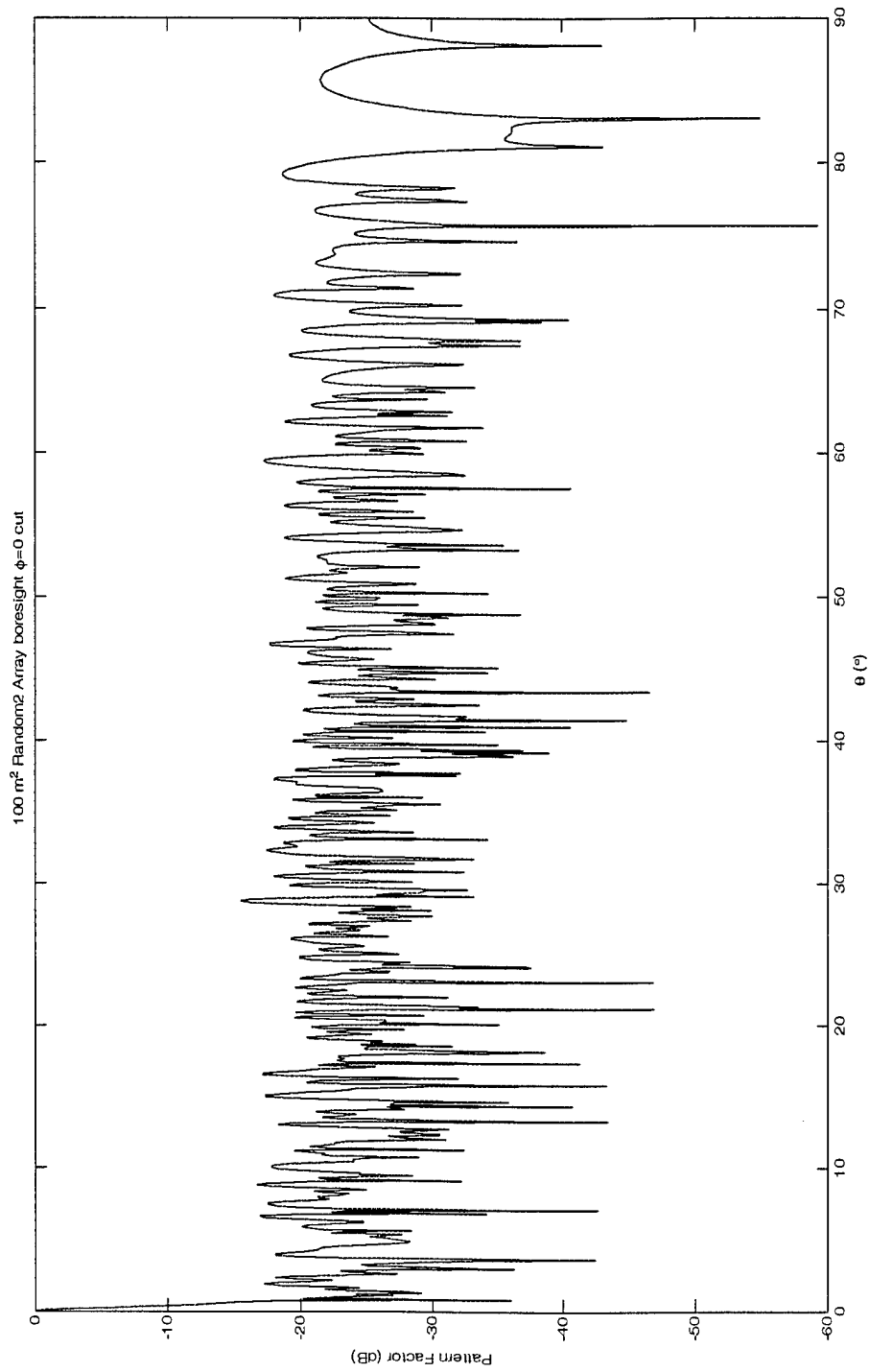


Figure C.6 Random2 $\beta=.999$ 100m² Array

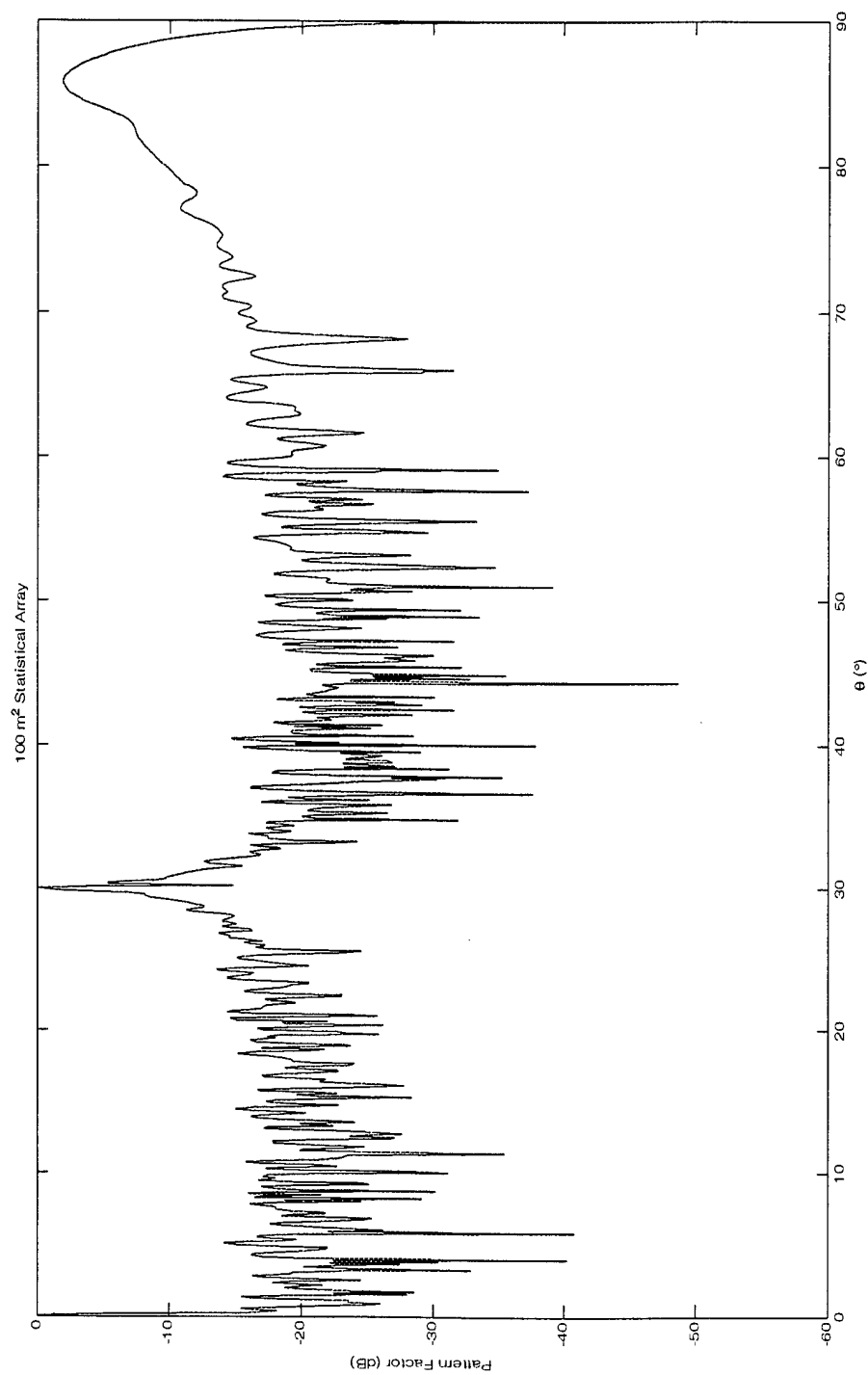


Figure C.5 Statistical 100m² Array

APPENDIX D: Nonprintable Materials List

The CD enclosed contains the following programs

- Th_main.exe: C++ program described in Appendix A.
- Th_avedb.exe: C++ program described in Chapter 5.
- Randanalysis.m: Matlab[®] script described in Chapter 5.
- Statanalysis.m: Matlab[®] script described in Chapter 5.
- Thmetric.m: Matlab[®] script described in Chapter 5.
- Metadj.m: Matlab[®] script to recalculate metric for all metric emphases.
- Resplot.m: Matlab[®] script that generates comparison pattern factor plots when used in conjunction with Thmetric.m.
- Singplt.m: Matlab[®] function that plots a pattern factor filename passed to it.
- Saprmetric.m: Matlab[®] function that computes the metric for a single thinning approach (same as Thmetric.m but only for one approach).
- Trends.m: Matlab[®] script that plots trend line plots for each thinning approach vs. array size.
- HPBW.m: Matlab[®] function for determining the half power beamwidth for a pattern factor.
- PSLE.m: Matlab[®] function that determines the number of angular samples that are greater than a given threshold level.

- Bwinterp.m: Matlab[®] function for use by HPBW.m function for interpolation purposes.
- Detelem.m: Matlab[®] script for generating plots of deterministic element location for the full array.
- Readme.txt: brief text file explaining the contents of the required input file for thmain.exe.

BIBLIOGRAPHY

ANDREASEN, M. G., "Linear Arrays with Variable Interelement Spacings," *IRE Transactions on Antennas and Propagation*, Mar 1962, pp. 137-143.

COLLIN, ROBERT E. and ZUCKER, FRANCIS J., ARRAY THEORY PART 1, 1969, pp. 138-234.

ISHIMARU, AKIRA, "Theory of Unequally-Spaced Array," *IRE Transactions on Antennas and Propagation*, Nov 1962, pp. 691-702.

KING, D. D., PACKARD, R. F., AND THOMAS, R. K., "Unequally-Spaced, Broad-Band Antenna Arrays," *IRE Transactions on Antennas and Propagation*, July 1960, pp. 380-385

LO, Y. T. and R. J. SIMCOE, "An Experiment on Antenna Arrays with Randomly Spaced Elements," *IEEE Transactions on Antennas and Propagation*, Vol. AP-15, No 2, March 1967, pp. 231-235.

LO, Y. T., "Random Periodic Arrays," *Radio Science*, Vol. 3, No 5, May 1968, pp. 425-436.

MAFFETT, A. L., "Array Factors with Nonuniform Spacing Parameter," *IRE Transactions on Antennas and Propagation*, March 1962, pp. 131-136.

SANDLER, SHELDON S., "Some Equivalencies Between Equally and Unequally Spaced Arrays," *IRE Transactions on Antennas and Propagation*, Sept 1960.

SKLAR, BERNARD, DIGITAL COMMUNICATIONS, 1988.

STEINBERG, BENARD D, "The Peak Sidelobe of the Phased Array Having Randomly Located Elements," *IEEE Transactions on Antennas and Propagation*, March 1972.

STEINBERG, BENARD D, Principles of Aperture and Array System Design: Including Random and Adaptive Arrays, 1976.

STUTZMAN, WARREN L., and THIELE, GARY A., ANTENNA THEORY AND DESIGN, 1998.

Vita

Captain Daniel R Richards Jr. was born 24 April 1973 in Phoenix, Arizona. In 1991, he graduated from Kofa High School in Yuma, Arizona. He continued his education by attending Northern Arizona University in Flagstaff, Arizona, where he graduated with a Bachelor of Science degree in Electrical Engineering in December 1995. In February 1996, he received his commission through AFROTC Detachment 027 of Northern Arizona University.

He was assigned to the Air Force Information Warfare Center, Headquarters Air Intelligence Agency, Kelly AFB. Where he was an electronic warfare systems engineer. He also served on the HQ Air Intelligence Agency Honor Guard for two years, spending the second year as the commander. In August of 1998, he entered the Air Force Institute of Technology graduate program in Electrical Engineering. His primary sequence is communications, and secondary sequence of radar. Upon graduation, his follow on assignment is to the Apertures and Receivers Branch of the Sensors Directorate at the Air Force Research Laboratory located at Wright-Patterson AFB.

Permanent Address: 7323 E 26th St
Yuma, AZ 85365

1. Type of Product: Computer (Floppy) Disk	2. Operating System/Version: WINDOWS	3. New Product or Replacement: New	4. Type of File: Software
5. Language/Utility Program: MICROSOFT VISUAL C++ V6 MATLAB			
6. # of Files/# of Products: 29/0	7. Character Set: ASCII	8. Disk Capacity: 1.44 MB	
	9. Compatibility: PC	10. Disk Size: 3 1/2	
11. Title: APERIODIC ARRAY PATTERN FACTOR GENERATION AND COMPUTATION SOFTWARE(U)			
12. Performing Organization: AIR FORCE INSTITUTE OF TECH GRAD SCHOOL OF ENGR & MGNT 2950 P ST WPAFB OH 45433	13. Performing Report #: AFIT/GE/ENG/00M-14	14. Contract #:	
		15. Program Element #:	
16. Sponsor/Monitor: AF RESEARCH LAB SENSORS DIRECTORATE 2241 AVIONICS CIRCLE WPAFB, OH 45433	17. Sponsor/Monitor # Acronym: AFRL/SNRP	19. Project #:	
	18. Sponsor/Monitor #:	20. Task #:	
		21. Work Unit #:	
22. Date: March 15, 2000		23. Classification of Product: Unclassified	
24. Security Classification Authority:		25. Declassification/Downgrade Schedule:	
26. Distribution/Availability: A Approved for public release; distribution is unlimited.			

27. Abstract: This thesis provides a method to reduce physical resource requirements along with cost reduction in Space Based Radar (SBR) platforms, and provides a rule of thumb for randomization effects on arrays. A trend analysis is performed on 4, 8, 12, and 16 square meter arrays. Three aperiodic thinning approaches are examined. They are an equal current density element distribution, a random periodic grid of elements, and random element distribution based a peak sidelobe indicator. According to the metrics used, the statistical and deterministic array thinning approaches performed best for these small arrays. However, the statistical arrays have a scan angle limitation of $\theta_0=30^\circ$ due to the interelement spacing of two wavelengths. The deterministic does poorly with peak sidelobes. The random array performance was limited due to the relatively small array sizes for the random approach used. The small size limits the array's capability to meet the peak sidelobe threshold requirement, due to a reduced confidence level, along with limiting the effective area to be randomized. However, as the array size increased, the thinning levels and performance increased to become competitive with the other array approaches. With these trends, the random array is the ideal solution.

28. Classification of Abstract:

Unclassified

29. Limitation of Abstract:

Unclassified Unlimited

30. Subject Terms:APERIODIC ARRAYS
NONUNIFORM ARRAYS (U)**30a. Classification of Subject Terms:**

Unclassified

31. Required Peripherals:**32. # of Physical Records:****33. # of Logical Records:****34. # of Tracks:****35. Record Type:****36. Color:****37. Recording System:****38. Recording Density:****39. Parity:****40. Playtime:****41. Playback
Speed:****42. Video:****43. Text:****44. Still
Photos:****45. Audio:****46. Other:****47. Documentation/Supplemental Information:****48. Point of Contact and Telephone Number:**PETER J. COLLINS, MAJ, USAF
2950 P ST
93725565654304
peter.collins@afit.af.mil

REPORT DOCUMENTATION PAGE					Form Approved OMB No. 0704-0188	
<p>The public reporting burden for this collection of information is estimated to average 1 hour per response, including the time for reviewing instructions, searching existing data sources, gathering and maintaining the data needed, and completing and reviewing the collection of information. Send comments regarding this burden estimate or any other aspect of this collection of information, including suggestions for reducing the burden, to Department of Defense, Washington Headquarters Services, Directorate for Information Operations and Reports (0704-0188), 1215 Jefferson Davis Highway, Suite 1204, Arlington, VA 22202-4302. Respondents should be aware that notwithstanding any other provision of law, no person shall be subject to any penalty for failing to comply with a collection of information if it does not display a currently valid OMB control number.</p> <p>PLEASE DO NOT RETURN YOUR FORM TO THE ABOVE ADDRESS.</p>						
1. REPORT DATE (DD-MM-YYYY) 21-03-2000		2. REPORT TYPE Master's Thesis			3. DATES COVERED (From - To) 07-1998 - 03-2000	
4. TITLE AND SUBTITLE NONUNIFORMLY SPACED ARRAY ELEMENTS				5a. CONTRACT NUMBER		
				5b. GRANT NUMBER		
				5c. PROGRAM ELEMENT NUMBER		
				5d. PROJECT NUMBER		
6. AUTHOR(S) RICHARDS, DANIEL, R, JR				5e. TASK NUMBER		
				5f. WORK UNIT NUMBER		
7. PERFORMING ORGANIZATION NAME(S) AND ADDRESS(ES) Air Force Institute of Technology Graduate School of Engineering and Management AFIT/ENG 2950 P St. WPAFB OH 45433-7765				8. PERFORMING ORGANIZATION REPORT NUMBER AFIT/GE/ENG/00M-14		
9. SPONSORING/MONITORING AGENCY NAME(S) AND ADDRESS(ES) Air Force Research Lab Sensors Directorate ATTN: Dr Stephen Schneider 2241 Avionics Circle WPAFB OH 45433				10. SPONSOR/MONITOR'S ACRONYM(S) AFRL/SNRP		
				11. SPONSOR/MONITOR'S REPORT NUMBER(S)		
12. DISTRIBUTION/AVAILABILITY STATEMENT APPROVED FOR PUBLIC RELEASE; DISTRIBUTION UNLIMITED						
13. SUPPLEMENTARY NOTES Advisor: Maj Peter J. Collins, ENG, DSN: 785-6565 x4304						
14. ABSTRACT This thesis provides a method to reduce physical resource requirements along with cost reduction in Space Based Radar (SBR) platforms, and provides a rule of thumb for randomization effects on arrays. A trend analysis is performed on 4, 8, 12, and 16 square meter arrays. Three aperiodic thinning approaches are examined. They are an equal current density element distribution, a random periodic grid of elements, and random element distribution based a peak sidelobe indicator. According to the metrics used, the statistical and deterministic array thinning approaches performed best for these small arrays. However, the statistical arrays have a scan angle limitation of $q_0 = 30^\circ$ due to the interelement spacing of two wavelengths. The deterministic does poorly with peak sidelobes. The random array performance was limited due to the relatively small array sizes for the random approach used. The small size limits the array's capability to meet the peak sidelobe threshold requirement, due to a reduced confidence level, along with limiting the effective area to be randomized. However, as the array size increased, the thinning levels and performance increased to become competitive with the other array approaches. If trends continue as array size increases, the random array is the ideal solution.						
15. SUBJECT TERMS Aperiodic Arrays; Nonuniform Arrays; Random Arrays; Aperiodic Array Element Distributions; Nonuniform Array Element Distributions						
16. SECURITY CLASSIFICATION OF:			17. LIMITATION OF ABSTRACT	18. NUMBER OF PAGES	19a. NAME OF RESPONSIBLE PERSON	
a. REPORT	b. ABSTRACT	c. THIS PAGE			Peter J. Collins, Maj, USAF	
U	U	U	UL	141	19b. TELEPHONE NUMBER (Include area code) (937) 255-3636 x4619	

INSTRUCTIONS FOR COMPLETING SF 298

1. REPORT DATE. Full publication date, including day, month, if available. Must cite at least the year and be Year 2000 compliant, e.g. 30-06-1998; xx-06-1998; xx-xx-1998.

2. REPORT TYPE. State the type of report, such as final, technical, interim, memorandum, master's thesis, progress, quarterly, research, special, group study, etc.

3. DATES COVERED. Indicate the time during which the work was performed and the report was written, e.g., Jun 1997 - Jun 1998; 1-10 Jun 1996; May - Nov 1998; Nov 1998.

4. TITLE. Enter title and subtitle with volume number and part number, if applicable. On classified documents, enter the title classification in parentheses.

5a. CONTRACT NUMBER. Enter all contract numbers as they appear in the report, e.g. F33615-86-C-5169.

5b. GRANT NUMBER. Enter all grant numbers as they appear in the report, e.g. AFOSR-82-1234.

5c. PROGRAM ELEMENT NUMBER. Enter all program element numbers as they appear in the report, e.g. 61101A.

5d. PROJECT NUMBER. Enter all project numbers as they appear in the report, e.g. 1F665702D1257; ILIR.

5e. TASK NUMBER. Enter all task numbers as they appear in the report, e.g. 05; RF0330201; T4112.

5f. WORK UNIT NUMBER. Enter all work unit numbers as they appear in the report, e.g. 001; AFAPL30480105.

6. AUTHOR(S). Enter name(s) of person(s) responsible for writing the report, performing the research, or credited with the content of the report. The form of entry is the last name, first name, middle initial, and additional qualifiers separated by commas, e.g. Smith, Richard, J, Jr.

7. PERFORMING ORGANIZATION NAME(S) AND ADDRESS(ES). Self-explanatory.

8. PERFORMING ORGANIZATION REPORT NUMBER. Enter all unique alphanumeric report numbers assigned by the performing organization, e.g. BRL-1234; AFWL-TR-85-4017-Vol-21-PT-2.

9. SPONSORING/MONITORING AGENCY NAME(S) AND ADDRESS(ES). Enter the name and address of the organization(s) financially responsible for and monitoring the work.

10. SPONSOR/MONITOR'S ACRONYM(S). Enter, if available, e.g. BRL, ARDEC, NADC.

11. SPONSOR/MONITOR'S REPORT NUMBER(S). Enter report number as assigned by the sponsoring/monitoring agency, if available, e.g. BRL-TR-829; -215.

12. DISTRIBUTION/AVAILABILITY STATEMENT. Use agency-mandated availability statements to indicate the public availability or distribution limitations of the report. If additional limitations/ restrictions or special markings are indicated, follow agency authorization procedures, e.g. RD/FRD, PROPIN, ITAR, etc. Include copyright information.

13. SUPPLEMENTARY NOTES. Enter information not included elsewhere such as: prepared in cooperation with; translation of; report supersedes; old edition number, etc.

14. ABSTRACT. A brief (approximately 200 words) factual summary of the most significant information.

15. SUBJECT TERMS. Key words or phrases identifying major concepts in the report.

16. SECURITY CLASSIFICATION. Enter security classification in accordance with security classification regulations, e.g. U, C, S, etc. If this form contains classified information, stamp classification level on the top and bottom of this page.

17. LIMITATION OF ABSTRACT. This block must be completed to assign a distribution limitation to the abstract. Enter UU (Unclassified Unlimited) or SAR (Same as Report). An entry in this block is necessary if the abstract is to be limited.